DEVELOPMENT AND CHARACTERIZATION OF NEW OPTICAL FIBRE BASED RADIATION DOSIMETERS

MOSTAFA GHOMEISHI

THESIS SUBMITTED IN FULFILLMENT
OF THE REQUIREMENTS
FOR THE DEGREE OF DOCTOR OF PHILOSOPHY

FACULTY OF ENGINEERING
UNIVERSITY OF MALAYA
KUALA LUMPUR

2015

UNIVERSITI MALAYA
ORIGINAL LITERARY WORK DECLARATION

Name of Candidate: **MOSTAFA GHOMEISHI**

Registration/Matric No.: **KHA110074**

Name of Degree: **DOCTOR OF PHILOSOPHY (PhD)**

Title of Thesis:

DEVELOPMENT AND CHARACTERIZATION OF NEW OPTICAL FIBRE BASED RADIATION DOSIMETERS

Field of Study: **PHOTONICS (ELECTRONICS AND AUTOMATION)**

I do solemnly and sincerely declare that:

1. I am the sole author/writer of this Work;
2. This Work is original;
3. Any use of any work in which copyright exists was done by way of fair dealing and for permitted purposes and any excerpt or extract from, or reference to or reproduction of any copyright work has been disclosed expressly and sufficiently and the title of the Work and its authorship have been acknowledged in this Work;
4. I do not have any actual knowledge nor do I ought reasonably to know that the making of this work constitutes an infringement of any copyright work;
5. I hereby assign all and every rights in the copyright to this Work to the University of Malaya ("UM"), who henceforth shall be owner of the copyright in this Work and that any reproduction or use in any form or by any means whatsoever is prohibited without the written consent of UM having been first had and obtained;
6. I am fully aware that if in the course of making this Work I have been infringed any copyright whether intentionally or otherwise, I may be subject to legal action or any other action as may be determined by UM.

Candidate's Signature Date

Subscribed and solemnly declared before,

Witness's Signature Date

Name:
Designation:

ABSTRACT

For past few years, the optical fibre dosimetry has been started to significantly grow in different ionising radiation applications due to their inherent advantages in terms of dosimeter characteristics and capability are used as both real-time or off-line monitoring.

Several case-studies reported characteristics of optical fibres under the different dosimeter aspects instant various radiation sources and wide ranges of doses. However, in most cases, commercial available optical fibres have been used, which provided lots of ambiguous in terms of dosimeter characteristics regarding to various fabrication process, materials doped and element concentrations used by different manufacturers.

This study demonstrates characterisation of different home-made optical fibres where their fabrication parameters, doping elements and concentrations, and physical characteristics are varied in classical approaches to carefully address the main sources and factors that influence the sensitivity and characteristics of optical fibre dosimeters. For fair and consistency in analysis, a set of relatively fixed characterisation methods are adapted based on the availability and accessibility of resources; for instance, the study is performed based on thermoluminescence (TL) dosimeter with the main irradiation of MeV electron/photon within 0.5-10 Gy of applied dose.

The study is benchmarked with a couple of commercial available standard single mode fibres and conventional used lithium-fluoride dosimeter family, i.e., TLD-100.

The main effect of fibre structure/shape on performance of dosimeter is investigated by fabricating different types of undoped and doped optical fibres including capillary optical fibre, conventional cylindrical fibre, flat fibre (FF) and photonic crystal fibre (PCF). Performance of undoped fibres are compared with doped fibres; all items have been fabricated from the same Ge-doped preform. The TL response of capillary fibre can be significantly improved with our novel proposed FF, especially, if some dopant element exists in the collapsing region of FF.

The effect of cylindrical and flat fibre size on TL response is thoroughly investigated by fabricating several different sizes of fibres with fixed and varying core-

to-cladding ratios. For FFs, this is performed by considering different collapsing methods during fabrication process. It is shown that the effect of fibre size with fixed core-to-cladding ratio on TL response is insignificant for cylindrical fibre, but it is significant for FFs.

The effect of Ge concentration on TL response of optical fibres is also investigated by fabricating ten fibre preforms with different concentrations. Furthermore, performance of the other rare elements doped in optical fibres are demonstrated.

The study is furnished by providing discussion on structural defects with the aid of computational glow curve deconvolution (CGCD) analysis almost for every different optical fibres used.

ABSTRAK

Sejak beberapa tahun kebelakangan ini, dosimetri gentian optik mula berkembang dengan pesat dalam pelbagai aplikasi radiasi pengionan kerana kelebihan mereka dari segi ciri-ciri pengukur Dosis dan keupayaan untuk penggunaan kedua-dua pemantauan mase sebenar atau luar talian.

Beberapa kajian kes ciri-ciri gentian optik di bawah aspek pengukur Dosis yang berbeza dengan pelbagai sumber radiasi segera dan pelbagai dos telah dilaporkan. Walau bagaimanapun, dalam kebanyakan kes, gentian optik komersial telah digunakan menpunyai banyak ketakpastian dari segi ciri-ciri pengukur Dosis kerana terdapat pelbagai proses fabrikasi, bahan didopkan dan kepekatan unsur yang digunakan oleh pengeluar yang berbeza.

Kajian ini menunjukkan pencirian buatan gentian optik yang berbeza di mana parameter fabrikasi, unsur-unsur dan kepekatan dop, dan ciri-ciri fizikal yang berlainan dalam pendekatan klasik untuk menangani dengan teliti sumber-sumber utama dan faktor-faktor yang mempengaruhi kepekaan dan ciri-ciri dosimeter serat optik. Untuk memastikan keadilan dan konsisten dalam analisis, satu set kaedah pencirian tetap diterima pakai berdasarkan penyediaan dan penggunaan sumber-sumber untuk kajian dilakukan berdasarkan thermoluminescence (TL) pengukur Dosis dengan penyinaran utama MeV elektron/foton dalam 0.5-10 Gy dos gunaan.

Kajian ini ditanda aras dengan beberapa standard gentian mod tunggal komersial dan biasa digunakan pengukur Dosis keluarga lithium-fluorida (iaitu, TLD-100 untuk di sini).

Kesan Struktur gentian / bentuk di atas prestasi pengukur Dosis disiasat dengan mereka-reka pelbagai jenis gentian optik undoped dan Terdop termasuk serat optik kapilari, serat silinder konvensional, serat rata (FF) dan gentian kristal fotonik (PCF). Prestasi gentian undoped dibandingkan dengan serat Terdop; semua diperbuat daripada preform yang sama Ge-terdop. Kami telah menunjukkan bahawa tindak balas TL daripada kapilari boleh meningkat dengan ketara dengan FF yang kami dicadangkan, terutama, jika beberapa elemen pendopan ada di rantau runtuh di dalam FF.

Kesan silinder dan FF saiz kepada sambutan TL ini disiasat dengan teliti dengan beberapa saiz yang berbeza bagi gentian dengan nisbah teras-ke-pelapisan tetap dan berbeza. Untuk FF, ini dilakukan dengan mempertimbangkan kaedah runtuh yang berbeza semasa proses fabrikasi. Ia menunjukkan bahawa kesan saiz serat dengan nisbah teras-ke-pelapisan tetap adalah tidak penting untuk silinder, tetapi ia adalah penting untuk FF.

Kesan kepekatan Ge kepada sambutan TL gentian optik juga disiasat dengan menyediakan beberapa preform serat dengan kepekatan yang berbeza. Tambahan pula, prestasi unsur-unsur nadir lain bumi yang berbeza didopkan dalam gentian optik telah ditunjukkan.

Kajian ini dilengkapi dengan menyediakan perbincangan mengenai kecacatan struktur dengan menggunakan pengiraan lengkung cahaya analisis deconvolution untuk setiap gentian optik yang berlainan digunakan.

To my family, with greatest love...

my wife with her lovely company, my parents with their endless supports, and my dearest sons, Nima and Pouriya.

ACKNOWLEDGEMENTS

This thesis has benefited greatly from the support of many people, some of whom I would sincerely like to thank here:

My supervisors, Professor Dr. Faisal Rafiq M. Adikan and Dr. Ghafour Amouzad Mahdiraji. Their guiding, support and valuable suggestions and advices have given me the confidence to complete this research work;

Professor Dr. David A. Bradley, for his consultations on some of the details and ideas during the commencement of the research and Dr. Ung, for his help and patient in sample collecting of this research;

Examiners of this thesis, Professor Dr. Sylvain Girard, Dr. Claus E. Andersen, and Dr. Jeannie Wong Hsiu Ding, for their valuable comments and suggestions to improve the quality of this thesis;

Present and past members of the Integrated Lightwave Research Group (ILRG) of University of Malaya, especially Dr. Peyman Jahanshahi, for their directly and indirectly contribution to the constructive ideas and the time together in the lab.

Last but not least, I owe sincere and earnest thankfulness to my family and all my friends who gave me encouragement and uphold me in prayer when I having hard time in life and study.

Mostafa Ghomeishi
Department of Electrical Engineering
Faculty of Engineering, University of Malaya
March 2015

TABLE OF CONTENTS

LIST OF FIGURES

LIST OF TABLES

ABBREVIATIONS

CB	Conductive band
EDX	Energy dispersive x-ray
ESR	Electron spin resonance
FF	Flat optical fibre
FOM	Figure of Merit
FWHM	Full width half maximum
GEC	Germanium electron trapped centre
Gy	Gray
HF	Hydrofluoric acid
MCVD	Modified chemical vapour deposition
MDD	Minimum detectable dose
MMF	Multi-mode fibre
NBOHC	Non-bridging oxygen hole centre
ODC	Oxygen deficiency centre
OSL	Optically stimulated luminescence
PL	Photo luminescence
PMT	Photo multiplier tube noise
PCF	Photonics crystal fibre
POL	Peroxy linkage
POR	Peroxy radical
QA	Quality assurance
ROI	Region of interest
S	Sensitivity
SEM	Scanning electron microscope
SMF	Single mode fibre
STE	Self-trapped excitation

TL	Thermoluminescence
TLD	Thermoluminescence dosimeter
TTP	Time temperature profile
VB	Valance band
Wt	Weight
XPS	X-ray photoelectron spectroscopy
XRD	X-ray diffraction
XRF	X-ray luminescence

CHAPTER 1: INTRODUCTION

1.1 Overview

In the past two decades, the fibre dosimetry has grown to become a reliable substitution for radiation detection in different range of dose and environmental conditions. The importance of this measurement is due to the potential harmful nature of ionising radiation, and some historical finding. Ionising radiation have various natural (i.e. cosmic radiation, radioactive elements and etc.) and artificial sources (nuclear plants, radiotherapy sources and etc.) in the earth that not always harmful.

Since 1985 there has been marked decrease in the use of film dosimeters for personal monitoring, largely being replaced by thermoluminescence dosimeters (TLDs) [2]. In-vivo TLD dosimetry has also become prevalent [3, 4], as illustrated by the therapeutic level work of White et al. [5], the dosimeters monitoring photon radiation. To this can be added other examples of in-vivo studies making use of TLDs as the main dosimetry system, for doses typically ranging from 0.1-10 Gy [4, 6–9] and for experiments performed on the total body, within a similar range of dose [10]. When sensitive parts of body have been targeted for radiation (including the eyes, glands, head and neck), the spatial resolution of the TLD has become that much more important [11, 12].

Optical fibres have been shown to be a potential candidate for such radiation dose sensors, with particularly high spatial resolution, linear response over wide range of doses, energy and temperature independence and acceptable sensitivity, the latter at a level that has now become comparable with that of commercially available dosimeter sensors [13]. Furthermore, optical fibres are immune to electromagnetic interference, impervious to water (suitable for in-vivo application), and capable to be used in real time or offline monitoring systems with significantly lower cost compared to the commercially available dosimeters.

In radiation therapy, a highly sensitive dosimeter would be extremely helpful in precision measurement of dose delivery, both to the tumour as well as in out-of-field

measurements, potential neutron contributions from accelerators operated at high energies ($\geq$ 10 MeV) becoming an important consideration [14]. Such performance can be expected to aid in obtaining an improved treatment outcome, in terms of enhanced tumour control and reduced post-radiation therapy complications [15]. Several different materials have been used to dope the silica glass and optical fibres in an effort to improve the radiation dose sensitivity, including germanium [13, 16–18], lithium and barium [19], aluminium [18], zirconium oxide (ZrO_2) [20], manganese doped calcium tetraborate (CaB_4O_7:Mn) nonocrystal [21], lithium potassium borate glass doped with titanium oxide (TiO_2) and magnesium oxide (MgO) [22].

1.2 Problem statement

Although commercial TLDs have typically developed, following up upon the favourable outcome of studies of various constituents, for optical fibres the study of TL yield have been much more limited to the commercially available fibres. Beside the commercial optical fibres with specific dopants, it is possible to use the tailor made optical fibres with specific characteristics. Different dopants, different sizes and even different patterns or structures can be examined for this purpose, where the information of such variations' effect on performance of optical fibre dosimeters are never classically reported.

The performance of different types of commercially available optical fibres such as standard single mode fibres (SMFs) and multimode fibres (MMFs) [23] doped with different rare earth materials for instant Germanium [23, 24], Phosphorus [23, 25–28], Aluminium [18, 29], Fluorine [30] are demonstrated. The performance comparison between SMFs and MMFs in terms of higher sensitivity against radiation dose detection suggest outperformance of MMFs that is related to their larger fibre core area; however, there is no such a classical report clearly evaluating performance of such optical fibres neglecting the influence of fibre manufacturing process and the dopant concentrations since most of those reported optical fibres are fabricated by different manufacturers using different recipes.

Zahaimi et al. [31] compared the thermoluminescent (TL) response of optical

fibres with different core diameters, from 8 to 50 μm, showing that the larger core fibre generates higher TL. However, the optical fibres used in that study were fabricated by different manufacturers with even different Ge concentrations leaving unclear the effect of manufacturing process and dopant concentrations. The effect of fibre drawing condition on characteristics of optical fibres is reported since earlier 1970s, as an example showing absorption induces in 215 nm and 248 nm [32], 630 nm [33, 34], and 1530 nm [35] at higher fibre drawing tension; and the refractive index reduction with the increase of residual stress (or drawing tension) [36]. However, to the best of our knowledge, the influence of fibre manufacturing process on irradiation characteristics of optical fibres for dosimeter applications, on the other hand, are not studied in detail yet.

Recently, Girard and Alessi et al., demonstrated the influence of manufacturing process on radiation induced attenuation (RIA) of optical fibres considering both the preform fabrication using modified chemical vapor deposition (MCVD) process and the fibre drawing conditions [25, 30, 37, 38]. In [25], Girard et al., have observed a slight reduction in RIA at 1550 nm by lowering the fibre drawing tension. Also, they observed that by lowering the preform deposition temperature during MCVD process the RIA at 1310 nm and 1550 nm reduces for short times after irradiation. In [30, 37, 38], the authors have shown the insignificant effect of drawing parameters on RIA of optical fibres within a range of fibre drawing parameters used for special fibre fabrications. However, these studies are limited to RIA involved with high radiation doses in the range of kGy – MGy.

Furthermore, the relationship between the irradiation dose sensitivity of optical fibre against fibre core diameter/area is not very clear yet. Although, Zahaimi et al., have shown a linear response of y = 24x or 25x; this relationship would not be accurate enough since the optical fibres are made with different Ge concentrations and fabricated by different manufacturers.

In terms of Ge-concentration, so far there is not any report showing the optimum dopant concentration that leads to higher radiation dose detection sensitivity.

In terms of fibre structure effect, very limited study reported performance of

some microstructure optical fibres under ionising radiation [39–42]. However, there is no any study to explain if there is any specific effect on radiation dosimeter performance due to the change of the fibre structure.

1.3 Objectives

The main objective of this study is to investigate the effect of optical fibre physical properties and dopant concentrations on their thermoluminescence response. In specific, the objectives of this study are:

- *To understand the characteristics and behaviour of standard optical fibres in dosimetry applications compared with commercially available TLD*;
- *To evaluate the dosimetric characteristics of specific doped optical fibres*;
- *To understand and investigate the effect of fibre structure on its TL response*;
- *To investigate the effect of fibre size on its TL response*;
- *To investigate the effect of Ge-doping concentration on TL response of optical fibres*;
- *To analyse glow curves of optical fibres and provide the fundamental kinetics properties of them.*

1.4 Scopes and limitations

The first objective is to study the dosimetric characteristics of commercially available standard SMFs. This is performed by selecting two Ge-doped SMFs fabricated by two different manufacturers to understand their similarity/differences in terms of dosimetric characteristics. A commonly used commercial TLD (here TLD-100) is used in this study mainly as the benchmark to compare performance of optical fibre dosimeters. The TLD-100 is selected among the other lithium-fluoride TLD families mainly due to its widespread usage in the dose range adopted for this study. It should be noted that since the main object of this study is to investigate the effect of fibre

physical parameters on TL response, therefore, a fixed dose range mainly from 0.5 to 10 Gy and fixed sources of irradiation, i.e., LINAC that is a therapeutic linear accelerator source, with energies of 6 to 20 MeV/MV electron/photon radiation, are adopted in this study mainly due to the availability and accuracy of the LINAC machine.

To achieve the second objective, five types of optical fibres with special dopants are involved in the study. After standard dosimetric examinations, it is tried to make a general comparison after analysing their kinetics. The choice of these fibres were due to availability of their preforms provided by our collaborators, which are pulled using our drawing tower for other photonics applications.

For the third objective, a simple 7-ring hexagonal lattice form photonic crystal fibre (PCF) is developed by using a HXWG pure glass tube. Performance of this fibre is compared with a single capillary fabricated from the same preform. For better understanding the phenomenon occuring in PCF compared to within a single capillary, a tailor made optical fibre, i.e., flat fibre, is fabricated. Since the FF can be directly fabricated from a single capillary cane or preform tube, understanding of its characteristics difference compared to a single capillary is much easier than a PCF, that consists of hundreds of capillaries. Therefore, instead of PCF, FF is used as the main structure for further investigation and fabrication with Ge-doped preform. Due to availability, only Ge-doped FFs are fabricated in this study.

Then five different sizes for cylindrical and flat fibres are tested for forth objective. For the ultimate achievement, this study is done once with different fibre sizes with the same core-to-cladding ratio and next with varying core-to-cladding ratio by etching the fibre cladding.

The concentrations of 0.7 to 15 weight % germanium in the core of optical fibre are chosen for the fifth objective. Ten Ge-doped fibres were involve in this study, eight of them were home-made fibres and two were commercial fibres.

The defect analysis is mainly addressed using the glow curve analysis with the aid of computerized glow curve deconvolution method.

1.5 Organization

Chapter 2 presents an overview of radiation source and doses together with their detection methods and devices. Early studies on the TLDs, included the fibre TLDs and related defect centres are described here. Applications of TLDs in various fields of radiation are presented. Some of the studies done with the specific aim to improve the thermoluminescence detectors are discussed in current chapter. Particular emphasis is given to the fibre TLDs and method of their analysis are proposed for this thesis.

Chapter 3 describes the theory and development of fibre TLD, which are divided in two main sections. It starts with general information on preparation of fibre samples from doping to cutting. The necessary parts of experiment is including annealing, irradiation and readout is briefly explained and some diagnostics methods, which are used in our work are presented. Afterwards, this chapter is followed by characterisation of the samples, according to each application in the result chapters.

Chapter 4 addresses the thermoluminescence response of two commercial single mode fibres in which their sensitivity in comparison to TLD-100 are studied. In addition, dosimetric properties of some available optical fibres with special dopant are discussed. Electron trap parameters of all the samples are extracted and analysed by using computerised glow curve deconvolution method.

Chapter 5 discusses possibility of improvement in the quality of fibre TLDs and show that there is still room for improvement especially in the response intensity of the fibre TLDs by using micro-structure optical fibres. New types of fibres are, therefore, proposed with detailed characterisation.

Chapter 6 specifically studies the influence of different fibre size on the thermoluminescence response. Besides the basic examination on the samples with different sizes such as their response to irradiation in various doses, the cladding of the fibres under investigation is removed gradually by chemical etching technique to highlight the influence of dopant material in compare with undoped silica, fibre cladding. This study is followed by evaluating the accuracy of normalised result to weight using normalisation to volume. Some consideration on the effect of uniformity of flat fibre

during the fabrication is studied. Furthermore, effect of collapsing method during the making of flat fibre on its TL response was tested.

In chapter 7, effect of different concentrations of germanium, which is incorporated inside the fibre core is investigated to find the optimum available concentration.

Chapter 8 summarise the contents of the thesis and discuss the possibilities of future work in this direction.

CHAPTER 2: LITERATURE REVIEW

This chapter offers a brief literature review about history of radiation, dosimetry and fibre dosimetry. The term "thermoluminescence dosimeter" or "TLD" is defined as a base of our work and methods to analysis the thermoluminescence dosimeters.

2.1 Introduction

The study on radiation effects of different beams was always interesting because of the variety of their characteristic, intensity, source and their influence on their targets. Radiation beams can be classified as some are ionising and some are magnetic. In most cases magnetic radiation is not harmful but ionising radiation can be dangerous especially with high intensity. The radiation beams are made of either electromagnetic waves or particles in which the particles might be Beta, Alpha, neutron or charged ions [43].

Dosimetry or radiometry is the science of knowledge about radiations. The devices which are used to detect the radiations are called dosimeter. Depending on the characteristics of the radiation beam and dosimeters itself, various information can be provided through dosimeters [44–46]. Among the dosimeters, thermoluminescence dosimeter (TLD) is well known as a passive and effective dosimeter and it is still under development [47, 48].

Design and optimisation of TLDs are related to the parameters known as TL parameters. Material, size, response, fading, linearity and supra linearity are the most important parameters among them. Further information about the TLDs can be provided through the study of their defects and trapping/detrapping mechanisms.

In some definitions radiation is depicted as stream travel of electromagnetic waves or any composed of subatomic particles. Radiations are produced naturally in decay process of radioisotope sources, however, they can be produced in the accelerators

too. The photon energy related to the wavelength can be calculated by:

$$E = \frac{1.240 \times 10^{-6}}{\lambda} \tag{2.1}$$

where E is the photon energy in eV and λ is the wavelength in meters [43].

Absorbed dose is a fundamental dose quantity representing the mean energy imparted to matter per unit mass by ionising radiation. The SI unit is joules per kilogram and its symbol is Gy (gray). The CGS unit for measuring the absorbed dose is Rad which is 0.01 Gy.

There are numerous of useful applications for ionising radiation. They can be divided into various dose ranges as per their applications: Radiation medicine, main applications of radiation in medicine are *radiotherapy* (cGy to Gy) and *diagnostic imaging* (μGy to cGy); Industrial applications, for example, *radiation processing and sterilization* (10s of kGy) and *nuclear establishment*; Radiation protection, *area and personal monitoring* (μGy to cGy) and *environmental surveys* (μGy to mGy); Research, several researches are undergone by using the radiation science like *space investigation* and *materials studies*.

2.2 Dosimeter

A dosimeter is a system or instrument which measures either directly or indirectly, the quantities exposure, absorbed dose or equivalent dose, or their rates. A dosimetry system is referred to a dosimeter along with its reader. The result of a dosimetry systems measurement is the quantity expressed as the product of a numerical value with an appropriate unit [44].

Clearly, all characteristics cannot be satisfied by a single dosimeter. The choice of a radiation dosimeter and its reader must then be made carefully, considering the requirements of the measurement situation [44].

The main types of dosimeters, but not in order, are radiochromic film [15, 49], ceric-cerous [50, 51], semiconductor dosimeter, radiographic film, ionisation chamber, gel dosimetry systems, diamond dosimeter, plastic scintillators [44], lumines-

cence based dosimeters such as optically stimulated luminescence dosimeter and thermoluminescence dosimeter in which the details are discussed later.

2.3 Luminescence

Emission occurs when internal energy from one system is transformed into electromagnetic radiation. When an atom has energy transferred to it, either by collisions or as a result of exposure to radiation, it is said to be "excited". In another word, some materials hold part of the absorbed energy after absorption of radiation in metastable states. If this energy is released afterward in the form of light with visible, ultraviolet or infrared spectra, the phenomenon is called luminescence. There are two types of luminescence, fluorescence that occurs with time delay between 10^{-10} and 10^{-8} second, and phosphorescence with time delay exceeding 10^{-8} second [44].

The phosphorescence process can be accelerated with an excitation in most cases in the form of light or heat. If the excitation happens through light, the phenomenon is known as optically stimulated luminescence (OSL) [52]. But, if it occurs via heat, the phenomenon is referred to thermoluminescence (TL) and the material is called a thermoluminescent material, which is the main focus of this study.

Thermoluminescence phenomenon is defined by two stages: firstly, the perturbation of system from equilibrium into metastable state; and secondly, thermally stimulated relaxation of the system back to equilibrium [47]. The thermoluminescence is distinguished from incandescence by two characteristics. First one is the intensity of TL emission that varies even in a constant temperature and diminishes with time to cease. Second is that the TL spectrum is more depends on the material rather than on the temperature. To distinguish the TL emission from incandescence emission, while both are available at some temperatures of observation, it is possible to just remove the steady-state emission (incandescence) from the total emission and the transient one is TL.

Due to the transient nature of the TL emission only heating triggers the release of stored energy. This interpretation is supported by the fact that after the TL has

been decreased to background level by heating, the sample can be made thermoluminescent again by exposure to one of a number of energy sources. As a result a memory of exposure to an energizing source is carried by a TL material, and this memory is utilized in a number of applications [53].

In addition to luminescent centres in TL phosphors, some centres are produced in TL solids by ionising radiation that can lead to electrons or holes trapping. Although the luminescence centre can trap both electron and hole, but, it is usually the hole trap. If the trap depth is large and thermal energy is not enough to release the electron from the trap, it will remain trapped without luminescence. In this case if the temperature of the phosphor is gradually increased, electrons will receive thermal energy increasingly and it raises the escape probability of them from traps and may then go over to luminescent centres and recombine with holes trapped at or near these centres. The energy released by the recombination can excite the luminescent centres, causing them to emit light [53].

The photon energy deposition in matter is mainly caused by the highly energetic electrons that are produced in the photon-matter interactions. These electrons in the solid release low energy free electrons and holes. Then they either recombine or become trapped in the solid. Traps are of two kinds, intrinsic and extrinsic, traps are introduced in the crystal as a lattice imperfections including of impurities and vacancies [44]. As temperature raise in the solid, the release of stocked energy, which is comes from vacancy-interstitial or electron-hole recombination, is stimulated in the form of luminescence. In both cases, electrons are de-excited to the ground state from metastable excited states [47].

An amount of thermal energy is absorbed by electron when phonon is coupling between the solid lattice and the electron. The probability per second to here a sufficient amount of this energy to release the trapped electron from its localised state is given by Arrhenius equation:

$$p(T) = s(T)e^{\frac{-E}{kT}} \tag{2.2}$$

having considered that the electrons in the trap have a Maxwellian distribution

of thermal energies. In this equation T is the absolute temperature (K), k is the Boltzmann's constant, E is the activation energy, called trap depth, in eV given as a difference between the trap level and the bottom of the conduction energy band and $s(T)$ which is a weakly temperature dependent term known as "the frequency factor" (s^{-1}), depending on the frequency of the number of hits of an electron in the trap, seen as a potential well and it is related to the local lattice vibrational frequency and the entropy change associated with the charge release. Therefore, when the temperature is high enough, the electron will be released into the conduction band and will then be free either to retrap, become trapped at a different localised state, or recombine with trapped holes [47, 53–57].

An alternative energy release mechanism involves the thermally stimulated recombination between interstitial atoms and vacancies. The reaction may be described by:

$$Interstitial\ centres + Vacancy\ centres \Longleftrightarrow Perfect\ lattice + Photon_{TL} \quad (2.3)$$

A third type of mechanism is also possible, involving electron and/or hole release but not involving excitation to delocalised bands. If there is a strong spatial association between a trap and a recombination site one can have transfer of charge between these sites via localised states, i.e. states, which are neither in the conduction band nor the valence band. With any of the above mechanisms one observes an increasing luminescence emission as the temperature rises due to the increasing numbers of free charges (or interstitial atoms) released and decrease of the luminescence intensity with temperature [47].

Electrons released by a shallow trap may be captured by an interactive trap (deep thermally disconnected trap). The interactive traps are competing with the recombination centres to capture electrons released from the shallow traps. Recombination must be accompanied by emission of light in order to get luminescence, which means "radiative" transitions. A "non-radiative" transition is accompanied only by phonon emission [54].

A simple model is described in the Figure 2.1 to explain the theoretical treat-

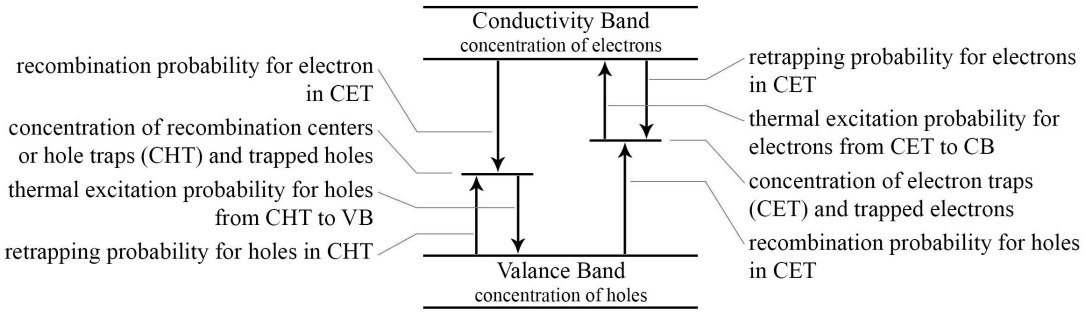

Figure 2.1: The energy level scheme proposed by Schon [54] for thermoluminescence phenomenon

ment of two delocalised bands, valance band (VB) and conduction band (CB) and two metastable states that one is trap and the other is recombination centre. The distance between the bottom of the CB and the trap is called activation energy or trap depth and being interpreted as the activation energy necessary to liberate of the trapped interstitial ions which then diffuse to vacancy sites.

2.4 Thermoluminescence Detectors

Thermoluminescence dosimeters (TLDs) are extensively used for observing integrated radiation exposure in hospitals, nuclear power plants and other installations where ionising radiations are likely to be faced. These dosimeters work with the fact that some part of absorbed energy of radiations in thermoluminescent phosphors are stored for long periods of time and when it is properly heated, the trapped energy will be released as luminescence. The intensity of this luminescence emission is proportional to the original radiation dose [53, 58].

The wide variety of TLDs by means of their different materials and shapes allows the determination of various radiations at different doses from μGy to kGy. As major advantages of TLDs are their small sizes and their independency to external equipment during the operation that make them suitable for many applications. However, still there are black arts for scientists who try to improve the TLD systems. Hence, the present literature intends to summarize the significant information that describe problems in the development of TLD systems in order to optimisation of TLDs.

2.4.1 Basic Theory of TLDs

As discussed in previous section, certain amount of ionising radiation energy absorbed by a thermoluminescent material, stimulate the excitation of electrons from the VB to the CB of the material. The free electrons in the CB may be trapped at a site of crystalline imperfection (i.e., impurity atom, lattice vacancy, dislocation). The trapped electrons have a certain probability per unit of time to be released back into the CB which is given by the Equation 2.2. This equation can lead to the TL intensity with respect to temperature and dose by defining the N as the concentration of empty traps in TLD:

$$I(D,T) = A.s.N.D.C.e^{\frac{-E}{kT}} \tag{2.4}$$

where A is radiation susceptibility and it is constant for each material, D is the absorbed dose and C is integration constant [54].

By heating of the sample, the filled traps can be evacuated by thermal stimulation of the trapped electrons which rise to the CB. From here the free electrons have a certain probability to recombine with a hole at some sites, called recombination centres which results in the emission of visible light and is called TL glow and can be monitored by a glow curve which is formed by some peaks. Each peak reflects a trap with defined activation energy [54]. There are few consideration to ensure that TL material can work as a detector and they are discussed as following.

2.4.1.1 TLD requirements

To choose an appropriate TL material for a specific or even general application, there are some properties that need to be considered [47, 54]:

- The recombination process should result in efficient light emission and high concentration of traps;
- Capability of stable storage of the trapped charges with negligible fading as a function of storage temperature and time;

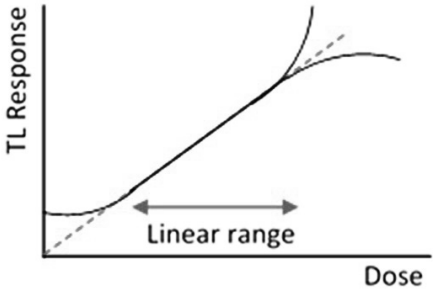

Figure 2.2: Typical TL response plotted vs dose

- The TL material should not suffer by environmental influences such as gases, organic solvents, humidity, and moisture; and also a good resistance against radiation damage in the applicable dose range;
- Low energy dependency and in case of medical and personnel applications tissue equivalency;
- Linearity of TL response with as low as possible lower limit of detection, and independent of dose rate and radiation incident angle;
- Non-toxic TL material (specially for in-vivo applications);
- And finally high accuracy and precision.

2.4.1.2 Nonlinearity

There might be different zones in the plot of TL response vs. dose. As it can be seen from the Figure 2.2, the TL response is not linear in all the dose ranges. To describe these zones, it is needed to introduce two terms: superlinearity and supralinearity. Superlinearity (or sublinearity) gives the indication of change in the slope of the dose response in all cases. Supralinearity is used to specify the size of the correction required for extrapolation of the linear dose region [54].

2.4.1.3 Sensitivity

The sensitivity (S) can be due to variation of the mass of the detectors, the optical density from sample to sample and dirt contamination of the sample surface [54].

The sensitivity of a TLD is defined as normalised TL response per unit dose. In the case that TL response is normalised per unit mass, it can be expressed as follow:

$$S = \frac{TL}{mass.Dose} \tag{2.5}$$

2.4.1.4 Repeatability

The stability of the chemical and physical properties of the TL material is referred to the repeatability of the TL material. In other word, if the cycle of using TLD (annealing, irradiation, and readout) is repeated, the glow curve and sensitivity of the TL material should not change. To check the repeatability, a group of TLDs should be chosen from the same batch of sensors and examined with a specific dose for few cycle [54].

2.4.1.5 Effective atomic number

Due to the vast range of radiological dosimetry, two properties of the TL dosimeters are beneficial for several applications, which are tissue equivalence and high sensitivity. High sensitivity thermoluminescent phosphors have high effective atomic numbers, Z_{eff}, hence in order to have photon energies almost lower than 100 keV, the response to a given absorbed dose of radiation must be significantly higher than the one at higher energies. In this range the photoelectric impact is dominant and the cross-section per atom is approximately Z^4 and on $Z^{4.8}$ for high and low Z materials, respectively. As each atom has Z electrons, the coefficient per electron relay upon Z^3 and $Z^{3.8}$ for high and low Z materials, respectively. In order to understand the expected TL response at different energies, the Z_{eff} of a TL material should be known. The reaction of materials to gamma and x rays contingents on the atomic number of the constituents and not on the chemical composition of these constituents [59–62].

$$\bar{Z} = \sqrt[x]{a_1 Z_1^x + a_2 Z_2^x + \cdots} \tag{2.6}$$

$$a_i = \frac{n_i(Z_i)}{\sum_i n_i(Z_i)} \quad \& \quad n_i = N_A.Z_i$$

where a_1, a_2, $\cdots$ are the fractional contents of electrons belonging to elements Z_1, Z_2, $\cdots$ respectively, n_i is the number of electrons, in one mole, belonging to each element Z_i and N_A is the Avogadro's number. The value of x is 2.94 [54, 63–65].

Those TLDs having an effective atomic number, Z_{eff}, similar to the effective atomic number of the body soft tissue (Z=7.4) are called as tissue equivalent TL dosimeters. The tissue equivalence is a feature for better accuracy in clinical, biomedical, and personal monitoring. The photon interactions' cross-sections in materials are directly proportional to the atomic number of elements in which they are raised to some numerical power. In cases that Z_{eff} is not satisfied the tissue equivalence, a correction factor need to be applied [54, 66–69].

2.4.1.6 Fading

Fading is the phenomenon of loosing the TL memory over time which has several causes. One of the most common fading is thermal fading. Thermal fading has half-life and the amount of fading can be concluded from rearrangement of Equation 2.2. The mechanism of this fading is the simple thermal release of trapped charges from defects thermally [47].

Athermal or anomalous fading express itself when the TL signal, which is not expected to decay thermally, is seen to decay significantly even at low storage temperatures. Quantum mechanical tunneling of the trapped charge to the recombination site [70], and localised transitions which do not take place via the delocalised bands [71] are believed to have a major contribution in anomalous fading. This fading can be characterised by an initial rapid decay followed by a decrease of the decay rate over long storage periods [54].

Optical fading is another fading that is the effect of light on an irradiated TLD which is included of a reduction of the TL signal, depending on the light intensity, its wavelength and duration of exposure [47, 54, 72].

2.4.2 Error sources in TLD measurements

Many sources of error were known in a TLD system, which a substantial effort should be done to reduce the influences of them and decrease the uncertainty on precision and accuracy of the TLD system. The errors in the system are usually originating from TLD or reader characteristics or may come out by the process of heat treatment either during the annealing or readout. The most important consideration in all cases, the whole procedure should put in practice in a reproducible way.

- Error sources due to TL material, which are the main sources of errors in TLDs and can be enumerated as optical properties, optical and thermal fading, energy dependency, directional dependency to the incident radiation, variations in the mass and size, and variation in sensitivity caused by radiation damage;
- Errors sources because of the reader, that usually are caused by instable and inappropriate readout cycle. An error can be generated by poor thermal contact of TLD and reader tray. Also performance of the built-in reference light could be important;
- Errors sources because of the annealing. It should be done in a reproducible way. So any deviation in the cycle of this procedure may results in a variation in the sensitivity of the TLD. Choosing proper temperature and heating cycle are also important to enhance the efficiency of the dosimeter.

2.4.3 TLD application - privilege and limitation

The determination of different radiation qualities over a broad range of absorbed dose is made possible by TLDs due to the variety of TL materials and their various physical shapes. This makes TL dosimeters useful in the range of μGy (monitoring of radiation protection) to the level of several Gray (dose measurement in radiotherapy). However the small physical size and remote dose assessment of TLDs are their major advantages that made them unique among the various dosimeters. Size matter, the TLD is good for point dose measurement in vivo dosimetry. It also can be applied in personnel dosimetry as an integrative dosimeter. In addition, TLDs are

easy to handle and transport and can be mailed [73]. Following are some application for the TLDs.

An important application of TLDs, is personnel dosimetry for observing the radiation dose that is delivered to personnel at routine working exposure (i.e. hospital radiotherapy technicians and reactor workers). The interested dose range in this category is from $\sim 10^{-5}$ to 10^{-2} Gy and accuracy of about $\pm 15\%$ is required [47].

Another application for TLDs can be named as environmental dosimetry. Nowadays, continuous monitoring of radiation released to the environment has become important for industrialized nations. For this purpose TLD is an ideal monitoring system. Low fading with high sensitivity is vitally important since the exposure levels are low (typically 10^{-2} mGy) and long exposure times are needed [47].

Clinical dosimetry was always an interest for TLDs. A TLD with small size is exploited in clinical diagnostics and therapies on the human body which are exposing to ionising radiations. By careful analysing the exposed TLD, physicians can measure the actual absorbed doses which is critical for internal organs. Most of the radiations in this application are gamma rays, electrons (up to 40 MeV), and x-rays (more than 10 keV). High sensitivity and linear response over a wide dose range is required due to the small size of the TLD and high doses in this application [47]. The two main clinical applications are diagnostic radiology (dose range of 10^{-5} to 10^{-2} Gy) and radiotherapy (up to 20 Gy).

Monitoring of high dose radiation (10^2 - 10^5 Gy) is another application of TLDs. The conventional TLDs have limitation because of the saturation in their response in high doses. The applications of this range are sterilization (food, cosmetics, surgical stuff, soil and etc.), nuclear reactors and material testing.

In this context, our focus in this study will be more on mid-range and high dose range of radiation detection using TL material. Generally, the radiotherapy dose range of about few Gy, and sterilization which is about several kGy were tested.

2.5 Fibre Thermoluminescence Dosimeter

After TLDs proved their efficiency in various applications, many attempts are done to improve these kind of detectors. Thermoluminescence materials subject to ionising radiation include but are not limited to calcium fluoride, lithium fluoride, calcium sulfate, lithium borate, calcium borate, potassium bromide and feldspar [44–46]. The TL capability of optical fibre is initially introduced in 1990 [74] and since then many experiments is done on this material [75–77] and the effect of radiation on optical fibres are investigated for various application like radiotherapy, radio-diagnosis, space studies, high and low doses and so on [78–82].

The phenomenon of thermoluminescence in silica based optical fibre is interesting since TL effect in pure silica is very poor and negligible. Although ionising and elastic collision together cause luminescence in silica, but mostly impurities needed for a better observing of the luminescence and thermoluminescence in this material [83]. Therefore, transforming the silica glass preform to a fibre shape plays the key rule of this ability in the optical fibre to work as a possible TLD.

Many attempts are done to improve the sensitivity of optical fibres to radiation and some models are suggested [84–86]. In a brief study, the influence of environment in the sensitivity of optical fibre as a TLD is investigated by Zheng, *et.al*. [87]. They found out that optical fibre response is not changing subject to irradiation temperature, irradiation humidity and different illumination conditions. By the way, to make sure that optical fibre can role as efficient TLD, finding the appropriate dopant and its concentration is ineludible and effect of different irradiation source and dose should be studied.

2.5.1 Dopant in Optical Fibre

Interaction of ionising radiation with glass materials causes physical and chemical changes where make up the glass structure by breaking of SiO_2 bonds and the formation of new bonds with impurity atoms such as Ge, Al, or a variety of other elements in the glass crystalline net [88].

Germanium is an interesting dopant for dosimetry purpose in optical fibres [16,

24, 89]. Beside the interesting results of this kind of doped fibre, there are two main reasons for this. First, Ge is a semiconductor with four available valence bands just like Si in the silica network. Second, the similar behaviour of this element as Si in silica network with the O=Ge=O bond or other similar Si bonds. In many other researches, Al was found helpful for increasing the TL response in optical fibres [82, 90, 91], however, not as sensitive as Ge-doped fibres.

After Ge-doped and Al-doped optical fibre, the effect of some other dopant to TL response of optical fibres was also studied. As a sample of these dopants, oxygen molecule (O_2) is tried by Hshim *et.al.* [92]. Phosphorus doped optical fibre also studied for x-ray radiation dosimetry in the range of 1 Gy to 3 kGy [23, 93]. It is confirmed that the dose response of this doped fibre is linear and temperature independent. Other doped fibres such as N-doped, Er-doped, Yb-doped, F-co-doped were investigated under ionising radiation, however, the investigation were focused mainly on hardening effect of the optical fibres [23].

2.5.2 Optical Fibre Response versus Dose

It is important that a TLD shows a linear response to dose in the dose range of interest. The dose response examination is included in almost all of the works which is carried on the TL dosimeters. Dose range of 0.1 Gy to 20 Gy is the interest of radiotherapy and as it was shown by many researchers, the optical fibre TL is linear in this range [92, 94–96]. In addition there is also reported a considerable TL energy dependence for both photon and electron beam radiation [94]. More high dose ranges up to several kGy produced by synchrotron on optical fibre are also reported [97].

2.5.3 Optical Fibre Response versus Source

The TL response of optical fibres were examined against different sources of radiations. The TL response of doped commercially available optical fibre subject to electron and photon irradiation were investigated by Hashim *et.al.* [90] in radiotherapy dose range. It is shown in their research that beside the sensitivity of the

samples, the results are linear with low degree of fading. Similar researches were done for x-ray therapy in the kilo-voltage range and in-vitro intensity-modulated radiation therapy (IMRT) prostate dosimetry [14, 98].

Synchrotron microbeam is a source of very high dose gradient for hundreds of Gy over an area of about 10 μm which is used to radiation therapy too. Some experiments have studied the TL response of optical fibres at incident energies of 20-90 keV, for a wide range of doses, from 1 Gy to 10 kGy, revealing a linear response [97]. Synchrotron x-ray at European Synchrotron Radiation Facility (ESRF) is another similar types of device for producing high energy photon dose [99] which is tested to investigate the spatial resolution of radiation by Ge-doped optical fibre. In another work done by Ramli et.al. [100], optical fibre is tested for alpha particle beam where used in radiotherapy to deliver a more precise dose to the target volume while minimizing dose to the surrounding healthy tissue.

Even though neutron radiation is almost always accompanied with gamma rays, an attempt to test the TL response of optical fibre subject to fast neutrons has shown a sensitive linear dose response using ^{241}AmBe source [101].

2.5.4 Optical Fibre TLDs versus commercial TLD-100

Comparison of optical fibre TLD against commercially available TLDs is important. Although the cost of optical fibre is much less than available TLDs, on the contrary, their response must be at least comparable with them to be able to introduce the optical fibre as TLD. To comply this important aim, optical fibres are compared for different radiation sources.

The experiment, which is done for Ge- and Al- doped optical fibre together with TLD-100 rods, shows that the response of doped optical fibres for alpha particle irradiation were almost in the range of TLD-100 rods, but a bit less [100]. However, the response of these two fibres subject to electron [102] and photon [91] irradiation for clinical ranges indicates that Ge-doped fibre response was near to the one with TLD-100 while Al-doped fibre was less sensitive. The same concept was repeated for low doses of both electron and photon irradiation and the results remained similar

to the clinical dose range [18, 96].

Results obtained in a study comparing TL fading of Ge-doped optical fibre with TLD-100 (LiF) indicate that for both samples the rate of post irradiation fading is not depended to the dose, on the contrary to the storage temperature. In other word, reasonable fading of Ge-doped optical fibre dosimeter makes it suitable for transnational dose audit programs [103].

2.6 Defect centres in silica fibre

Generally, the TLD materials are predominantly insulators in which the absorbed radiation energy are caused the entire conduction electrons. Whether the material is amorphous or crystal, there is always a crystalline definition for arrangement of elements inside the materials. If this arrangement is influenced by any purposes, the crystal is defected. Basically two types of defects exist with the crystals.

Firstly, the intrinsic defects that only involve atoms of the host matrix and can be: 1) vacancies (when one atom is extracted from its place without replacement) or missing atoms (Schottky defect); 2) interstitial defect (Frankel defect) that is including an atom that is misplaced in the proper crystalline lattice; 3) substitutional defect like halide ions in alkali sites; 4) a combination of mentioned defects [104, 105].

Secondly, the extrinsic defects which is an external impurity inside the crystalline lattice either from the diffuse, or melt, or implant at a later stage. They can be: 1) substitutional impurity which is a replacement of impurity atom with an atom inside the lattice; 2) interstitial impurity that is insertion of impurity atom in an additional site not belonging to the original lattice [104, 105].

2.6.1 Types of defects in silica fibres

The defect centre in silica is usually specified in the competition of a silica network, if the lattice site is occupied in a different way than in the perfect atomic arrangement [106]. The structure of a silica unit (Figure 2.3) is tetrahedron SiO_4, with angle of 109.5° for O-Si-O bond. Because of the large spread of tetrahedral linkage angle Si-O-Si, between 120° and 180°, the long-range atomic order is lacked. At this

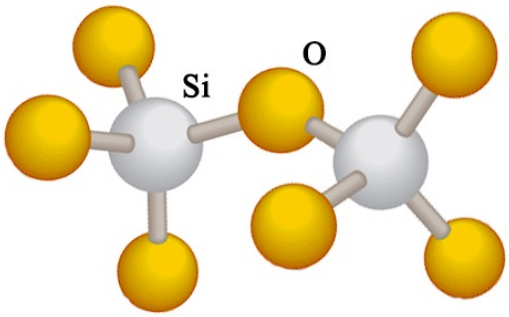

Figure 2.3: Silica molecule bounding

outline, when the array of Si-O atoms of the perfect silica lattice is decomposed by an imperfection, a point defect is presented [104, 106, 107].

All the intrinsic and extrinsic defects can be induced in the crystalline lattice by many ways. As the target of the TL material is fibre optic, it is tried to discuss more about the defects related to optical fibres. Point defects in different electronic states can cause optical transitions as absorption and luminescence which are defined as colour centre [106]. Furthermore, due to the amorphous nature of silica, defects can appear in various local rearrangements. It causes a large distribution in the transitional energy levels and as a result, a wide range of photon energy can be involved in the spectrum of luminescence and absorption [106].

There are many known defect centres for silica and optical fibres which are shown in Figure 2.4. The oxygen deficient centre (ODC), which are known as dominant intrinsic defect in a-silica[1] and its concentrations depends on processing conditions, as neutral defects in thermal oxides. During irradiation, they can capture holes and become positively charged E′-centres [105, 108]. The E′-centre is known as a paramagnetic defect observed in all forms of SiO_2 [109–111]. Creation of a combination of an E′ centre and a non-bridging oxygen hole centre (NBOHC) is another possibility from a normal Si-O-Si site. NBOHC centre can be visualized as the oxygen part of a broken bond. It is electrically neutral and paramagnetic and represents the simplest elementary oxygen-related intrinsic defect in silica [104, 105]. On top of that, the Si-H centre [112] seems to be capable of producing E′ centres. Lastly, species of the peroxy linkage (POL) and peroxy radical (POR) are recognized. POL

[1] Amorphous type of silica

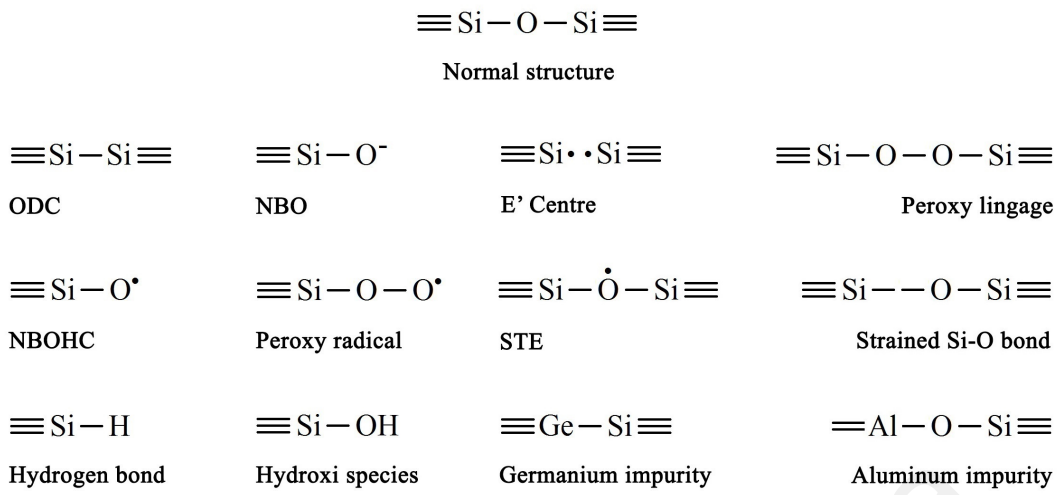

Figure 2.4: General defects associated with silica

centres are some of the excess oxygen is expected to form "wrong" oxygen-oxygen bonds in oxygen-excess silica, while, POR in silica is a paramagnetic defect with a hole delocalised over anti-bonding π-type orbitals of the O-O bond [105, 113]. Self trapped excites (STE) [25, 114] and interstitial oxygen [115] are another intrinsic defects known in silica network [116–121].

I: Drawing related defects

Drawing induced defect is raised in fibres due to the mechanical stress introduced by the pulling process. Such a stress can lead to an enhancement of the defect generation in optical fibres [122].

The analysis of the stress-induced crack growth in the delayed fracture, confirms that formation of the drawing-induced NBOHCs results from the breakage of the Si-O bond due to the tension applied to the viscous state. The formation rate of the drawing-induced NBOHCs is approximately given by the product of the tension and the temperature. It is found out that the pulling tension strongly influence the formation of the 630 nm absorption in optical fibres. Conjointly, by increasing the pulling speed, the peak height of the NBOHC is increased, while peroxy radicals are decreased [33, 123].

Although the E′ centres were not observed in low OH silica fibres [33], notwithstanding, in general, E′ centres can be produced through the evaporation of oxygen

atoms from the high OH silica lattice [34, 124]. The following changes in defects is expected by changing the pulling speed. Concentration of E′ centres is raised by increasing in the pulling speed. Then POR centres are formed via the reaction of oxygen molecules and E′ centres and its concentration is raised by decreasing the pulling speed. The concentration of POR centres is more than those in E′ centres and NBOHC which are produced via the mechanical break of Si-O bonds during the neck-down narrowing of preform to fibre. Thus, the concentration of NBOHCs decreases as pulling temperature increases and drawing speed decreases [34, 125]. The numerical analysis shows that the feeding speed is the most effective way to control dopant diffusion from the core into the cladding region [126].

Optical fibres contain more defects than bulk glass due to their rapidly cooling to room temp during pulling process. This difference is more in the fibre core-cladding interface, since it is cooled down most rapidly [127]. Residual stress has been investigated for pure silica core with fluorine doped silica clad single mode fibres. High residual stress in the core of the silica is proportional to drawing tension and it changes the refractive index and cut-off wavelength of the single-mode fibre [36, 128].

During the process of fibre fabrication due to the high temperature (above 2000 °C), high tension ($\sim$ 100 g), and rapid quenching ($\sim$ 10000 °C/s), some modifications in population and species are induced in the fibre lattice and it can affect the optical properties of silica fibre [32, 113]. However, concentration and types of the point defects in silica fibres depends on both drawing conditions and preforms that may differ in dopant content and/or amount of OH content in the silica basis. Increase in the drawing tension induces axial stress relaxation in the softened doped core but high axial tensile stress in the high viscosity doped core. Accordingly, a high concentration of oxygen deficiency centres (ODCs) and drawing induced defects can be expected in doped fibres. Most of these defects are generated in the neck down region [32, 129].

Drawing speed and temperature are controlling the change of tension, quenching rate and preform residence time in furnace. By increasing the drawing speed, tension

(shear stress) and quenching rate increase and it results in some structural defects. On the other hand, increase in drawing speed reduces the residence time of the preform in the furnace and this results in the further increase of strain stress, giving rise to more structural defects. The effect of temperature can be separated into two parts, by increasing it, the defects increase in first place however, it cause the decrease in the tension and it decrease the defects as well. So in general the effect of temperature in the formation of defect can be neglected [32].

The structure and formation of the drawing-induced centre can be changed by x-ray irradiation. The concentration of the x-ray-induced defect centres depends on the content of the pre-existing oxygen vacancies and stretched bonds. By comparing the preform and the fibre, more defects are created in the fibre rather than in the preform by x-ray irradiation. Radial distribution of residual strain becomes greater at the surface of the drawn fibre which affects the defect centres and increases them by decreasing the fibre diameter by chemical etching [130].

II: Dopant related defects

Structure and formation of radiation induced defect in doped optical fibre is studied for many dopants. Although the sensitivity of the pure silica to radiation is quite low, the radiation induced loss measured in Ge-doped fibres is about 500 times more [131]. On the basis of the electron spin resonance (ESR) results, the low-symmetry defect centres can be attributed to germanium-related defects rather than trace impurities or silicon-related defects [131]. Conjointly, it is found out that Ge lone-pair centre (=Ge··) radial distribution is different in preforms and fibres [122]. These spectroscopic properties depend on the host silica matrix [132].

The OH groups induced in the fibre as an impurity result in colour centres and increase the loss and luminescence of the optical fibre. Most of the Ge electron trapped centres (GECs) induced by gamma-irradiation at 77 K were bleached out by annealing in dry fibres, while some of the GECs changed into Ge-E′ centres in irradiated GeO_2-SiO_2 glass containing a considerable number of OH groups [133].

Temporal evolution of photo-darkening in Yb-doped fibre was shown that the

colour centres represent deep trap states. The behaviour of the Yb-doped fibre at total environmental doses over 2-5 of years in low-Earth orbit represent the relative radiation hardness of Yb-based silica fibres [134].

III: Other related defects

Rare-earth materials exhibit a variety of point defects in optical fibres and due to the self-irradiation or charge imbalance, they play an important role in luminescence properties of fibres [135]. Besides, germanium is one of the most common dopant which cause the material base defects inside the fibres, however, it is shown that in Ge-doped fibres there is no evident of Ge diffusion at the core [136]. In another research, diffusion of both Ge and Si is observed at low drawing speed (below 10 m/min) and high temperature of about 2100 °C. Most of the diffusion is occurred in the neck-down region as it is simulated and the most effective parameters found out to be drawing temperature and feeding rate, but, the diameter of preform had no magnificent effect on the diffusion [137, 138].

Apart from defects that induced by material and fabrication process, ionising radiation produces further defects in materials. It may cause permanent damage to the defect centres and impurities by changing their charge states [139]. These defects are called colour centres, which are absorption centres. As a result of ionising radiation, an electron is free to wonder in the matrix and it can be attracted by a Coulomb force to the localised positive charge and can be trapped in the vacancy. Similarly, a positive ion vacancy represents a hole trap. Furthermore, the knowledge of the TL phenomenon can be improved by study these centres using various luminescence techniques [53, 54, 140].

When optical fibres undergo radiation, few effect is expected: 1) Absorption loss in optical fibres increase. The additional loss are caused by the mechanism of colour centre. 2) Changes in refractive index of optical fibres. 3) Development of optical fibre luminescence which is usually considered to be fluorescence. It is theoretically possible that energetic gamma displace the atoms; but, has a very low possibility and can be ignored in first approximation [141–144].

2.6.2 Defects characterisation

The identification and characterisation of the defect centres form an essential step in understanding the mechanism of TL. The defect centres created by ionising radiations are usually responsible for TL in the TL material [145]. So it is important to get information about the defect inside the TL material. There are some diagnostics experiments to find the defects inside the materials. Among them, photo luminescence (PL), Raman spectroscopy, x-ray photoelectron spectroscopy (XPS), electron spin resonance (ESR), x-ray diffraction (XRD), x-ray luminescence (XRF) and cathodoluminescence can be named. It should be noted that due to the unavailability and inaccessibility of proper microscopic devices, the defect diagnostics of the fibre samples used in this study are not considered experimentally. Instead, theoretical modelling by using computational glow curve deconvolution method is used to address the related associated defects in the fibre samples.

2.7 Glow curve and defect

Modelling of thermoluminescence is started by simple models including separation of recombination centres and trapping and highly localised defect centres. Data attained from spectra of TL emission indicate the direct interactions of ions by coupling between the recombination and trapping sites [146]. The spectrum exploration of TL emission, which is known as glow curve analysis is widely used for dosimetric studies [147].

2.7.1 Introduction to glow curve and glow peak

The plot of TL intensity as a function of temperature or alternatively time during the read out is called "glow curve". Trapping level in the TL material leads to an associated glow peak. Therefore, a glow curve can be shaped by many glow peaks that associated to different trap centres in which they might or might not be determined in the glow curve.

$$I = -c\frac{dn}{dt} \tag{2.7}$$

that shows the simple relationship between TL intensity and detrapping rate;

$$n(t) - n_{\infty} = \int_{t}^{\infty} I.dt' \tag{2.8}$$

If $N_{\infty} = 0$ means that dealing with only one peak; therefore,

$$n(t) = \int_{t}^{\infty} I.dt' \implies n(T) = \frac{1}{\beta}\int_{T}^{\infty} I(T').dT' \tag{2.9}$$

where assumed that heating rate is linear. Practically, it is possible to evaluate $n(T)$ from the area under the peak from initial rise region of the peak, T_i, to a temperature at the end of the peak T_f.

$$n = \int_{t_i}^{t_f} I dt' = \frac{1}{\beta}\int_{T_i}^{T_f} I dT' \tag{2.10}$$

Hence, the concentration of trapped charge, n, is proportional to the absorbed dose to the TL sample, the concept stated by Equation 2.10 is important in radiation dosimetry [54].

2.7.2 Zero dose glow

One of the most important parameter should be considered in all dosimetry procedures is "zero dose level" read out of TL dosimeters. Zero dose readout is caused by the additive doses arising from other sources than irradiation processes.

By deconvolution of the glow curve before and after the zero dose subtracting, it was found that readout of zero doses usually accompanied by changes in glow curves quantitatively (i.e. area under the curve increases), and qualitatively (relative changes in glow curve peaks intensities and their maxima positions). Although in many cases Zero dose can be neglected, even so, readouts of this parameter should be performed for enhancements arise in TL glow curves and thus better performance [148].

2.7.3 Peak parameters related to TL

Activation energy or trap depth, E_a, assigned to a metastable state inside the impermissible band gap between the VB and the CB of a crystal. The metastable level can be an electron trap near to the CB, or a hole trap near the VB, or a luminescence centre somewhere in the middle of the band gap and originated from defects of the crystal structure. If E_a is greater than several kT, where k is the Boltzmann's constant and T is absolute temperature, then the trapped charge can remain in the trap for a long period. Then by heating the irradiated solid with heating rate of β, trapped charges can be released from traps by quantity of thermal energy which leads to the relationship between activation energy and applied temperature Equation 2.11.

$$\frac{\beta.E_a}{k.T_M^2} = s.e^{\frac{-E_a}{kT_M}} \tag{2.11}$$

It is observed that T_M increases as E_a increases. Actually, for $E_a \gg kT_M$, T_M increases almost linearly with E_a [54, 149].

There are few methods to calculate the activation energy. Among them, the three methods of '*initial rise*', '*double H.R*', and '*May-Partridge area*' are more interesting. The initial rise method is related to the tangent calculation technique and it has a strong dependency on the plot shape of glow peak. Therefore it is important to find the accurate glow peak. An eventual limitation of the initial rise method is given by the risk to underestimate the actual E value in comparison with the other computational methods and that may be caused by non-radiative phenomena that lead to a computation of a different energy from the real one by an amount W which is related to non-radiative traps. Efficiency decline during the temperature rise is called thermal quenching. Hence, an alternative expression for the initial rise part of TL intensity is suggested as:

$$I = s.n\ e^{-\frac{E-W}{kT}} \tag{2.12}$$

where the $E_{initial-rise}$ will be smaller than E by an amount W. The thermal quenching is experimentally demonstrated by the luminescence emission during irradiation

at different temperatures [150].

The frequency factor, s, is known as the *attempt to escape* frequency and is expressed as

$$s = \nu.\kappa.e^{\frac{\Delta S}{k}} \tag{2.13}$$

where ν is the number of times that an electron interacts with the crystal network per second, κ is the transition probability, ΔS is the changes in entropy associated with the transition from a trap to the delocalised band, and k is the Boltzmann constant [54]. Maximum value of s is expected to be similar to the lattice vibrational frequency (Debye frequency). Nevertheless, according to Equation 2.11, frequency factor expression can be written as:

$$s = \frac{\beta.E_a}{k.T_M^2}.e^{\frac{E_a}{kT_M}} \quad Hz. \tag{2.14}$$

Finding the order kinetics (b) of the traps in a TL material may lead us to more accurate estimation of the glow peaks and therefore a better evaluation of activation energy and frequency factor. In spite of any order other than first and second order lead to excessive calculations to find the other kinetic parameters.

2.7.4 Computerized glow curve deconvolution

The computerized glow curve deconvolution (CGCD) analysis has been widely applied since 1980 to resolve a complex thermoluminescent glow curve into individual peak components. The trap centres parameters can be evaluated once the components of glow peaks is determined. The problem in this computation is the numerous parameters that need to be consider during the deconvolution:

$$I = I(T, E, s, n_0) \tag{2.15}$$

The two parameters of s and n_0 are unknown and have to be transformed to substitution parameters which are easier to estimate. Therefore:

$$I(T, E, s, n_0) \implies I(T, E, T_M, I_M) \tag{2.16}$$

T_M and I_M are the temperature and TL intensity at the glow peak maximum. The advantage of the transformed equation is the two free parameters (I_M and T_M) that can be directly found from the experimental glow curve [54, 151].

2.7.4.1 Order Kinetics and Methods for Deconvolution

The transformation of glow peak equation can be done by the different order kinetics expressions [152]. The TL intensity of a glow peak following a first order process is given by:

$$I(T) = sn_0 e^{\frac{-E}{kT}} exp\Big(\frac{s}{\beta}\int_{T_0}^{T} e^{\frac{-E}{kT'}} dT'\Big); \tag{2.17}$$

By using the condition of maximum and after some algebra and approximations:

$$I(T) = I_M\ exp\Bigg(1 + \frac{E}{kT}.\frac{T - T_M}{T_M} - \frac{T^2}{T_M^2}.\Big(1 - \frac{2kT_M}{E}\Big) \\ exp\Big(\frac{E}{kT}.\frac{T - T_M}{T_M}\Big) - \frac{2kT_M}{E}\Bigg). \tag{2.18}$$

From this equation s can be found by applying the following boundary condition:

$$T = T_M \Rightarrow \frac{dI}{dT} = 0 \ \longmapsto\ s = \frac{\beta.E}{kT_M^2}.e^{\frac{E}{kT_M}}. \tag{2.19}$$

Hence, for a constant heating rate T_M shifts toward higher temperatures as s decreases or E increases; and for a constant values for E and s (in a single trap), T_M shifts to higher temperatures as heating rate increases. Another important remark of this relation is that T_M is independent of n_0. The important property of a first order peak namely that its shape does not vary with the n_0 and that at each point along the curve the TL intensity is proportional to n_0, cannot be automatically used in the reverse direction. If a TL peak exhibits a linear dependence of the maximum intensity of the dose with no appreciable shift of the maximum temperature with the dose, it cannot be taken as conclusive evidence that the kinetics are strictly of first order [153].

The second order kinetic equation is expressed by:

$$I(T) = sn_0 e^{\frac{-E}{kT}} exp\Big(1 + \frac{s}{\beta}\int_{T_0}^{T} e^{\frac{-E}{kT'}} dT'\Big)^{-2}, \tag{2.20}$$

with boundary condition at the maximum intensity of:

$$s = \frac{1}{1 + \frac{2kT_M}{E}} . \frac{\beta . E}{kT_M^2} e^{\frac{E}{kT_M}} . \tag{2.21}$$

the expression after some algebra and approximations forms to:

$$\begin{aligned} I(T) = 4I_M exp\Big(\frac{E}{kT} . \frac{T - T_M}{T_M}\Big) \times \\ \Big(\frac{T^2}{T_M^2}\Big(1 - \frac{2kT}{E}\Big) exp\Big(\frac{E}{kT} . \frac{T - T_M}{T_M}\Big) + 1 + \frac{2kT_M}{E}\Big)^2 . \end{aligned} \tag{2.22}$$

The shape of the TL glow curve for second order kinetics depends in part on the level of irradiation of the material before the measurement of the TL glow curve [154]. A developed general order kinetics model is used by Shah et.al. for glow curve deconvolution [155]. The model expression with assumption of linear heating rate is:

$$I(T) = \frac{n_0 s'' e^{-\frac{E}{kT}}}{\Big(1 + \big(\frac{(b-1)s''}{\beta}\int_{T_0}^{T} e^{-\frac{E}{kT'}} dT'\Big)^{b/(b-1)}} \tag{2.23}$$

Some modifications have been done on these models to improve the fitting values [155–158]. In these works, the order of kinetics is modified with the heating rate, annealing or other experimental values to be able to explain the different systems. In this way some softwares are developed to ease the deconvolution of TL glow curves [159, 160]. Merely, most of them are working with the first order kinetics model. The quality of fitting is usually reported by a parameter called figure of merit (FOM) in percentage.

2.7.4.2 Glow peaks analysis

Information about the behaviour of traps in a luminescent material is usually derived by fitting the glow curves in the thermoluminescence spectrum of the material to a general formula. From the fit one seeks to obtain values for the depth of the traps, the frequency factors governing the release of electrons from the traps, and some indication of the rates of trapping and retrapping [151, 154, 161, 162].

In some cases, silica based phosphors was analysed with their glow peaks. The difference in the method of doping shows magnificent changes in the main shape of glow curve and subsequently in the position and intensity of the glow peaks and even in their number [82]. In other studies the trapping parameters of silica in the crystalline form is studied and the related glow peaks are found out [163].

The fading properties of TL material can be demonstrated by analysis of the glow peaks [164]. Decrease and increase in the intensity of the glow peaks as well as the vanishing of the thermal traps during the fading can be observed.

The increase in lifetime has important implications in long range TL dating. The lifetime of trapped electrons relevant to TL glow peaks is studied using different order kinetics [165]. Generally, lifetime of trapped electrons corresponding to TL peak obeying non-first order kinetics. The lifetime of trapped electrons in an insulating material exhibiting thermoluminescence is closely related to activation energy and frequency factor.

2.8 summary

In the chapter, the theoretical overview of radiation, thermoluminescence, defects and glow curves were studied based on the research of this thesis.

The researches about radiation dosimetry and fibre thermoluminescence dosimeters are growing fast. The variety of radiation sources with different energies and dose caused to use assorted dosimeters to detect the radiation doses, however, attempt to find a unique dosimeter for almost all of the radiation area is not a far goal to achieve with optical fibre dosimeters. Low fading, high sensitivity, high saturating and many other factors along with the low price make this concept more

feasible.

In this thesis, it has been tried to do a multilateral investigation on the optical fibres as well as developing the new fibre architectures for increasing the TL sensitivity and reduce the threshold of TL saturation.

CHAPTER 3: METHODS AND MATERIALS

This chapter presents the experimental procedures and methods applied to achieve the objectives of the present study. The fibre development and fabrication for both undoped and doped fibres are presented in this chapter, followed by the sample preparation, irradiation, and description of other characterisation and measurements.

3.1 General approach

3.1.1 Preparation of fibre samples

The fibre TLD samples used in this study are made of doped and undoped optical fibres. The process is of preform doping, fibre pulling and fibre preparation are the first steps to prepare the fibre TLD samples, which are explained here.

3.1.1.1 Doped fibre preform fabrication

Optical fibres are made of silica with some additional elements as the dopant to change in refractive index of core from cladding. To make doped fibres, so called modified chemical vapour deposition (MCVD) process is applied in the ultra pure silica preform, Suprasil F300 glass tube. Germanium is the primary dopant for increasing the refractive index of silica to form a guiding structure.

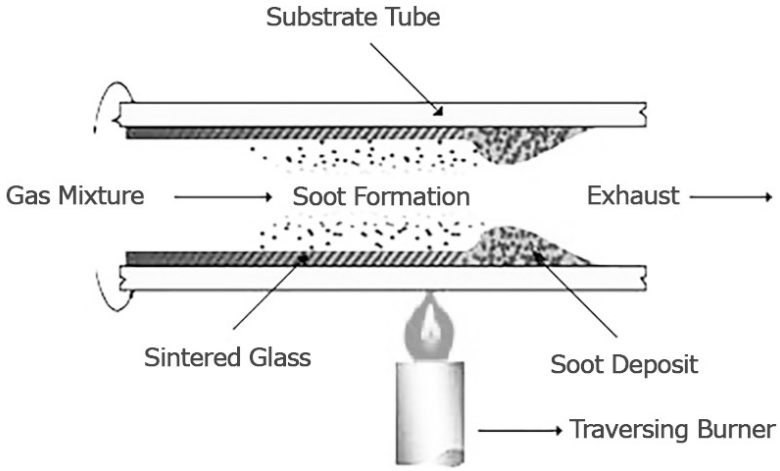

Figure 3.1: Schematic of MCVD process [166].

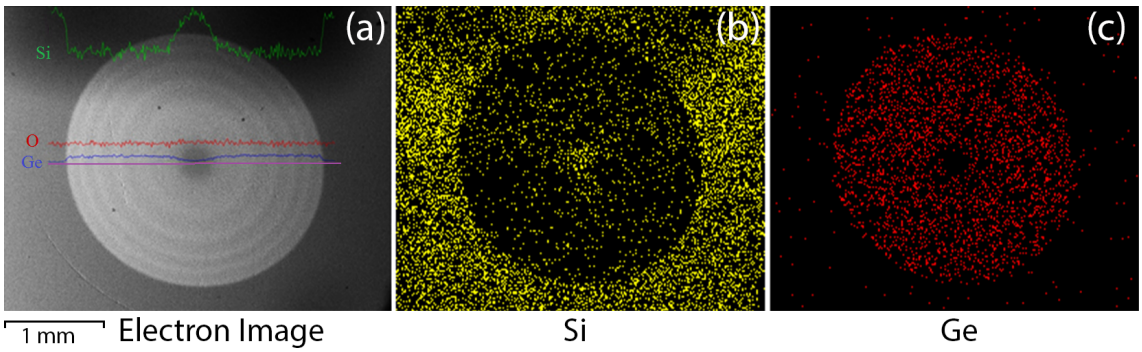

Figure 3.2: Ge-doped preform; (a) SEM images,(b and c) EDX image with material concentration at the core.

In this method, the reactants in the process are usually $GeCl_4$, $SiCl_4$, and O_2, often along with $POCl_3$, flowing in a silica support tube heated from the outside with an oxy-hydrogen flame. According to Figure 3.1, the oxide reaction products, which are formed in hot zone deposit as small particles downstream on the walls of the tube, and are consolidated into clear glass layers as the hot zone is traversed in the direction of flow [167].

The main preform used in this thesis was Ge-doped with different concentration of germanium at the core. Figure 3.2 shows the scanning electron microscope (SEM) and x-ray energy dispersive (EDX) images with the concentration of Ge versus Si at the core of a Ge-doped fibre. Material line-scan is attached on the SEM image.

3.1.1.2 Fibre fabrication

There after preparation of fibre preform, it is installed on the fibre pulling tower. The preform is fed toward the furnace and heat up to 2100 °C to get a drop. Then the tail of the drop is pulled with higher speed using tractor (for large diameter fibres) or capstan (narrow fibre smaller than 350 μm in diameter) and it caused the formation fibre from preform (Figure 3.3).

For puling the fibre with shapes of capillary or cylindrical, the pulling is straight forward from hollow tube or collapsed preform subsequently to the final fibre. It is only needed to calculate the speed of feeding and pulling according to the direct relation of surface area with speed (Equation (3.1)).

$$A_{feeding} \times v_{feeding} = A_{pulling} \times v_{pulling}, \tag{3.1}$$

in which, $A_{feeding}$ is the initial area of preform that enters the furnace with the speed of $v_{feeding}$ and $A_{pulling}$ is the final area belongs to the fibre that exit from the furnace with speed of $v_{pulling}$. This equation can be easily concluded from the conservation of mass. However, to make a flat fibre, a hollow tube preform or capillary cane is required. Then by applying vacuum from the top of the preform, and pulling from the bottom, the fibre is fabricated with flat shape. In another method, first a bigger size FF cane is pulled from the main preform and then the big size flat cane will be re-pulled to the desire flat fibre size according to Equation 3.1.

Figure 3.3: Fibre preform drop - transform of silica preform to optical fibre in fibre pulling tower.

The photonics crystal fibre (PCF) has been fabricated by using the stack-and-draw method (Figure 3.4), stacking a hexagonal shaped array (Figure 3.5) of small diameter capillaries within a greater diameter tube and then pulling the assembly into a PCF cane ($\sim$ 1 - 2 mm diameter) followed by repulling the PCF cane into the desired PCF diameter $\sim$ 125 - 250 μm.

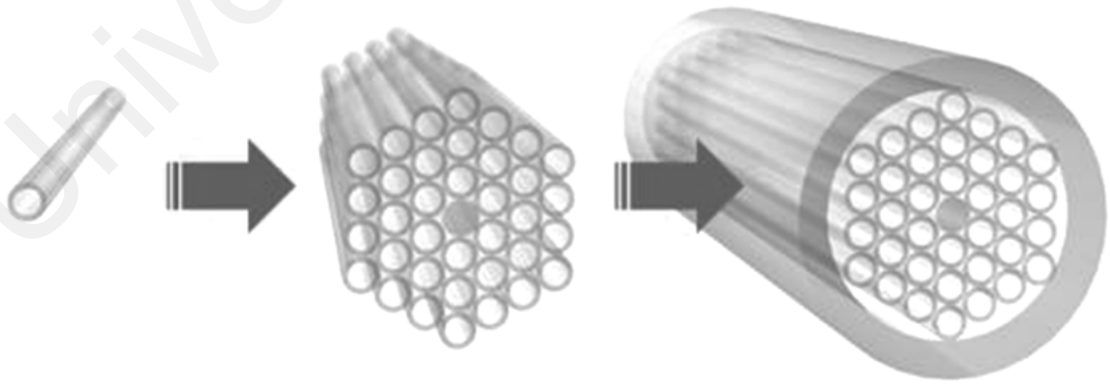

Figure 3.4: Schematic of PCF stacking.

The proper optical fibres should be cut to precise same lengths one by one. Prior to cut, the outer polymer cover to the coated fibres has been carefully removed using a chloroform solution, soaking the fibres in the solution for 30 seconds. The length

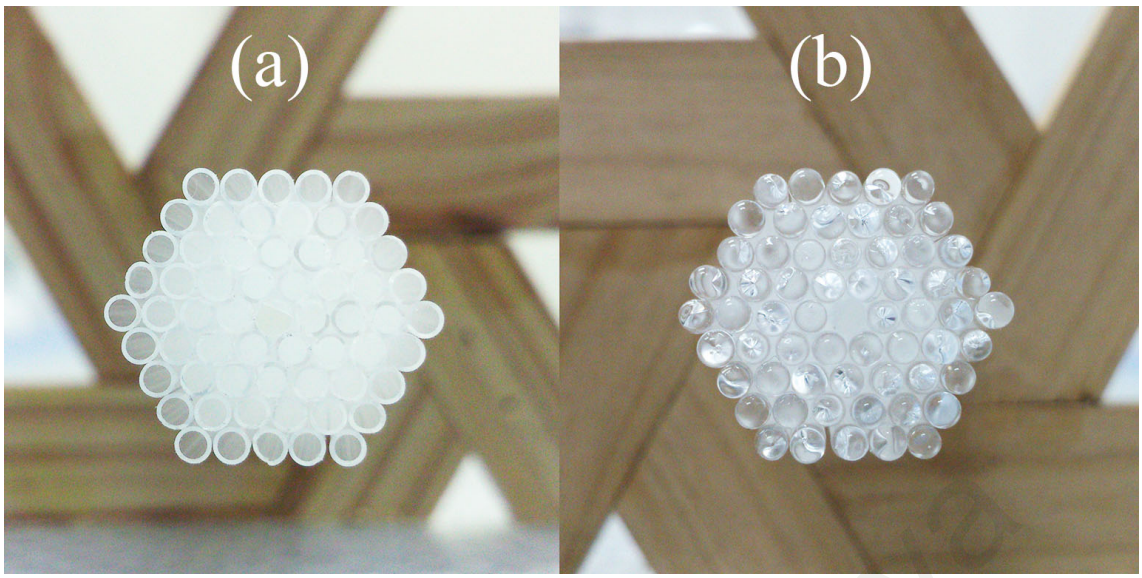

Figure 3.5: Example of a stacked PCF preform a) Open end of capillaries for pressurising b) Fused end of capillaries for avoiding the vacuum suck.

of cut fibres is limited to the planchet of TLD reader device which is 5 mm for our case. For this purpose, two methods are applied in this study. In the first method, a Sumitomo Electric FC-6S fibre cleaver (Sumitomo, Japan) is modified to cut the fibre in 5 mm for smaller diameter fibres. In the second method, pen diamond (either cone or flat tip) is used to cut larger size fibres manually.

After the samples are cut, they are weighed for normalisation. For this purpose, accurate electronic balance with 0.1 mg accuracy was used to measure the weight of fibre samples. For the samples that were too light (usually with diameters less than 350 μm such as commercial fibres), a group of 10 to 15 pieces of fibre (from the same samples) were scaled together and then the average weight is calculated. This approach is used for all measurements in this study, unless otherwise stated.

Furthermore, in some special cases, where the mass normalisation were very critical, the volume of every individual sample is measured one-by-one by using a table top electronic microscope with accuracy of 10 μm as shown in Figure 3.6. This is highlighted throughout the results chapters, whenever this method of normalisation is performed.

The fibre drawing parameters used in this study are $\sim$ 35 $\pm$ 10 g for tension, low drawing speed of $\sim$ 1 - 2 m/min, and furnace temperature of $\sim$ 2000 $\pm$ 50 °C.

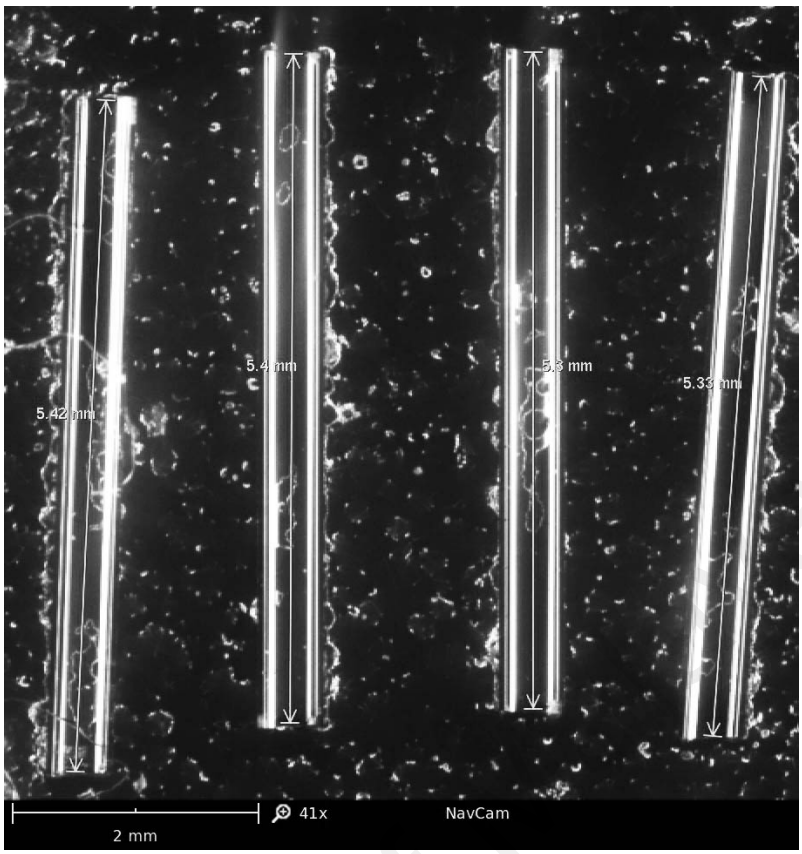

Figure 3.6: Length measurement using microscope measurement facility.

Since the drawing parameters are relatively fixed, the influence of drawing effect on performance of TL response of optical fibre is expected to be negligible. This is proven by studying the effect of drawing tension from 25 g to 100 g on TL response of a home-made-fibre as shown in Figure 3.7. As the temperature were keep constant during the fibre pulling, the one that can be considered as the main parameter was the tension. However, as it is shown in Figure 3.7, no significant effect is been found by pulling a uniform Ge-doped silica fibre in six different tensions. Since the tension cannot be measured for large scale fibres, the experiment is done for one middle size fibre with 240 μm diameter.

3.1.2 Irradiation

Before the fibre samples undergo for irradiation, for standardizing the thermal history within the fibres and removing any residual TL signal, they were placed in ceramic plates and annealed at 400 °C for a duration of one hour using electric oven. There after annealing, the samples left to cool at room temperature. How-

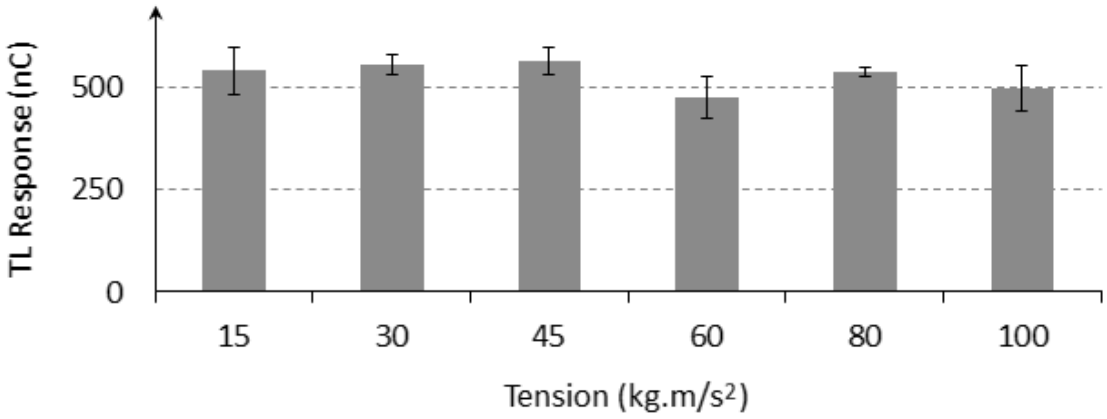

Figure 3.7: Effect of tension in the thermoluminescence activity of Ge-doped fibre.

ever, the annealing process for commercial TLD-100 is a bit different, in which they need to undergo heating temperature of 400 °C for an hour followed by 100 °C for two hours.

Since the objective of this study is to evaluate the performance of optical fibres with different characteristics, a fixed range of dose adopted for clinical therapy range from 0.1 to 10 Gy is used. A secondary range of applied dose (up to kGy) is considered to evaluate few fibre samples for industrial applications.

3.1.2.1 Clinical dose range

For clinical dose range, both photon and electron sources were tested. Therefore, the fibre samples were placed at the surface of a *solid water*^{TM} phantom (Gammex RMI) whose function is to provide for the standardized full-scatter condition (reference conditions) as conventionally adopted and were exposed to 6, 9 and 20 MeV electron beams, 600 cGy/minute dose rate, with accumulation doses from 0.5 to 8 Gy, delivered by a Varian Model 2100C linear accelerator (Varian Medical System, Palo Alto, USA). A field size of 20×20 cm^2, source to skin distance of 100 cm and applicator size of 20×20 cm^2 were used for all irradiations. This device is also capable of producing photon beam with energy of 6 and 10 MV. The setup for photon is almost the same as electron irradiation, with this difference that applicator is omitted. For consistency in results and fair comparison, this irradiation setup is kept for all samples in this study, unless otherwise stated.

In addition, the recorded absolute radiation dose delivered by the linac is based on adoption of the procedures detailed in the International Atomic Energy Agency Report TRS398, the output being ensured to be within ± 2% of the intended delivered dose. Measurements of dose from electron beam irradiation have been performed by the in-house medical physicists, supported by monthly quality assurance (QA) checks made using a Roos ionisation chamber IBA PPC40 with a Supermax electrometer.

3.1.2.2 High dose range

For high dose irradiation, up to 100 kGy, an electron beam source (EPS-3000) [168] and a gamma source (^{60}Co) were used. The EPS-3000 electron beam is capable to generate up to 3.0 MeV high energy electrons. It is a fast process with high efficiency, high uniformity with appropriate control. The EPS-3000 is widely used in R&D and commercial irradiation for cross-linking and polymeric materials in the form of wire insulation and heat shrinkable tubes, sterilization of cosmetic product and treatment of silicon wafers. Some specification for EPS-3000, used in this study, is mentioned in Table 3.1.

Table 3.1: EPS-3000 specification.

Accelerator Voltage (MeV)	Beam Current (mA)	Max Beam Power (kW)	Beam Width (cm)	Dose Uniformity	Conveyor Speed (m/min)
0.5 - 3.0	1 - 30	90	30, 60, 120	± 5%	1 - 20

^{60}Co is a synthetic radioactive isotope of cobalt with a half-life of 5.2714 years. It is produced artificially by neutron activation of the isotope ^{59}Co. ^{60}Co decays by beta decay to the stable isotope ^{60}Ni. The activated nickel nucleus emits two gamma rays with energies of 1.17 and 1.33 MeV, hence the overall nuclear equation of the reaction is

$$^{59}_{27}Co + n \rightarrow ^{60}_{27}Co \rightarrow ^{59}_{28}Ni + \beta + \nu_e + \gamma. \tag{3.2}$$

The β-decay energy is low and easily shielded; however the gamma-ray emission lines have energies around 1.3 MeV, and are highly penetrating. ^{60}Co is mainly applied

as a tracer for cobalt in chemical reactions and sterilization of medical equipment. Also, it is a good radiation source for medical radiotherapy, industrial radiography, leveling devices and thickness gauges, pest insect sterilization, food irradiation and laboratory mutagenesis. The activity of ^{60}Co that is used in this study was 220 kCi (Ci = Curie = 3.7×10^{10} atoms decaying per second).

3.1.3 TL measurement

After irradiation, the samples are stored for a day. This allow the thermal luminescence to be faded and reduce the noise in the glow curves [54].

The TLD reader used to measure the intensity of sample luminescence is Harshaw 3500 series with 5 mm × 5 mm planchet size, which is limiting us to prepare the fibre samples in small size of 5 mm. The acceptable spectral range of TL emission by this model is 350 - 700 nm. The time temperature profile (TTP) of the reader is set to preheat temperature of 50 °C, maximum temperature of 400 °C, applied voltage of 700 V, acquired temperature rate at 25 °C/s, post annealing of 6 s and acquisition time of 20 s. The readings were performed under nitrogen gas flow to suppress possible spurious light signals from triboluminescence and also to reduce oxidation of the heating element. Vacuum tweezers with micro needle were used to move the fibre samples. A careful attention is going to the small samples as during the movement they might be sucked by vacuum tweezers. This TL measurement setup is fixed for all samples read in this study, unless otherwise, stated.

3.1.4 Kinetic model

In this thesis, the analysis on kinetics of thermoluminescence is carried out using computerized glow curve deconvolution and the glow peaks, in most cases, are found out with the second order kinetics estimation of intensity [54]:

$$I(T) = sn_0 e^{\frac{-E}{kT}} \left(1 + \frac{s}{\beta}\int_{T_0}^{T} e^{\frac{-E}{kT'}} dT'\right)^2 \tag{3.3}$$

where s is the frequency factor of trapped electrons, n_0 is the initial concentration of traps, E is the energy of a trap in eV, T is temperature in K, β is heating rate

and k is the Boltzmann constant. However, in some cases that shape of the first order kinetics (Equation 3.4) was more efficient to fit to a glow curve or part of it (see Figure 3.8a), use of this model was mixed with the second order kinetics. The shape of peak according to the first order kinetic is shown in Figure 3.8b.

$$I(T) = sn_0 e^{\frac{-E}{kT}} \left(\frac{s}{\beta} \int_{T_0}^{T} e^{\frac{-E}{kT'}} dT' \right) \tag{3.4}$$

In general, calculations of the activation energy (E_a) of each trap and other parameters of any glow peaks, resulted of an accurate deconvolution of our glow curves. The TLAnal [169] software is employed and based on the order kinetics of each traps, then the glow peak parameters were computed.

According to the CGCD method, the initial number of glow peaks should be estimated and then the software can help to optimise the peaks in order to find the best fit for the glow curve under analysis. At the glance, it seems that several numbers and combination of peaks can be chosen to fit the curve, however, there are some limitations and concerns. The shape of the peaks, as shown in Figure 3.8, must follow the kinetic model, so not any types of continuum can be added for deconvolution. Furthermore, by increasing the number of peaks, which are following the proposed kinetic model, just some low intensity peaks will be appeared such all satellite peaks. Erasing these satellite peaks can be explained as when the irradiated samples getting post anneal prior to readout, most of the low intensity peaks (related to weak defects) will be eliminated. It is good to keep in mind that there are some limitation in the range of kinetic parameters that should be applied during the deconvolution which raise the ultimate limitation in choosing the number of peaks. The acceptable numbers of glow peaks can be found after some trial and error after the initial estimation.

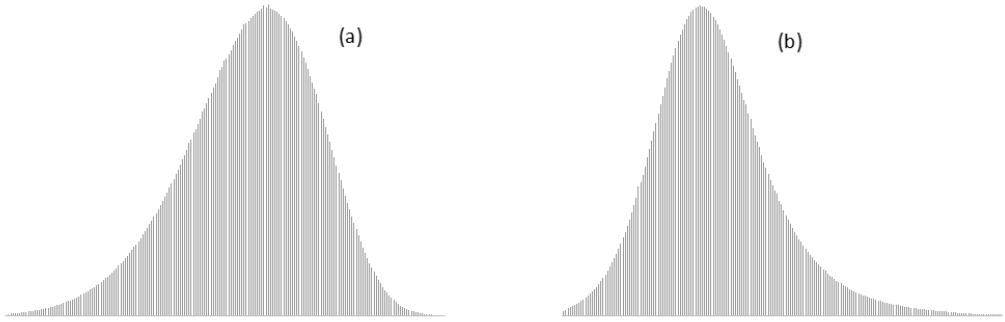

Figure 3.8: Typical glow peak generated by TLAnal for a: first order and b: second order kinetics.

3.2 Characterization of Samples

In the following subsections, the general characterizations, in terms of physical and elemental parameters/analysis, of every optical fibre sample used in this study are presented in detail. Then, the detailed dosimetric properties and performance of each fibre are presented in next chapters (Chapters 4-7).

3.2.1 Single mode fibres

Two commercially available SMFs fabricated by two different manufacturers are characterised in this study to understand their behaviour and performance similarity/differences in respect to dosimeter application. The general characteristics in terms of physical and elemental parameters of these fibres are presented in this chapter, while the detailed dosimeter performance and characteristics compared to TLD-100 is shown in result chapter. Both SMFs have similar core and cladding diameters of about 8.5 μm and 125 μm, respectively. EDX analysis was used for elemental measurement. For each SMF type, five sets of EDX measurement were done by using different samples of the same fibre type. For each fibre sample, 6-10 region-of-interests (ROIs) are selected within the fibre core area. Table 3.2 shows the results of average compositional analysis over all ROIs per fibre sample for SMF-1 and -2. On average, SMF-1 and -2 indicate the presence of Ge at about 4.9 and 4.3 weight%, respectively. Details of the Ge concentration variability per ROI for the five samples are presented in Figures 3.9(a) and (b) for SMF-1 and -2, respectively. Over and above the overall average value presented in Table 3.2, it is noted that the

Table 3.2: EDX analysis of SMF-1 and SMF-2.

	SMF-1						SMF-2					
	Weight (%)			Atomic (%)			Weight (%)			Atomic (%)		
	O	Si	Ge	O	Si	Ge	O	Si	Ge	O	Si	Ge
Sample 1	69.6	25.5	4.9	81.7	17.0	1.3	70.2	25.2	4.7	82.0	16.8	1.2
Sample 2	69.6	25.5	4.8	81.7	17.1	1.3	66.0	30.1	3.9	78.6	20.4	1.0
Sample 3	72.0	22.7	5.4	83.6	15.0	1.4	66.2	28.9	5.0	79.1	19.6	1.3
Sample 4	52.8	42.7	4.6	67.6	31.2	1.3	50.6	45.5	3.9	79.1	19.6	1.3
Sample 5	53.1	42.3	4.8	67.7	30.9	1.4	51.8	44.1	4.1	65.4	33.5	1.1
Average	63.4	31.7	4.9	76.5	22.2	1.3	60.9	34.7	4.3	76.8	22.0	1.2
STD	9.6	9.9	0.3	8.1	8.1	0.1	9.1	9.4	0.5	6.5	6.6	0.1

majority of Ge concentrations in SMF-1 are found to be greater than that in SMF-2. As an instance, 22 out of the 50 readings made in SMF-1 showed a concentration greater than 5 weight% compared to 9 out of 42 readings in SMF-2. In regard to concentrations of ~ 4 weight%, there are 19 over 42 readings for SMF-2 and 12 over 50 readings for SMF-1. This suggests that the concentration of Ge in SMF-1 and -2 can best be characterised as ~ 5 and 4 weight% respectively. Figures 3.9(c) to (e) illustrate the result of Si, O, and Ge concentrations across the fibre core surface, respectively, obtained as averages of line scanning over the cross-sections of fibre Samples 4 and 5 under EDX inspection. Results in Table 3.2 and Figure 3.9 are in agreement that Ge and O concentrations in the SMF-1 core area are greater than that in the SMF-2 core area, while Si is greater in SMF-2. It should be noted that the EDX analysis over fibre cladding is also performed. However, almost similar Si and O concentrations are observed for both fibre samples in the absence of detecting any other elements. Figures 3.9(f) and (g) show SMF-1 and -2's cross sections obtained by SEM imaging.

After the exposures (details were discussed in section 3.1.2), the optical fibre TL yield was read out using TL reader. All TL responses were then normalised to the mass of the sample. In this study, mean masses of 0.132 mg for SMF-1 and 0.136 mg for SMF-2 were used to normalise the TL yield for individual fibre samples.

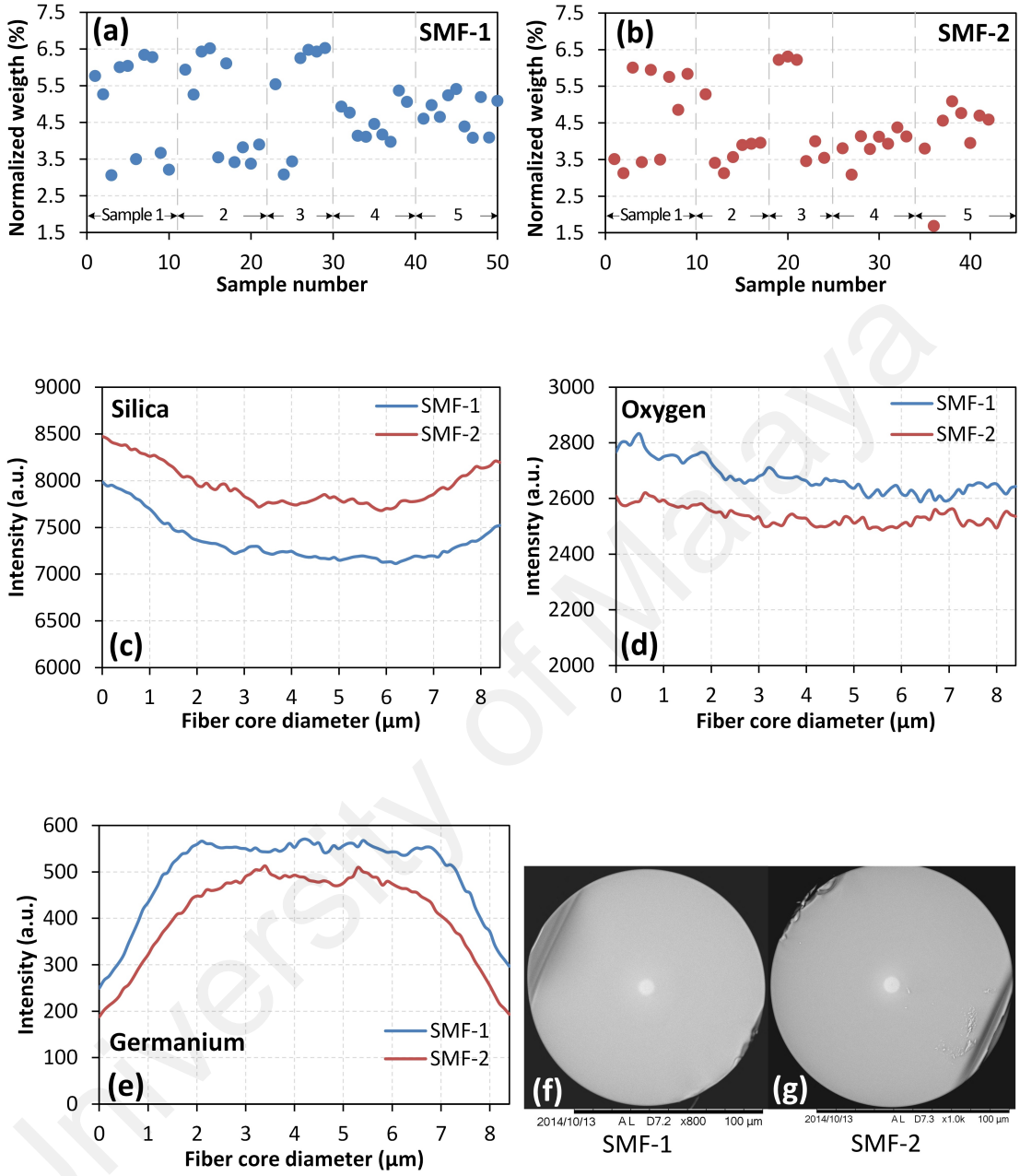

Figure 3.9: Chemical element concentration distribution across the fibre core cross section, obtained using EDX. (a) and (b) Normalized weight (%) Ge concentration for 50 and 42 ROIs measured within fibre core area of five different fibre samples for SMF-1 and -2, respectively. The result of ROIs per fibre sample are identified in (a) and (b). (c), (d), and (e) showing silica, oxygen, and germanium intensity concentration, respectively, measured by line scanning across fibre core area (averaged from fibre Samples 4 and 5 in Table 3.2). (f) and (g) show cross section area of SMF-1 and -2 taken by SEM imaging.

3.2.2 Other doped fibres

The second groups of samples are standard circular cross-section optical fibre of 125 μm outer diameter. The 9 μm central core that forms the dopant channel has been confirmed using the EDX facility of an SEM, doped-core and silica cladding mappings being obtained for all but one of the samples (Figure 3.10). For fibres that contain Al as a co-dopant, i.e. Al:Tm and Al:Y:Tm, EDX mapping of the core represents a severe challenge, due to the neighbouring atomic numbers of Al (Z = 13) and Si (Z = 14), providing for limited differential x-ray fluorescence production, further confounded by the associated low energy emissions (Figure 3.10b). The doped elements are compared with SiO_2, BaF, GaP, Al_2O_3, TmF_3 as a reference for EDX identification. The characteristic peaks through which the dopant materials are detected are $K_{\alpha 1}$ for O, Si, Al, Y, Ba and Ga and $L_{\alpha,\ \beta}$ for Tm. Table 3.3 shows the concentration of each element present in the different samples.

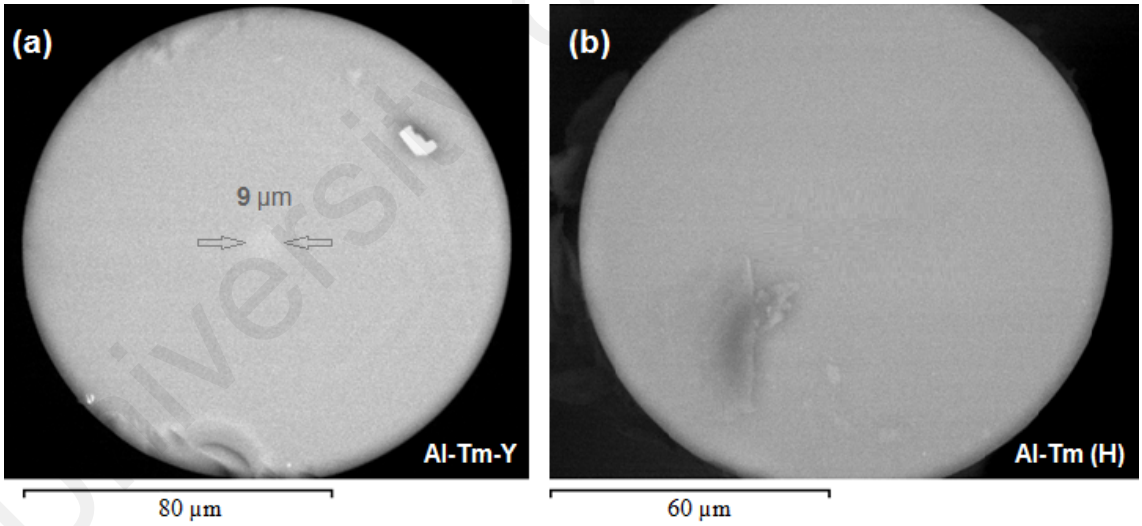

Figure 3.10: SEM-EDX fibre cross-section mappings of (a) Al:Tm:Y and (b) high-Al:Tm doped silica fibre.

3.2.3 Different fibre types

These different types of undoped optical fibre have been fabricated for this study (Figure 3.11), made using the same undoped preform. The undoped fibres include capillary optical fibre, flat fibre, and photonic crystal fibre (PCF) are shown in

Table 3.3: EDX results for the different doped fibre samples. In this table the weight percentage of each material is shown.

Element	Al-Y-Tm	Ba	Al-Tm (H)	Al-Tm (L)	Ga
O	52.66	51.13	54.52	55.09	52.79
Si	46.42	43.27	40.11	41.02	41.81
Ba	-	5.60	-	-	-
Ga	-	-	-	-	5.40
Tm	0.25	-	0.24	0.18	-
Al	0.54	-	5.13	3.71	-
Y	0.13	-	-	-	-

Figure 3.11a to 3.11c, respectively. The images were took using Phenon table-top electronic microscope. These fibres are made from a pure silica glass tube termed HXWG (Heraeus Holding GmbH, Hanau, Germany), with outer and inner diameter of 25 mm and 19 mm, respectively.

The capillary form has been fabricated at a temperature of 2000 °C by pulling a 25 mm diameter silica glass tube into a fibre of diameter $\sim$ 200 μm. The flat fibres have been fabricated in a similar way, the one difference being the use of a vacuum pressure of $\sim$ 10 kPa applied from the top of the glass tube in order to collapse the tube into a flat shape, the faces of the internal walls are coming into contact with each other. The undoped flat fibre used in this study have cross-sectional dimensions of 300 μm $\times$ 70 μm. The specification of the PCF used in this study was explained earlier in this chapter.

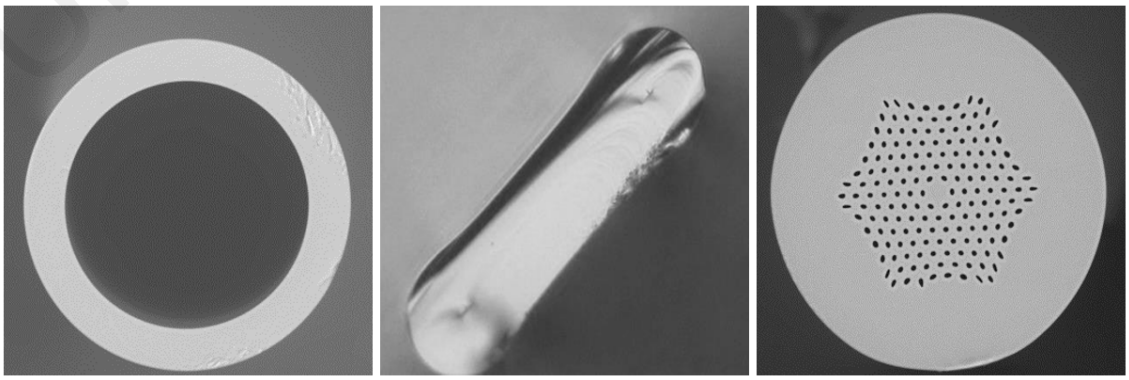

Figure 3.11: Optical fibre images: (a) undoped capillary fibre; (b) undoped flat fibre; (c) undoped PCF.

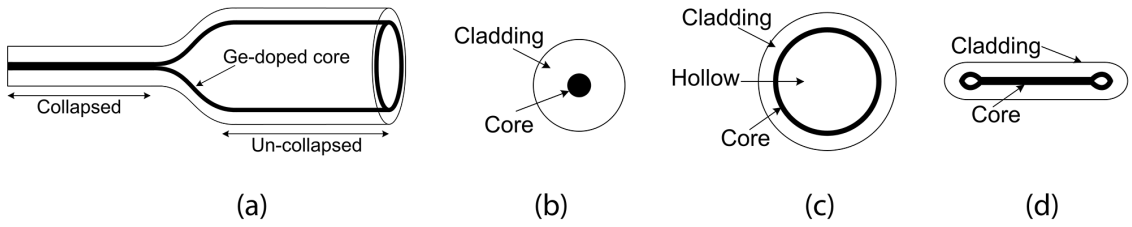

Figure 3.12: (a) Original Ge-doped preform, (b) Cylindrical fibre, (c) Capillary fibre, and (d) Flat fibre.

A Ge-doped core preform has been fabricated using the MCVD process, with ultra-pure fused silica Suprasil F300 glass tube as the substrate. During the MCVD process one part of the preform has been made to collapse for allowing the fabrication of conventional optical fibre, while the other part has been left hollow as shown in Figure 3.12a. The preform has then been pulled into conventional optical fibre (hereafter referred to as cylindrical fibre) with 125 μm diameter using the collapsed part (Figure 3.12b). The hollow part of the preform has been used to fabricate capillary optical fibre of 125 μm outer diameter and flat fibre with cross section of 60 μm $\times$ 180 μm as shown in Figure 3.12c and 3.12d, respectively. The flat fibre has been fabricated by applying vacuum pressure from the top of the hollow preform during the drawing process [170]. Note is made that the capillary fibre in this study is fabricated from the boundary between the collapsed and uncollapsed region of the preform, which leads to smaller hole-to-outer diameter in the capillary compared to the uncollapsed part of the preform.

The elemental measurement is pursued using EDX analysis. Table 3.4 shows the involvement of materials and their concentration in the core of each types of fibre used in this study. According to the EDX measurement, an average of 7.8%, 7.5%, and 7.4% of weight is germanium in the cylindrical, capillary and flat fibre, respec-

Table 3.4: EDX results for concentration of Ge, Si and O in the core.

	Cylindrical		Capillary		Flat	
Element	Weight (%)	Atomic (%)	Weight (%)	Atomic (%)	Weight (%)	Atomic (%)
O	53.6 $\pm$ 0.43	69.3 $\pm$ 0.40	47.1 $\pm$ 0.61	63.1 $\pm$ 0.51	74.1 $\pm$ 0.15	85.9 $\pm$ 0.12
Si	38.6 $\pm$ 0.81	28.4 $\pm$ 0.54	45.4 $\pm$ 0.92	34.7 $\pm$ 0.61	18.5 $\pm$ 0.29	12.2 $\pm$ 0.18
Ge	7.8 $\pm$ 0.81	2.2 $\pm$ 0.24	7.5 $\pm$ 1.07	2.2 $\pm$ 0.33	7.4 $\pm$ 0.31	1.9 $\pm$ 0.08

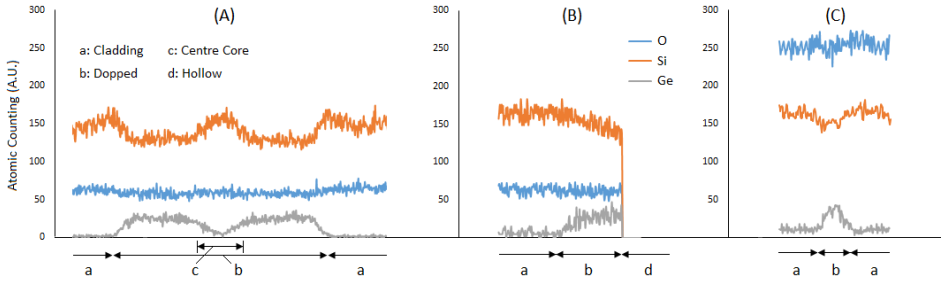

Figure 3.13: EDX elemental line scan for (A) cylindrical, (B) capillary, and (C) flat fibre at the doped core.

tively, which is averaged from four different fibre sample measurements. Figure 3.13 shows the result of material concentration across the surface for each type of fibres obtained by EDX material line scanning over fibre core cross section.

3.2.4 Different fibre sizes

Two sets of optical fibres, one cylindrical fibre and the other one flat fibre, each in five different cross-sectional surface sizes is tested to find the effect of surface size in optical fibre TLDs. Figures 3.14 and 3.15 illustrates the surface of 5 different cylindrical and flat fibres consequently.

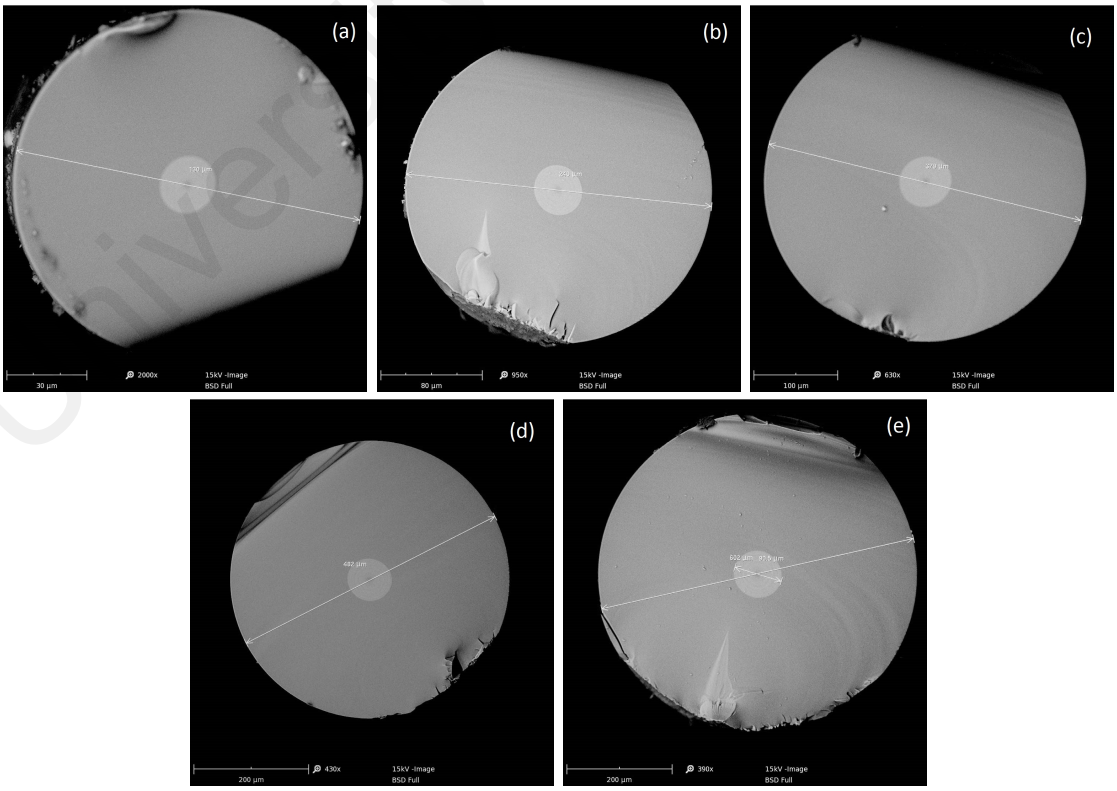

Figure 3.14: SEM images of cylindrical fibres in 5 sizes. From a to e, diameters increases from about 120 μm upto 600 μm.

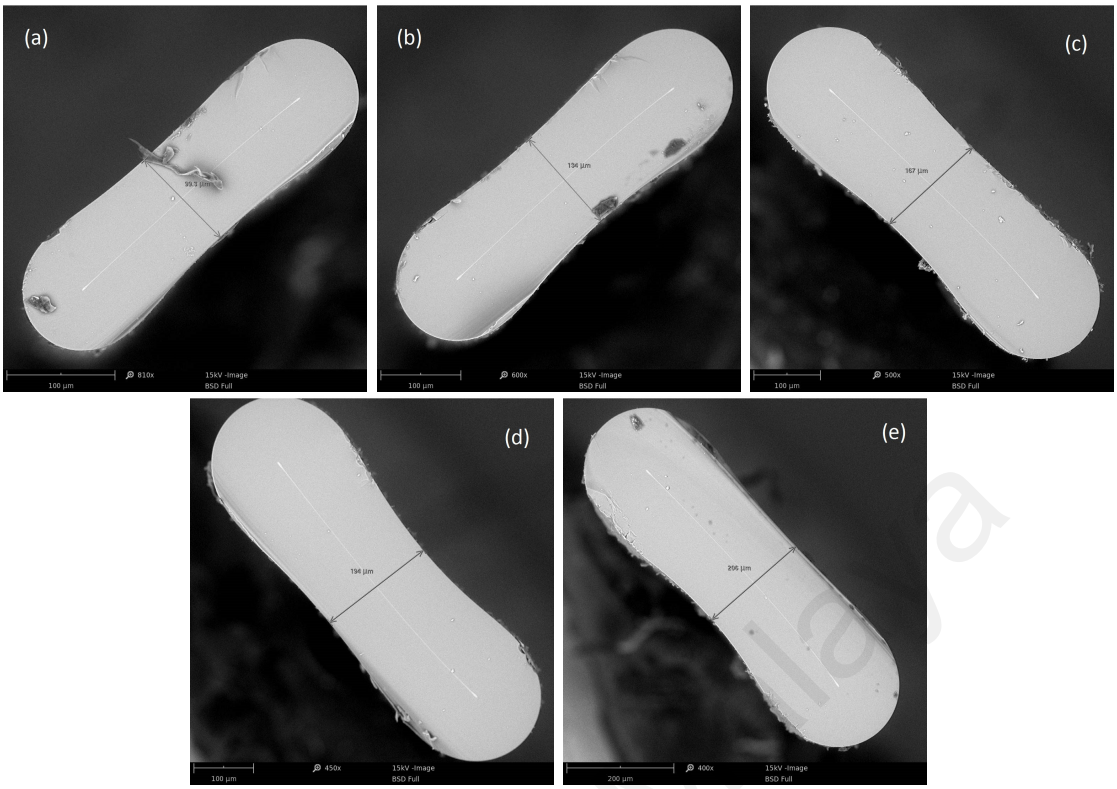

Figure 3.15: SEM images of flat fibres in five sizes. From a to e, their thickness is increased from about 100 μm up to 200 μm.

In this study HF acid were used to etch the outer surface of doped fibres (cladding) for investigating the influence of core and cladding on the TL response separately. To have a uniform etching, samples were rotated smoothly during the etching process.

3.2.5 Fibres with various Ge concentration

The Ge-doped fibre parameters used in this study are gathered in Table 3.5. Since all the core size of each fibre was different, the relation between the core area in comparison with the cladding area is calculated using SEM imaging measurement facility (Table 3.5 last column) and the TL response of each samples were divided to this proportion to make the different samples comparable to each other. This concept comes from the fact that almost all the TL is generated from the doped area (core) and cladding has the least effect on it (Chapter 6). The cross-section of each Ge-doped fibre is illustrated in the Figure 3.16.

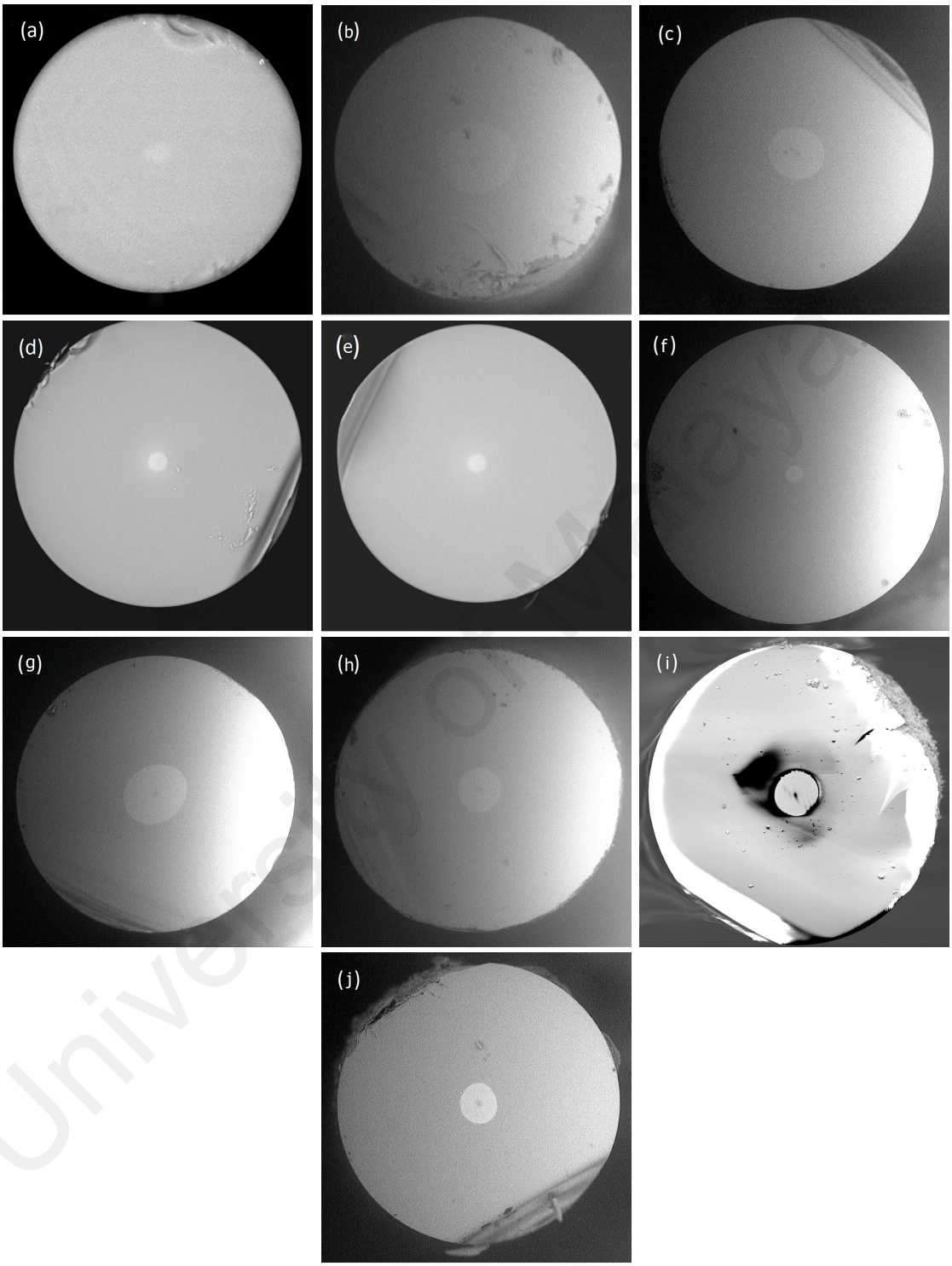

Figure 3.16: SEM images of different Ge-doped fibres (Ge01-Ge10) used in the concentration study. The germanium concentration at the core of above fibres from (a) to (j) is varying from about 0.7 to more than 16 weight percent. According to the different core sizes, a correction factor should be considered in calculation of TL response.

Table 3.5: Core parameter and chemical analysis of different Ge-doped fibres.

Attribute	Concentration (Weight (%))			Size Relation
	Germanium	Silicon	Oxygen	(core : cladding)
Ge01	0.7	35.5	63.7	0.004
Ge02	3.1	34.8	61.8	0.067
Ge03	3.8	34.6	60.8	0.038
Ge04	4.3	34.7	60.9	0.004
Ge05	4.9	31.7	63.4	0.005
Ge06	6.3	34.7	59.0	0.003
Ge07	7.0	31.7	61.3	0.049
Ge08	8.2	38.4	53.5	0.025
Ge09	12.1	36.9	51.0	0.024
Ge10	16.7	31.5	47.8	0.021

3.3 Chapter summary

In this chapter, the general method of sample preparation, irradiation and readout, which is applied in this thesis was discussed. The measurements were defined and relevant devices were introduced. It was shown how to dope a fibre preform and the method of fibre pulling is generally discussed in more details for PCF and flat fibre. The sample measurement methods were introduced and effect of fibre pulling parameters were shown. After presenting the used radiation sources for this study, the model used for kinetics study were illustrated.

Thereafter general approach to the methodology, the samples used in this study were characterised in more details introducing the direction of the results and discussion chapters. Doped and undoped samples including capillary, cylindrical, PCF and flat fibre were introduced and relevant SEM images and EDX results were presented.

CHAPTER 4: DOSIMETRIC EVALUATION OF VARIOUS DOPED OPTICAL FIBRES

Thermoluminescence dosimeters are widely used, serving the needs of various radiation applications. In recent times, optical fibres have been introduced as alternatives to more conventional phosphor-based TLD systems, with many efforts being carried out to improve their TL yield. While there have been extensive studies of many of the various TLD characteristics of optical fibres, including TL response, linearity, reproducibility, repeatability, sensitivity and fading, far more limited studies have concerned dependence on the type of TL activator used in optical fibres, promoting the TL mechanism.

4.1 Introduction

New perspectives are evolving in respect of the wide range of potential TLD applications of various forms of optical fibres [16, 82]. It is demonstrated that the TL response of fibres will vary depending upon core dopant concentration as well as core size [31]. On the other hand, a variety of works reported on designing special photo-, radio-, and/or thermoluminescence material with high sensitivity in detecting irradiation in which all these studies emphasized the importance of dosimeter with high sensitivity.

The characterisation of the defect centres forms a crucial step in understanding the mechanism of TL [157]. In this context, analysis of glow curves offers a sensitive and suitable technique for such study. Here, in present chapter, two types of standard single mode fibres (SMF) namely, SMF-1 and SMF-2 are compared with TLD-100. Besides, TL response and kinetic parameters of optical fibres doped with rare elements are examined.

4.2 Results

4.2.1 Single mode fibres

Figure 4.1 shows TL response of the two SMFs for the three different electron energy irradiations in comparison with TLD-100 TL yields. In terms of linearity, all samples show linear response (linear fitting curve $R^2 > 97.8\%$) over the investigated dose range, 0.5 to 8 Gy for all three energies. Taking TLD-100 as the benchmark, SMF-1 exhibits significantly greater response than the TLD-100, while SMF-2 approximately has half of the response of the TLD-100. On average, SMF-1 has a TL response that is about 3.2 times greater than that for TLD-100 at 6, 9 and 20 MeV, and the results also confirm SMF-1 to significantly outperform TLD-100. The potential of Ge-doped optical fibre as TLD has been reported earlier in the literature. Hashim et al. [90] compared the TL response of a Ge-doped commercial SMF with TLD-100, oxygen- and Al-doped fibres under electron and photon energies. Ge-doped fibre showed significantly better TL response oxygen- and Al-doped fibres but showed a TL yield about eight times lower compared to TLD-100. In another study, Yaakob et al. [102] confirmed the significant outperformance of Ge-doped fibres compared to Al-doped fibre, while the Ge-doped fibre used in their study could yield a TL half that of a TLD-100 chip. To the best of our knowledge there exist no previous reports showing SMFs to outperform TLD-100, certainly not to the present extent. Recently, Benabdesselam et al. [24] reported TL glow curve analysis of a multimode fibre (MMF) with 62.5 μm diameter with 2-layer Ge-doped fibre compared with TLD-500 and TLD-600. The MMF is shown to be relatively more sensitive than compared to TLD-500 and TLD-600. Zahaimi et al. [31] demonstrated that the TL yield in a SMF with 8-9 μm diameter can be improved upon by up to 6 times using a larger core MMF with 50 μm diameter with the same cladding size.

Figures 4.2 (a, b and c) show the energy dependency of the two SMFs compared to that of TLD-100 at 6, 9 and 20 MeV. Both SMFs show low sensitivity to change in radiation energy, sharing this dosimetrically favourable behaviour with that of

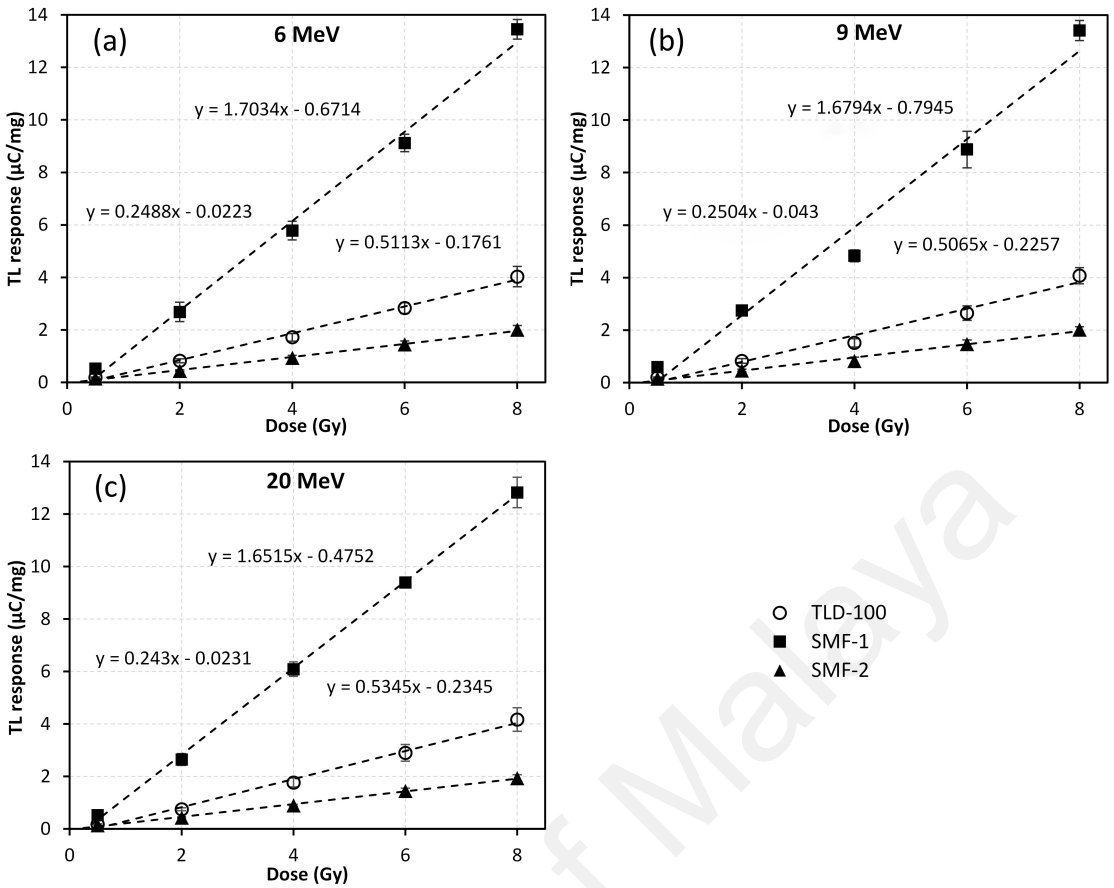

Figure 4.1: TL response of two different SMFs in comparison with TLD-100 irradiated to 6, 9 and 20 MeV electrons. SMF-1 shows significantly greater TL response than SMF-2 and TLD-100.

TLD-100. On the other hand, Figures 4.2 (right side) show the sensitivity curve of the optical fibres and TLD-100 calculated from their TL response divided by relative applied dose. Besides the irradiation energy insensitivity, both SMF-1 and TLD-100 have a positive sensitivity slope compared to SMF-2. Unlike SMF-2, SMF-1 and TLD-100 have slightly higher sensitivity at the higher doses compared to lower dose, showing them to be slightly dose dependent.

Uncertainty of the slope (ΔS) of the fitted curve in TL response (shown in Figure 4.1 and 4.2 (left)) and dose detection sensitivity (shown in Figure 4.2 (right)) is calculated based on the maximum (M) slope (S_M) and minimum (m) slope (S_m) calculated based on the variation or standard deviation (STD) in TL response as $\Delta S = (S_M - S_m)/2$, where $S_M = (Y_{M\ (at\ x_M)}/Y_{m\ (at\ x_m)})$ and $S_m = (Y_{m\ (at\ x_M)}/Y_{M\ (at\ x_m)})$. The $Y_{M\ (at\ x_M)}$ is the maximum value in Y-axis (mean + STD) at maximum value in x-axis, which here refers to the maximum TL value at dose 8 Gy and the $Y_{m\ (at\ x_m)}$ is

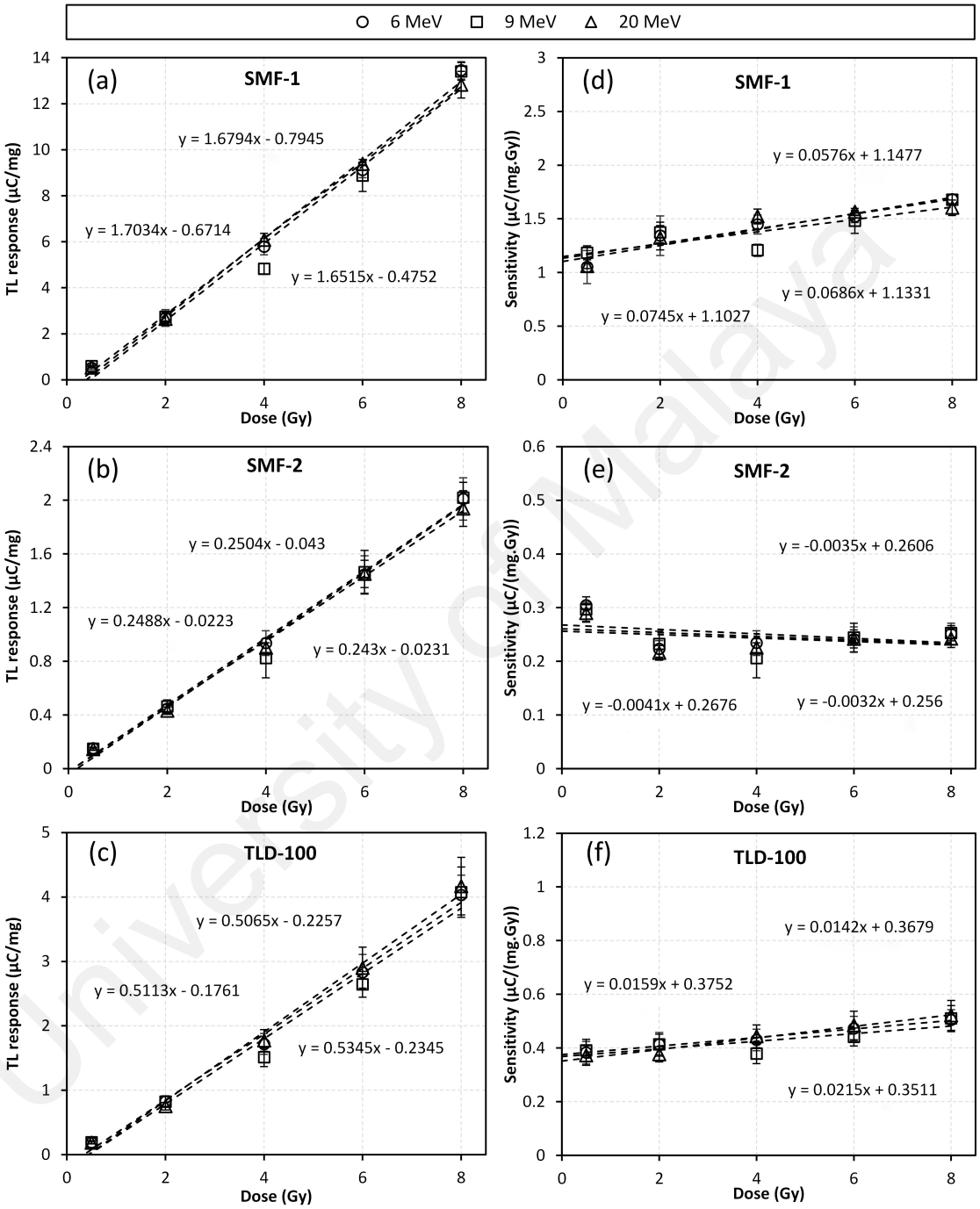

Figure 4.2: Comparison of energy dependencies of SMF-1, SMF-2, and TLD-100 for electron irradiations between 6 and 20 MeV.

Table 4.1: The slope and its uncertainty for (a) the fitted curves in TL response and (b) the fitted curves in sensitivity for SMF-1, -2, and TLD-100 for the three electron energies.

(a)	**TL response** (μC/mg)		
	6 MeV	9 MeV	20 MeV
SMF-1	1.70 ± 0.05	1.68 ±0.04	1.65 ± 0.06
SMF-2	0.25 ± 0.02	0.25 ±0.01	0.24 ± 0.02
TLD-100	0.51 ± 0.04	0.51 ±0.04	0.53 ± 0.05

(b)	**Sensitivity** (μC/(mg.Gy))		
	6 MeV	9 MeV	20 MeV
SMF-1	0.075 ± 0.020	0.058 ± 0.012	0.069 ± 0.010
SMF-2	0.004 ± 0.003	0.004 ± 0.004	0.003 ± 0.003
TLD-100	0.016 ± 0.008	0.014 ± 0.009	0.022 ± 0.010

the minimum value in Y-axis (mean - STD) at minimum value in x-axis, which here refers to the minimum TL value at dose 0.5 Gy. Table 2 shows the slope of fit and its uncertainty for TL response (Table 4.1(a)) and dose sensitivity (Table 4.1(b)) for SMF-1, -2, and TLD-100 for the three electron energies. The highest variation in the slope of the fit to the TL responses for SMF-1, -2 and TLD-100 are 6%, 2% and 5%; and to the dose sensitivity are 2%, 0.4% and 1%, respectively. These low variations in the slope of the fit reconfirm the stability of the SMFs in terms of both energy independency and dose sensitivity, comparable with commercially available TLD-100.

Table 4.2 shows the average sensitivity of SMFs compared to TLD-100, obtained by dividing the TL response by its corresponding dose over the three radiation energies. SMF-1 offers a dose sensitivity 3.2 and 5.6 times that of TLD-100 and SMF-2, respectively, and TLD-100 shows 1.7 times more sensitivity than SMF-2.

Figure 4.3 shows the glow curves of SMF-1, -2, and TLD-100 resulting from electron irradiation at 6 MeV, delivering doses of 0.5, 2, 4, 6, and 8 Gy. To pro-

Table 4.2: The average sensitivity of SMF-1, -2, and TLD-100 with standard deviation (STD).

	SMF-1	TLD-100	SMF-2
Sensitivity (μC/(mg.Gy))	1.40	0.44	0.25
STD	0.08	0.04	0.02

vide intercomparison between all three samples, the curves have been normalised to dosimeter mass, the time-temperature profile covering temperatures from 50 °C to 400 °C. Compared with TLD-100, with thermal luminescence at well-defined temperatures, at around 170, 220, 260 and 330 °C, it is apparent that the SMFs exhibit a broad range of thermal excitation, as expected of an amorphous system.

Using the so-called computerised glow curve deconvolution (CGCD) method, second derivative deconvolution of the glow curve of SMF-1 and -2 has been carried out as the resultant component peaks are shown in Figure 4.4. The trap parameters associated with the component peaks are shown in Table 4.3, a mixture of first and second order kinetics being applied. It is found that the first half of the glow curve follows first order kinetics since while the second half follows second order kinetics. The deviation of the fitted sub-component peaks from the gross glow curve is about 0.04%, with a figure of merit of 2.8%.

In SMF-1, glow curve peak number 1, with activation energy 1.6 eV, could be associated with Si nanoclusters, while peak number 2, activation energy 1.8 eV, could also be related to Si nanoclusters and the oxygen-deficiency centre (ODC) in the silica. Peaks numbers 3 and 4, activation energy 2.6 and 2.4 eV respectively, are probably due to the ion dopants Ge^+ and/or Si^+, peak number 3 being also

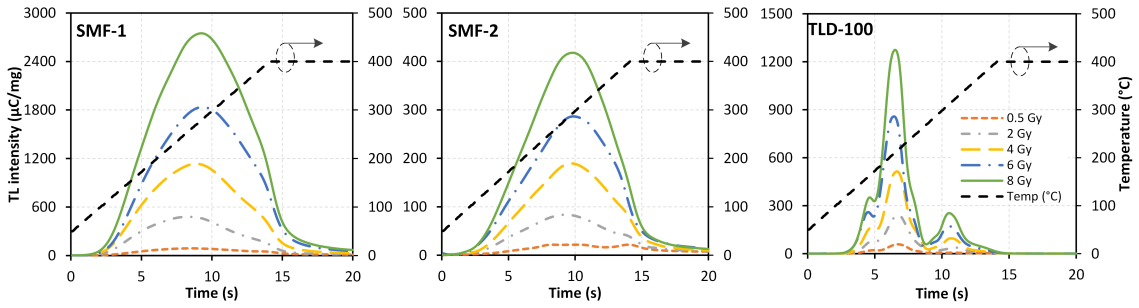

Figure 4.3: Glow curves of SMF-1, -2 and TLD-100 for doses of 0.5, 2, 4, 6, and 8 Gy obtained with 6 MeV electron irradiation, all normalised with sample mass.

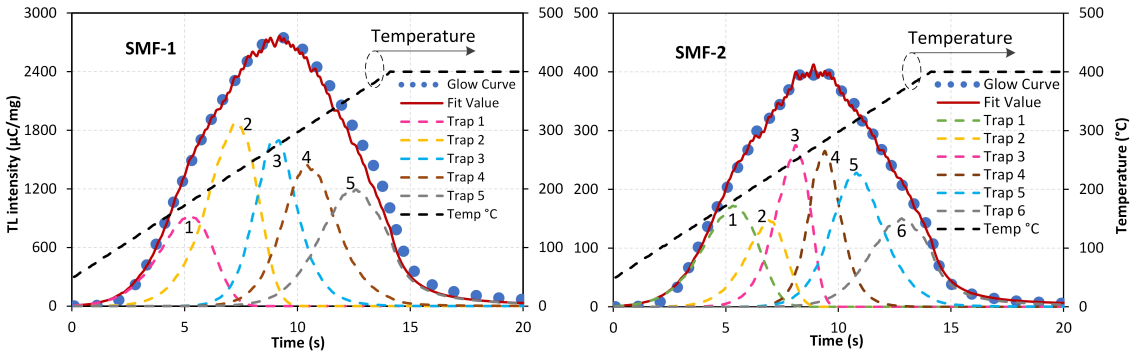

Figure 4.4: Glow curve deconvolution for SMF-1 and SMF-2.

probably related to the self-trapped exciton (STE) defect in silica. Peak number 5, with energy 2.2 eV, could be due to the STE, Si implantation, Si nanoclusters, and/or hydrogen defects [105].

In SMF-2, peak numbers 1 and 5 with 1st and 2nd order activation energy of 2.5 eV could be associated with the STE, Si implantation, and/or Si nanoclusters. Peak number 2, with activation energy 1.5 eV, is suggested to be due to Si nanoclusters in the fibre. Peak number 3 and 4, with activation energy 2.0 and 2.2 eV, is suggested to be mainly due to the STE, the ion dopant Si and C implantation, Si nanoclusters and/or hydrogen defects [105].

Minimum detectable dose (MDD) is a particularly important parameter, defining the realm of applicability, not least setting limits on use for low dose irradiation evaluations. The value of MDD depends not only on the medium but also on reader-based parameters including background noise (BG) and photo multiplier tube noise (PMT). The various influences act to define the slope of TL response (α) of the TLD medium and the standard deviation of the background TL signal (σ) of the samples. Various determinations of the MDD can be defined, based on the order of the background standard deviation. Here, the criterion of 2σ above background is applied in expressing the MDD [171], as follows:

$$MDD = (BG_{mean} + PMT_{mean} + 2\sigma)/\alpha \tag{4.1}$$

The average and σ of background noise for the TLD reader used in this study are 7.9 nC and 0.83, respectively. On the other hand, the variation in the slope of the fit in

Table 4.3: Glow peak analysis of SMF-1 and SMF-2. b is the kinetics order of the glow peaks, E is the activation energy of each trap, in units of eV, s is the frequency factor (s^{-1}), n_0 is the initial concentration of trapped electrons (cm^{-3}), Peak-I is the maximum intensity of glow peak, in units of nC, Peak-T is the temperature at maximum intensity of the glow peak in °C, FWHM is the full width at half maximum intensity of the glow peak, also in units of °C, and the peak emission wavelength in nm.

SMF-1	Trap : 1	Trap : 2	Trap : 3	Trap : 4	Trap : 5
b	1^{st} order	1^{st} order	2^{nd} order	2^{nd} order	2^{nd} order
E	1.6	1.8	2.6	2.4	2.2
s	1.3E+6	3.5E+7	9.5E+7	2.2E+5	7.7E+2
n_0	2.9E+6	5.5E+6	4.4E+6	4.7E+6	5.1E+6
Peak-I	933	1874	1693	1447	1195
Peak-T	177	227	277	307	362
FWHM	115	110	100	115	132
Emission	775	689	477	517	564

SMF-2	Trap : 1	Trap : 2	Trap : 3	Trap : 4	Trap : 5	Trap : 6
b	1^{st} order	1^{st} order	1^{st} order	2^{nd} order	2^{nd} order	2^{nd} order
E	2.5	1.5	2.0	2.2	2.5	3.5
s	6.1E+13	1.8E+5	1.2E+10	6.2E+3	8.7E+6	2.1E+16
n_0	4.6E+5	6.8E+5	4.7E+5	6.2E+5	7.1E+5	4.0E+5
Peak-I	172	147	275	265	228	150
Peak-T	392	227	177	307	277	362
FWHM	70	50	42.5	40	62.5	77.5
Emission	496	827	620	564	496	354

Table 4.4: Minimum detectable dose and its tolerance for SMF-1, -2, and TLD-100 for 6, 9, and 20 MeV electron irradiations.

	Minimum detectable dose (mGy)			
	6 MeV	9 MeV	20 MeV	Mean
SMF-1	6 ± 0	6 ± 0	6 ± 0	6 ± 0
SMF-2	39 ± 3	38 ± 2	39 ± 3	39 ± 3
TLD-100	19 ± 1	19 ± 2	18 ± 2	19 ± 2

the TL response reflects uncertainty on the MDD. Considering the slope of the fitted curve and its variation presented in Table 4.1, the MDD and its variation for SMF-1, -2, and TLD-100 over three applied energies are estimated based on Equation (4.1) as shown in Table 4.4. SMF-1 shows a detection threshold some 3.2 and 6.5 times lower than that of TLD-100 and SMF-2, pointing to considerable utility in detecting environmental doses.

In consideration of the potential repeated reuse of the samples, repeatability tests were performed on six samples from each of the SMF samples and TLD-100 each irradiated with 8 Gy dose at 6 MeV. Subsequent to each readout cycle, the same samples were re-annealed and re-irradiated for a total of four irradiation-readout cycles. The variation from the first TL yield is represented in Figure 4.5, the error bars on the y-axis values provided as the STD in TL yield. From the six samples per dosimeter type, the highest variation observed in SMF-1, -2, and TLD-100 are 13.1%, 13.1% and 10.9%, where the average repeatability variation over the six samples are 11.0%, 8.7% and 9.7%, respectively. The low variations suggest the SMFs to offer reusability as radiation dosimeter sensors. It should be noted that the TL response difference between samples 1 to 6 are mainly due to the cut length variation of the fibre samples.

The results of signal fading in the irradiated SMF samples are shown in Figure 4.6. In this experiment, initially, the fibres were irradiated at 6 MeV to a dose of 6 Gy and stored in a dark place under room temperature. The readout was started after 24 hours and continued up to six weeks from irradiation. The percentage of signal

reduction after every ten days is presented in the figure based on the exponential curve fitting. The TL signal of SMF-1 and -2 showed about 4 and 6% reduction after ten days from irradiation, 21 and 30% after 60 days, respectively.

A comparison study is made with TLD-100 based on the reported works in literature, suggesting higher fading in optical fibres compared to TLD-100 especially for the longer period of time. Izak-Biran et al. [172] have shown the fading in TLD-100 is about 11%, 19%, and 22% after 10, 30, and 90 days, respectively. Vasilache et al. [173] reported a fading of about 12% and 19% for TLD-100 after 10 and 25 days respectively, keeping the samples in a dark room. Noor et al. [103] presented fading analysis comparison between Ge-doped SMF and MMF with TLD-100, where after 133 days of storage, a TL loss of 11%, 8%, and 5% is observed with a preheat temperature of 160 °C, respectively.

4.2.2 Rare element doped fibres

The TL responses of the five sets of optical fibres with respect to a dose of 8 Gy are illustrated in Figure 4.7 for two applied energies of 6 MV photon and 6 MeV electron radiation. The fibres used in this study are doped/co-doped with Al-Y-Tm, Ba, Al-Tm (two concentrations), and Ga. The TL yields are similar for both the photon and electron irradiations, with a deviation between them of less than 4% based on the mean values.

In Figure 4.8(a)-(e) the main glow curves for each of the fibre samples have been deconvoluted, with a figure of merit (FOM) for fitting of about 3.4-5.2% and a

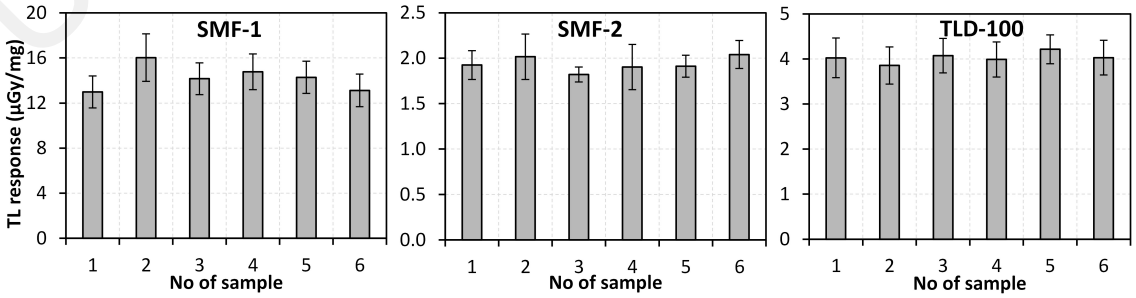

Figure 4.5: Four subsequent cycles repeatability test applied on 6 different samples for SMF-1, -2 and TLD-100, irradiated to a dose of 8 Gy dose using 6 MeV electron irradiations.

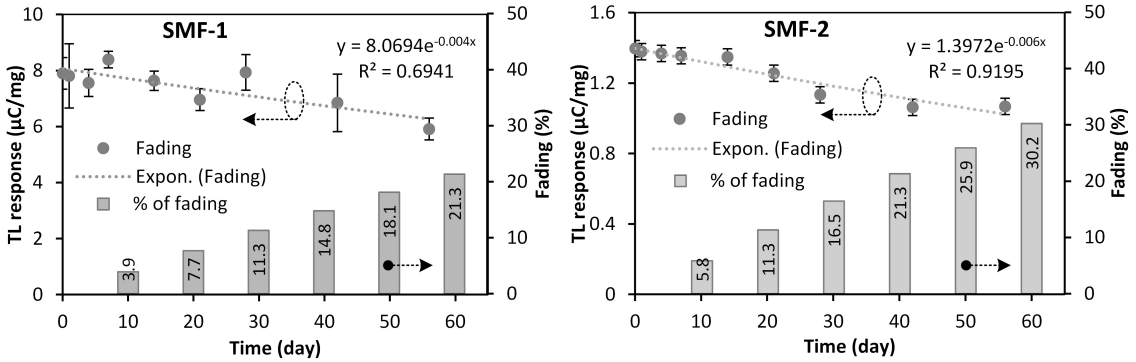

Figure 4.6: Fading effect for SMF-1 and -2 irradiated with 6 MeV electrons and a dose of 6 Gy measured with preheat temperature of 50 °C.

mean deviation of 0.8%. The extracted traps information from the deconvolution of glow curves are presented in Tables 4.5(a) to (e). These tables show the first peak (referred to as Trap 1) to have an activation energy of 0.9-1.1 eV, a peak intensity of 2-2.9 μC, and an emission wavelength of between 1100 and 1400 nm pointing to independence from the dopant material, instead being more related to the substrate or the silica preform itself. The activation energy suggests association between O^2 and O^{2-} defects in amorphous and fused silica [105].

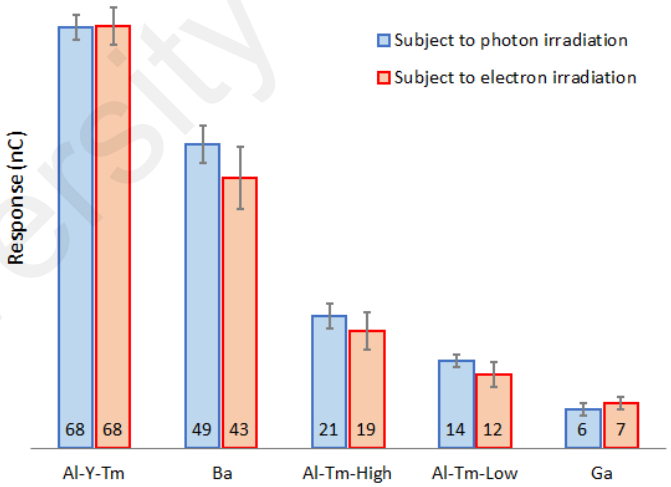

Figure 4.7: Typical responses for 8 Gy photon irradiation at 6 MV and electron irradiation at 6 MeV.

Examining Figures 4.7 and 4.8(a) and (b), the numerous traps in Al-Y-Tm-doped and Ba-doped fibre provide for the greater response of these two forms over that of other samples, each of which are composed of less traps (Figures 4.8(c) to (e)). This supports the underpinning basis of greater numbers of traps producing greater absorption. According to Figure 4.8(a) the combination of Al, Y and Tm as fibre

co-dopants results in an increased number of trap centres and, as a result, enhanced absorption. Figure 4.8(b) for Ba-doped silica, provides evidence for lower intensity glow peaks compared to that for Al-Y-Tm-doped fibre, albeit with similar energy traps formed in the two types of fibre.

In accord with Tables 4.5(a) and (b), the major difference between Al-Y-Tm-doped fibre and Ba-doped fibre is the intensity of the individual peaks. In the first case, the more energetic traps have a greater capacity for storing memory of the irradiation. The complex shape of the Ba-doped fibre glow curve is posited to be due to deep interactions of this element with the host silica preform.

Figures 4.8(c) and (d) show deconvolutions for optical fibres containing the same dopant (Al-Tm), one with a greater concentration of Al inside the fibre core than the other. Tables 4.5(c) and (d) show that in increasing this dopant concentration, there is no practical change in the peak positions (peak-$T \sim$ 160-166 & 193-206 for traps 2 and 3 respectively), but the intensity is increased, the exception being for trap 1 which is independent of dopant as discussed earlier (peak-I_1 = 1.5 & 1.6 $\rightarrow$ peak I_2 = 2.2 & 2.3 for traps 2 and 3 respectively).

The simple glow curve of Ga-doped fibre is shown in Figure 4.8(e). The main TL is generated from the first glow peak which is from the silica preform, while less TL is contributed from peak 2, from Ga traps.

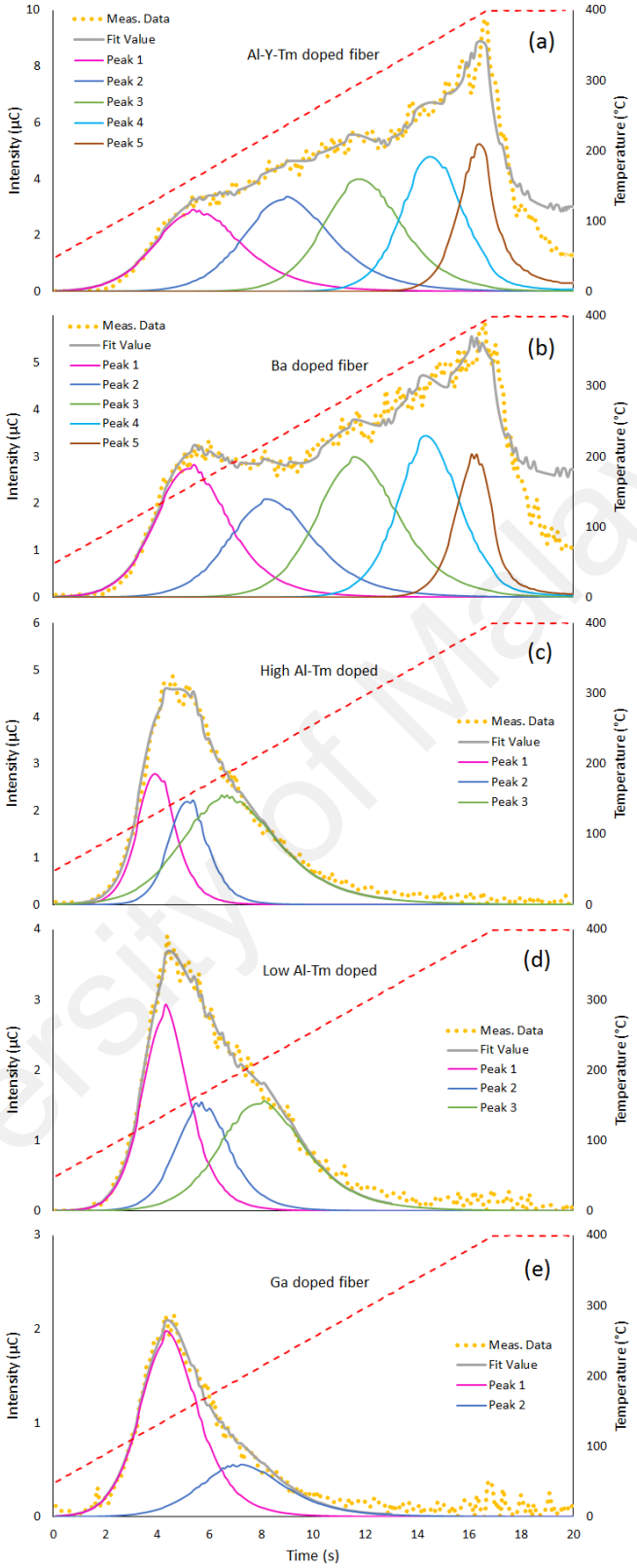

Figure 4.8: Glow curve deconvolution for (a) Al-Y-Tm-doped, (b) Ba-doped, (c) Al-Tm-doped, (d) Al-Tm-doped, (e) Ga-doped fibre TLD according to second order kinetics.

Table 4.5: Trap parameters for different doped fibres. Here, E_a is the activation energy of each trap in units of eV, s is the frequency factor (s^{-1}), n_0 is the initial concentration of trapped electrons (cm^{-3}). The Peak-I and Peak-T values are the glow curves maximum intensity (μC) and associated relevant temperature (°C) respectively. The full-width-half-maximum (FWHM) value is calculated on the absolute temperature scale and the TL emission wavelength is in units of nm.

	(a) Al-Y-Tm doped					(b) Ba doped fibre				
	Trap:1	Trap: 2	Trap: 3	Trap: 4	Trap: 5	Trap:1	Trap: 2	Trap: 3	Trap: 4	Trap: 5
E_a	1.1	0.9	1.2	2.0	3.0	1.0	0.8	1.2	1.9	3.0
s	1.3e3	1.6e4	5.7e6	5.3e11	9.0e19	6.7e4	3.7e4	2.3e6	4.7e11	1.5e21
n_0	1.4e4	1.6e4	1.6e4	1.5e4	4.1e3	1.1e4	9.2e3	1.2e4	1.1e4	1.0e3
Peak I	2.9	3.4	4.0	4.8	5.2	2.8	2.1	3.0	3.4	3.1
Peak T	162	237	295	353	393	166	241	297	345	403
FWHM	79	81	73	54	29	65	79	73	54	31
Emission	1138	1438	993	628	408	1238	1463	1055	644	408

	(c) High Al-Tm doped			(d) Low A	
	Trap:1	Trap: 2	Trap: 3	Trap:1	Tr
E_a	1.1	1.5	0.6	1.1	
s	1.9e13	1.6e14	7.2e2	7.6e9	2
n_0	5.8e3	4.5e3	1.1e4	6.8e3	4
Peak I	2.8	2.2	2.3	2.9	
Peak T	128	160	193	137	
FWHM	33	33	86	42	
Emission	1145	829	1916	1128	1

4.2.3 High dose gamma exposure

Doped fibres were shown up with low TL responses in current chapter, capability of them for high dose TL measurement were considered. Basically, delivered dose of more than 1 kGy is known as high dose. Two ranges of high dose ionising radiation is important for dosimetry application. One is started from 5 kGy upto 25 kGy, that is mainly used in food radiation and neutralisation. The next range is start from 25 kGy to 70 kGy which is the interested range for sterilization of products such as soil, surgical equipments and cosmetics. Hence, high activity ^{60}Co (details were discussed in Chapter 3) was applied to irradiate the samples with gamma (γ) ray from 50 Gy upto 100 kGy. Whilst, the complete study on high dose γ ray irradiation can be found in Appendix A, here, the TL characteristics of Al:TM-doped fibre at high dose exposure is described as it fits our dose range criteria (Figures 4.9 and 4.10).

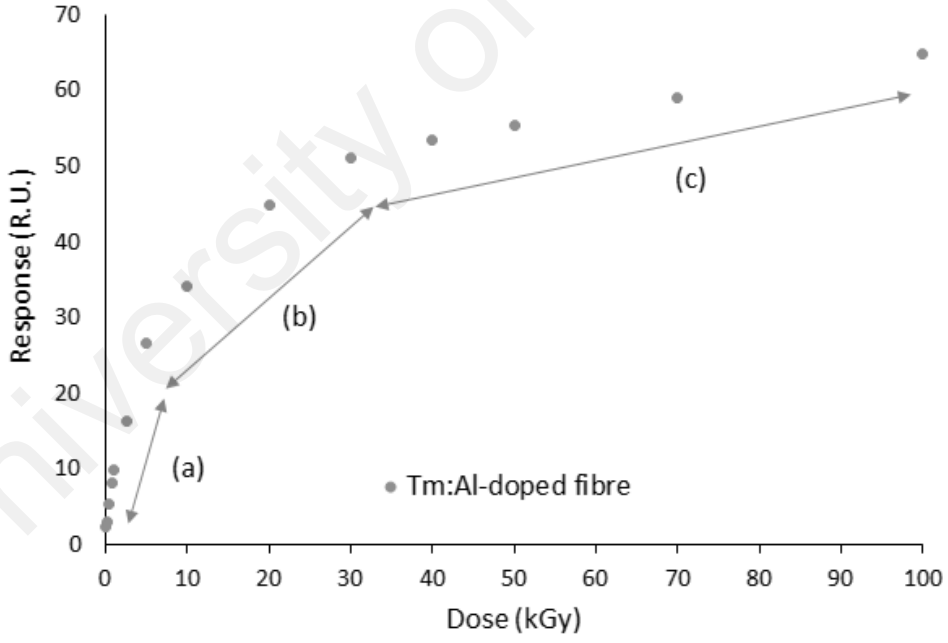

Figure 4.9: Al:Tm-doped fibre TL response subject to gamma ray irradiation from 50 Gy upto 100 kGy. An average of 6% standard deviation is calculated.

As shown in Figure 4.9, Al:Tm-doped fibre can stand long range of irradiation doses without saturating completely. This dose range (50 Gy to 100 kGy) can be divided to three linear part. The first parts started from several Gy and stays linear upto 5 kGy as shown in Figure 4.10a. On the other tail of the response curve, again

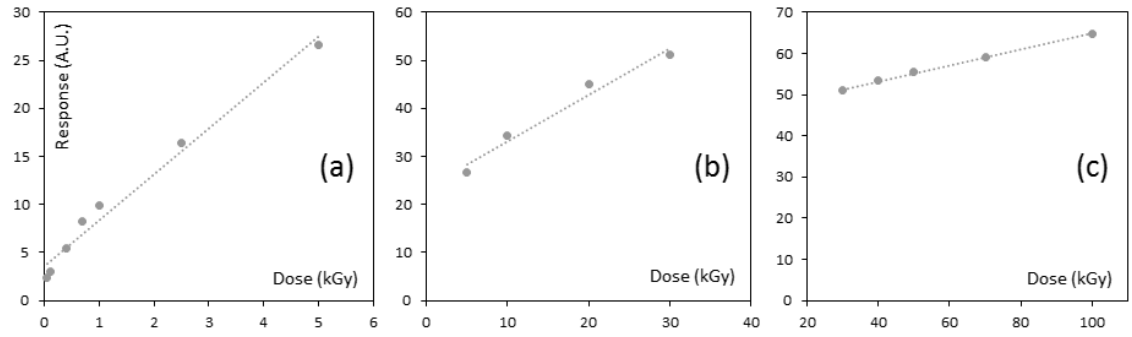

Figure 4.10: Three linear parts of Al:Tm-doped fibre TL curve; a) from 50 Gy to 5 kGy; b) from 5 kGy to 30 kGy; c) and from 30 kGy to 100 kGy.

there is a good linear part with smooth and slow gradient where started from 30 kGy to end. This is also shown in Figure 4.10c. Somewhere between the regions of (a) and (c), again can be assumed as a linear part that covers a dose range from 5 to 30 kGy. As it appeared in Figure 4.10b, the TL points can be reproduced with a linear trend-line and good accuracy. It should be noted that the results of high-dose presented here and in Appendix A are just the preliminary observations that required further study in future to develop high dose dosimeter.

4.3 Discussion

In standard optical fibres, to obtain the *total internal reflection* required for effective light guiding for telecommunication, the core or cladding needs to be doped to obtain the necessary refractive index situation. Fortuitously, it is the presence of the dopant that provides the defect centres for TL dosimeter applications, to first order a greater concentration of defects being expected to produce the greater TL response, albeit with saturation occurring (due to self-absorption) above a certain level. The EDX results of Table 3.2 show SMF-1 to contain slightly greater Ge-doping concentration compared to SMF-2, supporting the superior TL response of SMF-1 over that of SMF-2. It is remarkable that a small increment of about 10% in Ge concentration in SMF-1 compared to SMF-2, caused a large TL response difference of 6.3 times, important in designing high-sensitivity optical fibre with optimum Ge concentration.

In terms of dosimeter performance, SMF-1 significantly outperformed TLD-100 with 3.2 times greater TL response and dose detecting sensitivity. SMF-1 has ca-

pability in detecting a minimum dose of 5.7 ± 0.2 mGy. In addition, this fibre shows highly linear TL response with regression fitting of greater than 97.8%, relative independence to irradiation energy, low fading of less than 4% per 10 days, and repeatable dose measurement with an average variation of about 10%. These and other inherent advantages of optical fibres as mentioned in the introduction confirm the considerable capability of these optical fibres as dosimeter sensors. Thus said, comparison of the TL response of SMFs and MMFs in this study suggests that designing a larger core optical fibre like MMF, with Ge concentration similar to SMF-1, would significantly improve dose detection sensitivity of an optical fibre sensor.

By comparing different rare material doped and co-doped fibres (i.e. Tm, Ga, Ba, and Y) according to their TL yields subject to photon and electron irradiation which comes with different energies, similarity of the results with a deviation between them of less than 4% based on the mean values is in agree with their energy independency. Also their low response to the tested range of dose, suggests their efficiency to be used in high dose radiation detection. For this purpose, the fibre which is co-doped with Tm and Al is offered as a possible dosimeter for high doses. As shown in Figures 4.10b and 4.10c, it can be used separately for either food radiation dosimetry (5-25 kGy) or sterilisation radiation dosimetry (30-70 kG). However, further study is still required for understanding and performance development of these rare doped fibres especially for higher dose applications.

Finally, notwithstanding, the fibre samples are cut manually, the highest measured TL variation observed was less than 8%, which is related to 6 Gy, 9 MeV, SMF-1 (Figure 4.1(b)) with STD of 0.7 and TL yield of 8.9 μC/mg. This variation in TL yield of optical fibres can be reduced by cutting the fibre samples with an automated fibre cleaver. Albeit, due to use of bare optical fibre, without polymer coating, for thermoluminescence based dosimeter applications; the standard optical fibre sizes (125 um) would be brittle for harsh environments, which required extra care and appropriate container to protect the fibre samples from the harsh environment.

4.4 Chapter summary

The commercially SMFs with about 8.5 μm core diameter used herein reveal a linear dose response for 6, 9 and 20 MeV electron irradiations, up to at least 8 Gy, encompassing the range of fractionated doses normally used in radiotherapy. From this study, the SMF-1 produced elevated TL yields compared to SMF-2 and TLD-100, by a factor of around 6.3 and 3.2 times. Analysis shows SMF-1 contains slightly higher germanium concentrations compared to SMF-2. These results confirm that by using this optical fibre technology irradiation dose sensors with sensitivity beyond TLD-100 is possible.

Howbeit, the similarity in activation energy of first glow peak for all different doped fibre samples indicates the TL response of the substrate, regardless of the dopant in the fibre. It is concluded that different concentration of similar dopant will only affect on the intensity of relevant glow peaks, while other factors will be plateau. An interesting observation from this study is that co-doping of the fibre is associated with an increase in the TL yield, pointing to a need for optimisation of the choice and levels in use of co-dopants.

Finally, for the first time, based on our preliminary results, a unique doped fibre is offered that can stand high dose γ irradiation up to 100 kGy without completely saturation. This may leads to next generation of TLDs for use in such high dose ranges.

CHAPTER 5: EFFECT OF OPTICAL FIBRE STRUCTURE ON TL RESPONSE

Present chapter focuses on six types optical fibres with different structural arrangements and/or shapes, three of them undoped silica fibre, namely capillary fibre, flat fibre, and photonics crystal fibres (PCF) as illustrated on the SEM images in Figure 3.11, and the other three types of Ge-doped optical fibres, namely conventional cylindrical fibre, capillary fibre, and flat fibre, as the schematic diagram shown in Figure 3.12. The fabrication process and general characterisation of these fibres have been presented in Chapter 3.

5.1 Introduction

Nowadays, by increasing the demand of using optical fibres, in the potential of optical fibres as the foundation of next-generation thermoluminescence dosimeters (TLDs), the development of suitable forms of material and their fabrication has became a fast-growing endeavour. Investigations of the TL yield from such media have been rather rudimentary since recent decade. The researches which have been done were trial to use the conventional standard fibres, underlined by the lack of a firm linkage with the underlying mechanisms supporting the behaviour of the different types of fibre.

Using silica obtained from a single manufacturer, three forms of undoped fibre (capillary, flat, and photonic crystal fibre (PCF)) were fabricated for this study. The approach is entirely novel, to the best of our knowledge there exist no other published reports showing the method for improvement in the TL yield of undoped optical fibres. The proposed method can be further applied to doped optical fibre preforms (the doped silica starting material, prior to fibre production) to further enhance TL yield.

The Ge-doped preform has been developed by using the modified chemical vapour deposition (MCVD) method, with part of the preform is brought to a state of col-

lapse during the MCVD process that has been applied in fabricating conventional cylindrical fibre, the remaining part of the perform being kept uncollapsed as a hollow structure for fabricating capillary and flat fibres.

For doses from 0.5 to 8 Gy, obtained at electron and photon energies, standard TL characteristics of the optical fibres have been the subject of detailed investigation. Addressing the associated defects generating TL in each of the optical fibres, the study encompasses CGCD analysis of the TL glow curves with 2^{nd} order kinetics. The study was separated in two parts as mentioned above since the samples were not available from the same preform. The first group includes undoped fibres with the shapes of capillary, flat and PCF and the second group includes Ge-doped fibres with the shapes of capillary, cylindrical and flat.

The idea of flat fibre came from the collapsed part of the PCF. Considering this concept, a simple collapsed fibre, here we call it flat fibre, can explain the performance of PCF, which includes many collapsed parts that formed from joining of outer surface of each single capillary inside the PCF.

5.2 Thermoluminescence analysis

5.2.1 Group 1

The TL response of capillary and flat fibres (FF) following 6 and 20 MeV electron beam irradiations, for doses in the range 0.5 - 8 Gy, is shown in Figure 5.1. As expected, the capillary fibre shows minimal TL response, approaching that of the prevailing background noise. By collapsing the capillary into a flat shape, the resulting TL responses for 6 and 20 MeV irradiations have been observed to be about 12.0 to 12.5 times that of the capillary fibre. The approximate agreement between the results for electron and photon irradiation is in line with the equivalent linear energy transfer (LET) provided by these sources. It should be noted that both fibres were fabricated from the same preform, simultaneously exposed and read out on the same day, the latter reducing potential drift effects of the TL reader.

Considering Figure 5.1, the results strongly suggest the dominant TL mechanism to be associated with the generation of new defects in the FF, the inner surfaces

of the capillary fusing together during the drawing process, with subsequent strain relaxation on cooling and defects generation.

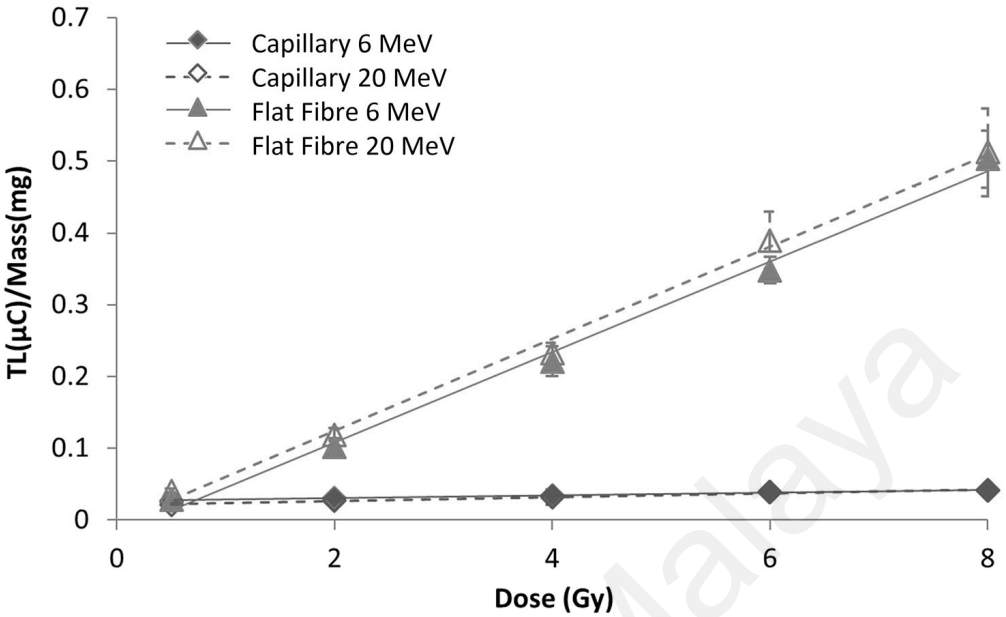

Figure 5.1: TL response of capillary and flat fibre under 6 and 20 MeV electron irradiation, for doses in the range 0.5-8 Gy. All fibres show linear TL response and low energy dependency. While capillary shows very low TL response with almost flat response, FF provides multiple times higher TL.

To seek support for this, a PCF has been fabricated, the resulting TL to be then compared with that of the capillary and FF. In the present PCF there are a bundle of 168 capillary fibres, their outer surfaces being fused together. Thus, even greater TL response is expected to result from the PCF compared to that from the capillary fibre or FF.

For the same irradiation conditions as previously, Figure 5.2 shows the TL response of flat fibre and PCF. The TL response of PCF is between 17.5 to 17 times that of capillary optical fibre for both 6 and 20 MeV irradiations, respectively. Compared to FF, the PCF provides a TL yield some 1.4 times greater. This strongly reaffirms the suggestion that the TL response in FF and PCF is predominantly generated from the fused surfaces of the collapsing region.

All three types of fibres represented up to this point show strong linear TL response, for the dose range applied, the fibres are seen to be insensitive to radiation energy. The variation of TL response at a given dose is primarily due to variation in fibre details, the variation being reduced to a certain extent by the mass normalisa-

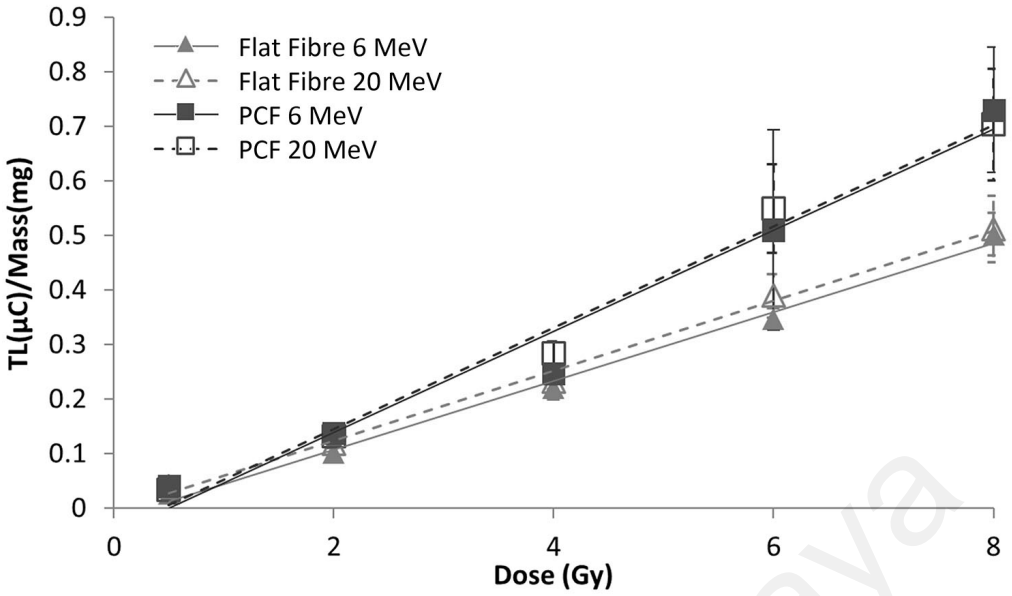

Figure 5.2: TL response of flat fibre and PCF following 6 and 20 MeV electron beam irradiation for doses covering the range 0.5 - 8 Gy. While PCF is more sensitive than FF, both fibres show linear TL response and minimal energy dependence.

tion procedure. A length variation of about ± 0.5 mm can lead to a 20% variation in TL response of fibre samples. Such variation can be reduced by characterising individual response to dose, a rather laborious procedure.

5.2.2 Group 2

Figure 5.3 shows the TL response of the three types Ge-doped optical fibres, as their detail have presented in Figures 3.12 and 3.13 and Table 3.4. Over the investigated dose range, a linear TL response has been obtained for all of the optical fibres. Of the three fibre types, the capillary fibre TLD shows the least TL response. On the basis of mean values, the cylindrical fibre provides a TL yield some 1.6 × that of the capillary fibre, while the flat fibre TLD produces a TL yield some 3.2 × and 5.5 × that of the cylindrical and capillary fibre samples respectively. In addition to the variation observed for each data point, the variation in the slope for each dosimeter type has also been calculated based on the maximum and minimum values for each dose and the transitional line across these points. These variations were about 8%, 6%, 10% and 13% (±0.040, ±0.004, ±0.013 and ±0.039) for the TLD-100 (the LiF dosimeter), capillary, cylindrical and flat fibre accordingly.

The results show that while all the optical fibres have been fabricated from the

same Ge-doped preform, their TL responses significantly differ (Figure 5.3). Since the TL response derives from the presence of defect centres [33], present results point to the presence of far greater numbers of defect centres in the flat fibre than in either the cylindrical or capillary fibre. The results further suggest that by collapsing the optical fibre wall surface, an additional form of defect is generated at the fused internal surfaces. While this defect type is also apparent in the central core of the cylindrical fibre, formed by collapse during the MCVD process, the numbers of defects produced in the flat fibre, formed by collapse during fibre drawing process, is significantly greater. This additional defect is due to the fast quenching rate and strain shearing effects at the fused walls formed during the fibre drawing process.

For 6 MV photon radiation Figure 5.4 provides sensitivity curves for the various fibre dosimeter samples, compared against that of TLD-100. In accord with expectation, the flat fibre TLD produces the greatest sensitivity of all of the fibre samples, also displaying uniform sensitivity over the full range of measured doses. Conversely, the capillary and cylindrical fibre TLDs are of greater sensitivity at low doses than at larger doses.

The results show that like the TLD-100, the flat fibre is linearly sensitive to dose within the investigated dose range, down to doses of 0.5 Gy at a minimum. Interchangeably, the cylindrical and capillary fibre are seen to show a supra-linear response [54] (Figure 5.4).

The effect of heating rate on TL reading is presented in Figure 5.5. The experiment was performed by selecting one batch of fibre samples and recycling through the irradiation-readout process a total of five times (annealed, exposed to radiation, and readout) using five different heating rates, from 15 to 40 °C/s, all other parameters defining the time-temperature profile (TTP) remaining fixed at the values recorded earlier. Using 6 MV photons, doses of 8 Gy were delivered. Apparent from the results for the various fibres are the inappreciable changes in response observed around the acquired temperature rate of 25 °C/s.

While with appropriate heating the trapped charges will always be released, at low heating rates the release is seen to be somewhat suppressed when compared to

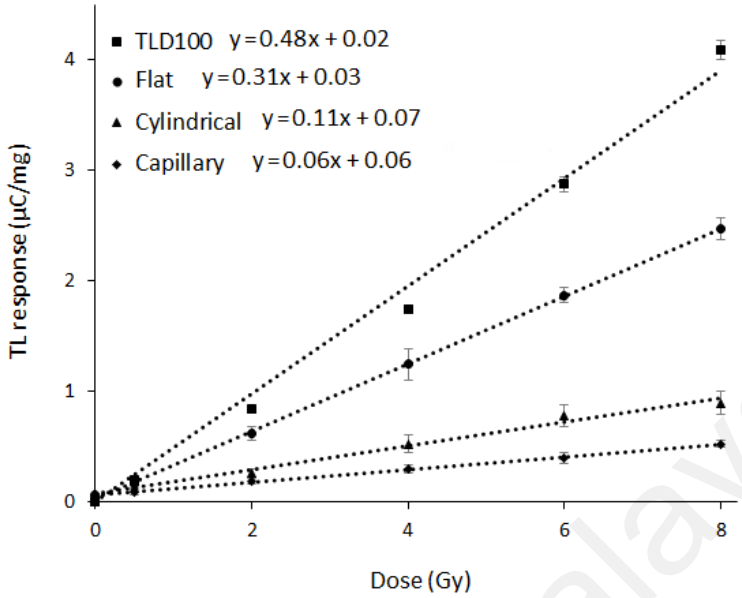

Figure 5.3: Comparison of the TL yield of the three different types of fibre TLD and of TLD-100 using 6 MV photon radiation. The error bars were based on the least square mean value of five different measurements.

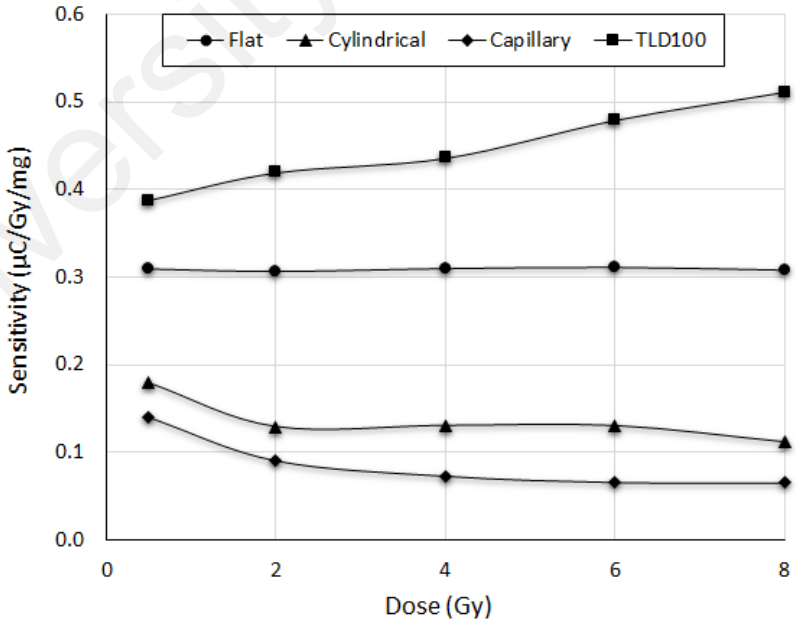

Figure 5.4: Calculated sensitivities for the three fibre TLD samples compared against that of TLD-100. The flat fibre displays uniform sensitivity across the entire dose range.

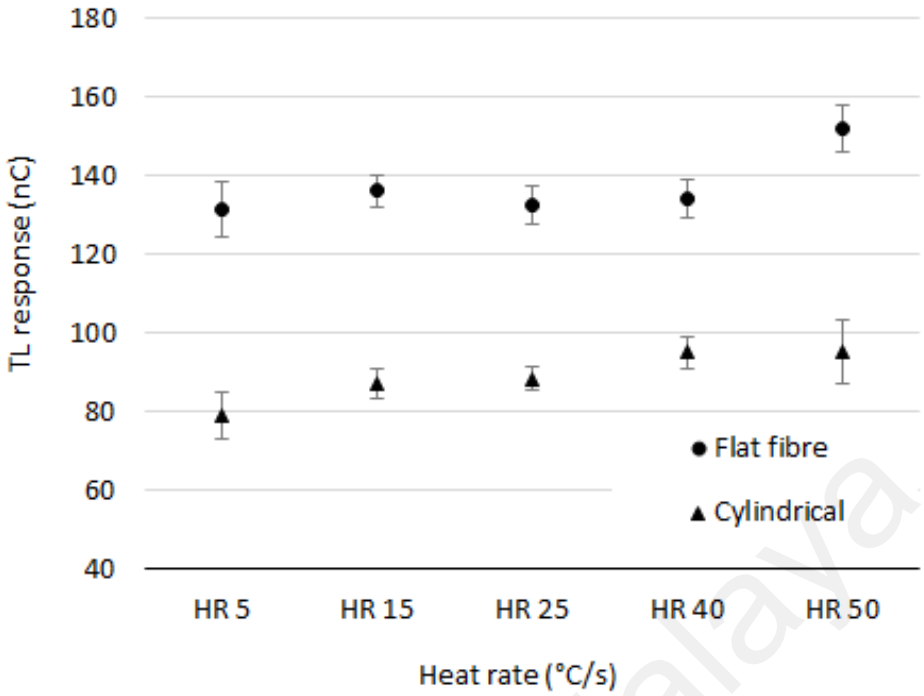

Figure 5.5: Effect of heating rate on TL yield of the irradiated samples. Apparent is the low variation in response around the mid-range heating rate.

the luminescence obtained at greater heating rates. At the low heating rates this suppression is due to a fraction of the traps releasing their charges in the form of kinetic phonons instead of photons. This necessitates choice of a heating rate that is optimum for TL response detection. Results herein have shown a heating rate between 15 to 40 °C/s to be appropriate for these particular materials, providing high response and low variation in readout.

The MDD for the TLD samples, calculated using Equation 4.1 for 6 MV photon irradiation, are shown in Table 5.1. The average background and PMT noise and its variation measured in this study were 8.98 ± 0.28 nC and 0.45 ± 0.09 nC respectively.

Further to this, the low dose detection limit of the flat fibre TLD has been shown to be some 30 mGy (Table 5.1), superior to the performance of either the other fibre TLD sample types investigated, as well as TLD-100. The noted characteristics of flat fibre is to potential for low dose detection applications, as in measurements directly made adjacent to the direct radiotherapy field (in other words, out-of-field measurements).

Table 5.1: Minimum detectable dose for TLD samples.

	α (μC/(mg.Gy))	MDD (mGy)
Flat fibre detector	0.305 ± 0.040	31 ± 8
Cylindrical fibre detector	0.108 ± 0.013	88 ± 22
Capillary fibre detector	0.057 ± 0.004	167 ± 24
TLD-100	0.480 ± 0.040	20 ± 3

One more important detector performance parameter is irradiation energy dependency. The samples were tested for two available photon energies that are regularly used in radiotherapy, 6 and 20 MV, plus one electron energy at 6 MeV. Irradiations were made using five different doses. The results are presented in Figure 5.6. For each type of TLD sample, there is no significant evidence for a difference in response with energy. In regard to the slope for each type, the maximum variation for the different energies was 11%, 8% and 14%, for the flat, cylindrical and capillary fibres respectively. Moreover, the standard deviations of the energy variation were found to be as low as 0.17 for the flat fibre and 0.05 for both the cylindrical and capillary fibres.

Due to the relative independence to radiation energy for the therapeutic range, to first order, the TL response can be directly related to the delivered radiation dose and not to the choice of energy, varying on average by less than 11% across the energies investigated.

Since it is typical for TLDs to be recalibrated and reused multiple times, a repeatability test has been performed, measuring the variation among four different samples per fibre type over six experimental cycles. Figure 5.7 shows the percentage variation observed over the six cycles. For flat fibre repeatability the variation range is from 5 to 15% for the four different samples. For the cylindrical fibre, the variation range is 11 to 16% while for the capillary fibre it is 11 to 19%; by comparison, for TLD-100, the range variation is 10 to 12%.

Fading analysis results are shown in Figures 5.8a to 5.8c, for the flat, cylindrical and capillary fibres respectively. All fibre samples were irradiated simultaneously, use being made of the 6 MV photon source, to a dose of 8 Gy. The TL yield of each

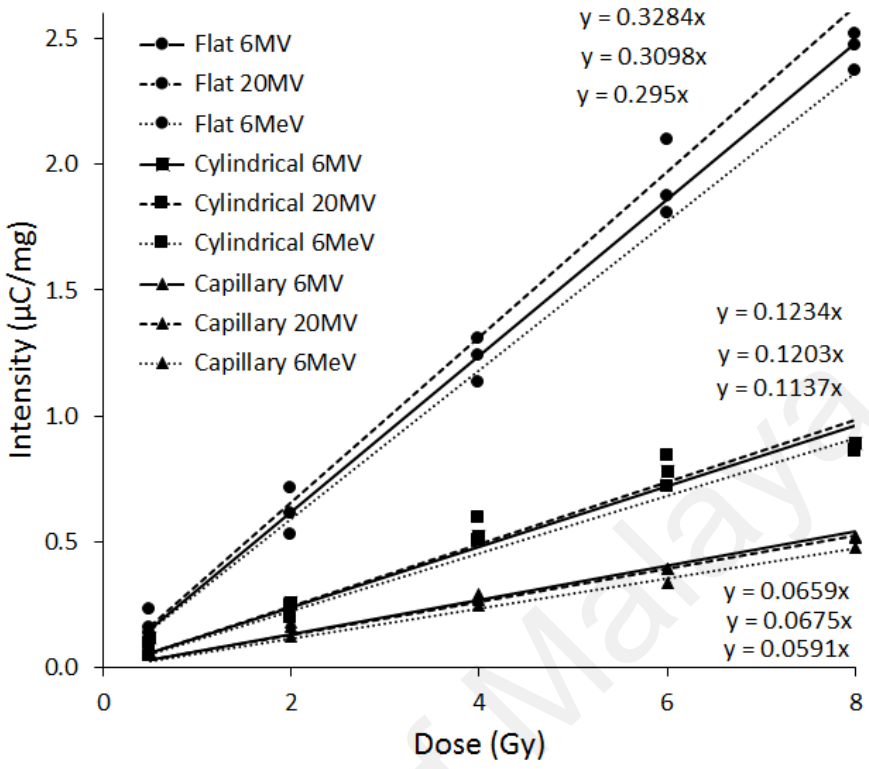

Figure 5.6: Energy dependency of the flat, cylindrical and capillary fibre TLD samples for two different photon energies, generated at 6 and 20 MV, and one electron energy, 6 MeV.

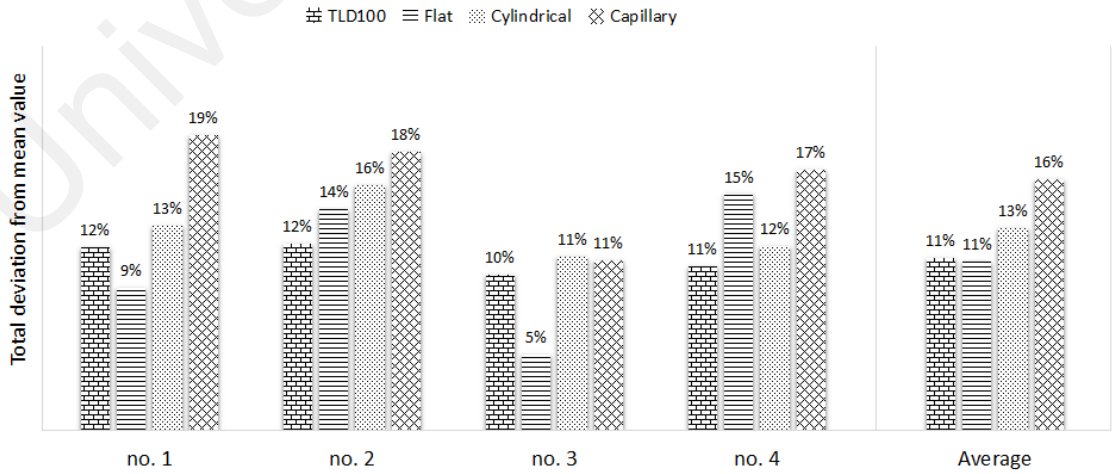

Figure 5.7: Repeatability test for four different samples from each fibre type. Each sample has been reused for six complete cycles and the average results are presented.

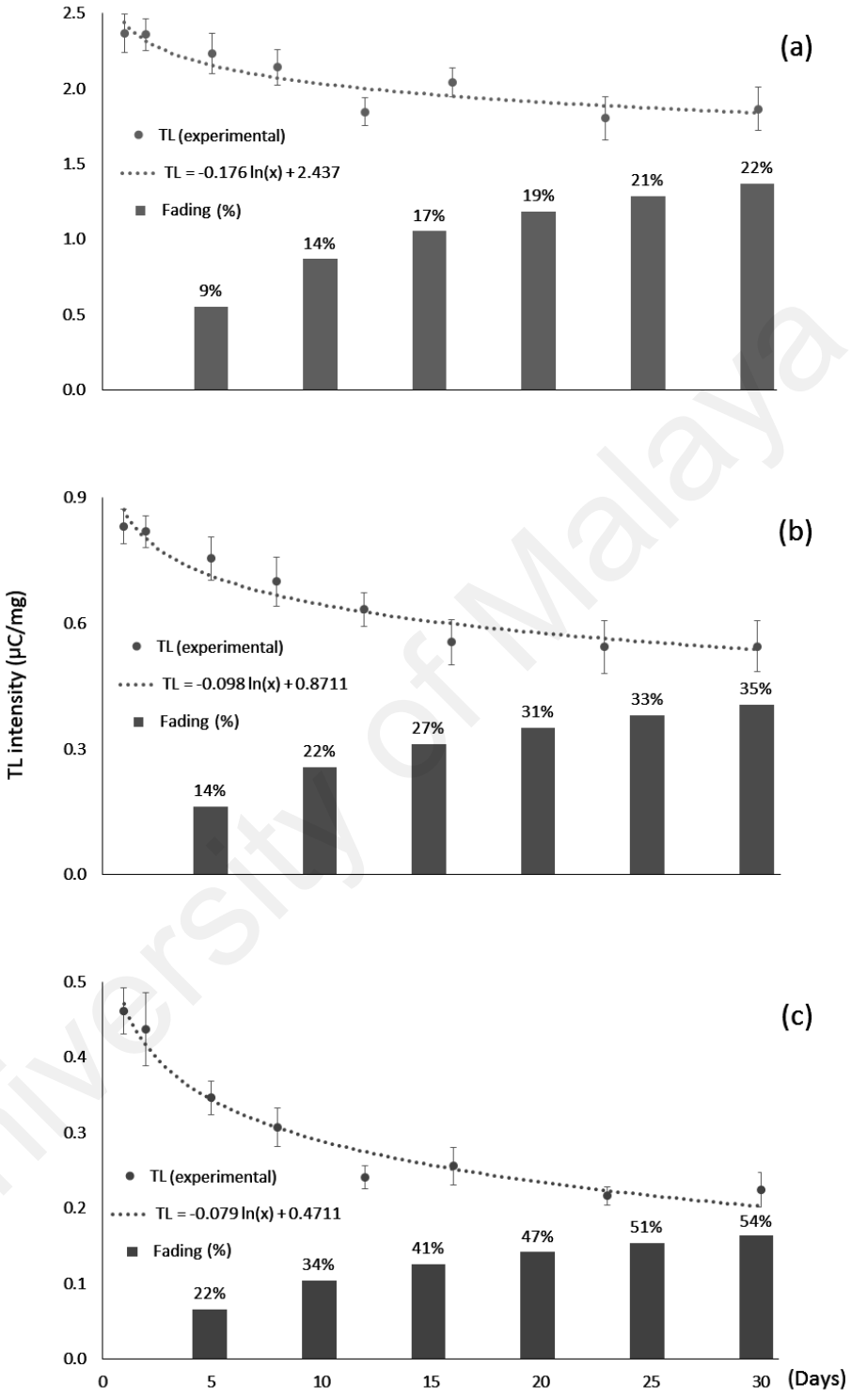

Figure 5.8: Fading of: (a) flat fibre; (b) cylindrical fibre, and; (c) capillary fibre, all for a period of one month subsequent to irradiation to 6 MV photons to a dose of 8 Gy.

set of 5 samples per fibre type were obtained over specified post-irradiation times, from one day to one month post-irradiation. The loss of TL response follows an exponential-like curve, showing rapid fading in the first few days followed by a more linear-like loss subsequently. After 30 days post-irradiation, the TL response for the flat fibre has reduced by 22% compared to that obtained one day after radiation. For the cylindrical and capillary fibres respectively the fading is about 1.6 and 2.5 times greater.

Furthermore, the low fading losses of the flat and cylindrical fibre when compared to that of the capillary fibre is to be noted, supported by the fact that in these two media there are proportionately greater TL contributions from deeper defects, sufficient to retain stable memory of the initially absorbed dose.

5.3 Kinetics study

5.3.1 Group 1

Figure 5.9a to 5.9c show representative glow curves for undoped capillary fibre, flat fibre and PCF, respectively subsequent to 6 and 20 MeV electron irradiation at doses of 4 and 8 Gy. Compared to the capillary fibre, and within the temperature range 250 to 350 °C, a substantial TL increment is observed for both the flat fibre and PCF. This is observed for both 4 and 8 Gy with 6 and 20 MeV irradiation energies. A further observation is the effect of energy on the glow curves, with mild shifts occurring. In the case of the capillary (Figure 5.9a), by increasing the electron energy from 6 to 20 MeV, the glow curve peak shifts towards higher temperature (pointing to deeper trapping levels). The same situation is observed for the PCF (Figure 5.9c). Conversely, an opposite shift is observed in the case of the flat fibre (Figure 5.9b), whereby for an increase in electron energy from 6 to 20 MeV, the glow curve peak shifts towards lower temperature (pointing to more superficial traps). For all of the fibres, glow curve peak shifts in the range 25 to 30 °C are observed. The situation becomes clearer when analysed through use of the computerized glow curve deconvolution (CGCD) method [174], as below.

Glow curve analysis has also been carried out for the undoped fibre samples as

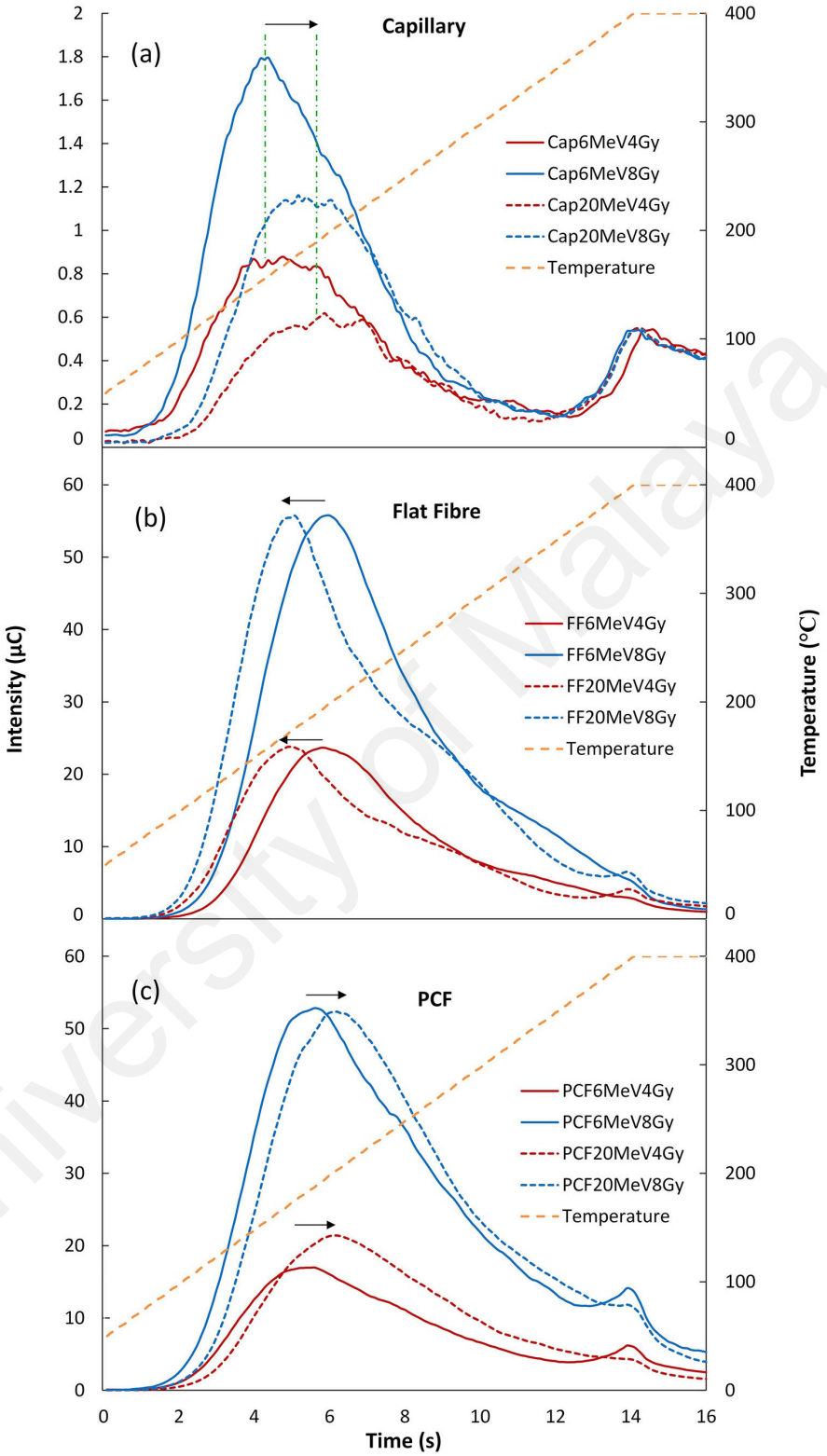

Figure 5.9: Glow curves of undoped fibres following 6 and 20 MeV irradiation at doses of 4 and 8 Gy. (a) Capillary optical fibre, (b) flat fibre, and (c) PCF. Glow curves were shifted by changing the radiation energy.

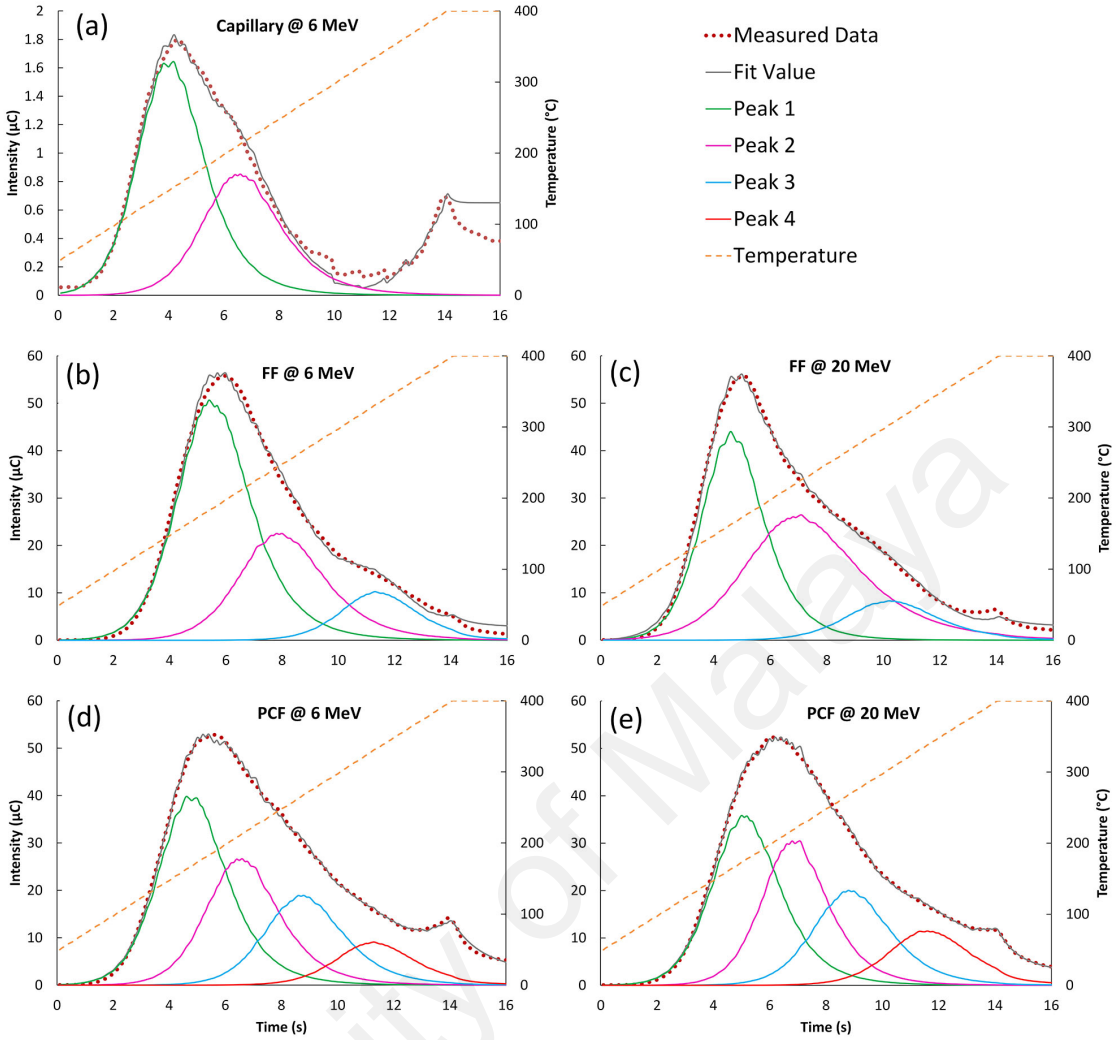

Figure 5.10: Deconvolved glow curves of undoped fibres for irradiations at 6 MeV (left) and 20 MeV (right). (a) Capillary optical fibre at 6 MeV; (b) and (c) flat fibre at 6 and 20 MeV respectively, and; (d) and (e) PCF at 6 and 20 MeV respectively. Each glow peak represents the energy of traps inside the dosimeter media.

shown in Figure 5.10. Using second order kinetics, the CGCD method has been applied in seeking to define the different trapping levels of the various fibre samples. The deconvolved glow peaks of the capillary fibre are shown in Figure 5.10a, accompanied by presentation of the trap energy details in Table 5.2. For this form of fibre, two traps are found, located at peak temperatures of approximately 150 and 210 °C and denoted as peak 1 and peak 2 in the accompanying Tables 5.2, 5.3 and 5.4.

Similar glow peaks to those observed for the capillary fibre are also observed for both the flat fibre and PCF, implying similar (if not the same) defect centres to be present in all of the fibre samples that have been investigated herein. However, additional traps are also observed in the case of the flat fibre and PCF. For the flat

fibre (Figures 5.10b and 5.10c and Table 5.3), peak 3 (T ≈ 300 - 330 °C) indicates the existence of a secondary, deeper trap, strongly suggestive of this being induced in forming of the collapsed wall surfaces during fabrication. In the case of the PCF, in addition to peak 3 a further even deeper secondary trap is observed to exist, as shown in Figures 5.10d and 5.10e with details of the parameters shown in Table 5.4. The two additional traps in PCF, namely peak 3 and peak 4, are also expected to be a direct result of defect generation in the fusing of the capillary wall surfaces. The glow curve analysis observed for 6 and 20 MeV are in good agreement and show that for both trap energies, all the traps are activated and absorbed during irradiation at the particular beam energies.

The increase of activation energy in the PCF and flat fibre glow peaks are in accord with expectation, the traps occurring at higher temperature, commensurate with elevated activation energies. The frequency factor (equivalently S' for second order kinetics) and initial number of trapped electrons n = n_0 (t = 0) have also been calculated together with the FWHM of each of the peaks and relevant emission frequency. Also are shown T_{max}, the temperature of maximum TL intensity, I_{max} (μC), and the time t_{max} along the temperature range at which this was obtained.

Table 5.2: Trap parameters of undoped capillary fibre for the electron radiation energy of 6 MeV.

	Peak 1	Peak 2
Energy (eV)	0.71	0.79
s	526	460
n_0	5.4 E +04	3.3 E +04
FWHM (K)	68	79
Emission (nm)	1758	1565
I_{max} (μC)	1.6	0.9
T_{max} (°C)	153	213
t_{max} (s)	4.2	6.6

Table 5.3: Trap parameters of undoped flat fibre for the electron radiation energies of 6 and 20 MeV.

	6 MeV			20 MeV		
	Trap:1	Trap: 2	Trap: 3	Trap:1	Trap: 2	Trap: 3
E_a (eV)	0.77	0.84	1.30	0.83	0.56	0.99
s	17	14	17711	330	0.02	102
n_0	1.8 E+6	9.4 E+5	3.6 E+5	1.3 E+6	1.5 E+6	3.6 E+5
FWHM (K)	76	85	76	60	113	90
Emission (nm)	1607	1470	954	1497	2203	1251
I_{max} (μC)	51	23	10	44	26	8
T_{max} (°C)	183	248	331	163	226	303
t_{max} (s)	5.4	8	11.3	4.6	7.1	10.2

Table 5.4: Trap parameters of undoped PCF for the electron radiation energies of 6 and 20 MeV.

	6 MeV				20 MeV			
	Trap:1	Trap: 2	Trap: 3	Trap: 4	Trap:1	Trap: 2	Trap: 3	Trap: 4
E_a (eV)	0.76	0.87	1.01	1.24	0.80	1.00	1.05	1.23
s	41	105	369	6723	85	1856	683	2856
n_0	1.4 E +6	9.5 E +5	7.1 E +5	3.4 E +5	1.2 E +6	9.6 E +5	7.3 E +5	4.5 E +5
FWHM (K)	68	72	80	78	67	65	76	80
Emission (nm)	1626	1431	1226	997	1554	1244	1186	1006
I_{max} (μC)	40	27	19	9	36	30	20	11
T_{max} (°C)	163	213	268	331	173	218	268	338
t_{max} (s)	4.6	6.6	8.8	11.3	5	6.8	8.8	11.6

5.3.2 Group 2

The distribution of TL peak intensity provides information on the distribution of electron trap energies, moderated by the particular irradiation conditions and heating rate used. Figures 5.11a to 5.11c are respective SEM cross-section images of cylindrical, capillary and flat fibre samples fabricated for this study. The germanium doped area is the brighter narrow strip within the samples. The TL yield versus readout time continua in Figures 5.11d to 5.11f reveal the uniformity of shape of the glow curves for each of the sample types across the different irradiated doses. Compared with commercial TLDs with thermal luminescence at well-defined temperatures, it is apparent that the fibre TLDs exhibit a broad range of thermal excitation, as expected from an amorphous system. In all optical fibres, the TL glow curves were generated from practically identical time/temperature profiles. Of note are the broad differences between the glow curves of the three types of fibre; the glow curve of the capillary fibre is essentially composed of one centrally located peak producing a maximum intensity value at a temperature of 235 °C (Table 5.5b), the distribution completing at the maximum temperature of 400 °C while for the cylindrical fibre, a small shoulder is seen to initiate at around 330 °C, growing in intensity with dose (Table 5.5a), its full intensity artificially terminating as a result of the maximum temperature of 400 °C. The abrupt termination at the maximum temperature set is indicative of deeper defects within the material, incompletely released as a result of the limited activation energy. This same situation is seen with even greater clarity in the case of the flat fibre glow curves, the deeper and more superficial defects being better resolved as a consequence of more noticeable defect localisation. Other than the fact that the TL intensity of the superficial defects peak in the flat fibre is markedly greater than that of the cylindrical fibre, the small shoulder observed in the cylindrical fibre glow curve is now revealed to be a new/secondary glow peak, peaking in intensity at a temperature of around 380 °C (Table 5.5c). This new source of thermoluminescence in the flat fibre is suggestive of the generation of new defect centres, clearly absent in the capillary fibre. The most apparent outcome of the flat fibre fabrication process is the formation of a

rather extensive fused internal surfaces interface, with other aspects of the treatment remaining otherwise common to that of the other fibre types. This suggests that the new defect centres are a result of the fusing of the Ge-doped layer available in the capillary fibre, fused in the cylindrical fibre during the MCVD process and in the flat fibre during fibre drawing process. The latter method shows a significant improvement to be available in defects generation, thought to be due to the strain induced in the collapsed surfaces and the fast quenching rate in the drawing process, essentially freezing in the material before atomic bonds are formed between the joining wall surfaces.

Figures 5.11g to 5.11i show glow curve deconvolutions for the cylindrical, capillary and flat fibres respectively, computed in accord with second order kinetics, the detailed glow peak parameters being presented in Table 2. For the cylindrical fibre glow curve (Figure 5.11g and Table 5.5a), five main glow peaks are found in which the first three are related to Si-O and Ge-O centres and the last two are Ge structural defects. However, for the capillary fibre glow curve (Figure 5.11h), three main glow peaks are found. Based on the simple shape and fabrication process for the capillary fibres, it is expected that these peaks are also representative of Si-O and Ge-O centres in the fibre. Finally, in Figure 5.11i, the flat fibre glow curve is deconvoluted into five main glow peaks. The first three clearly have the same origins as that of the other two sample types, while the remaining two are Ge structural defects. Although the second peak for both the cylindrical and flat fibres are a result of structural changes, the nature of the peak related defects are expected to be different, with different peak positions (i.e. at different T_{max}) and hence different activation energy. More definitively, the first and second peaks, with activation energies less than 1.2 eV are to be related to the existence of O^+ and O^- in the silica network, while the third peak with energy of round 1.2 - 1.4 eV has to be related to the formation of silicon/germanium nano-clusters in the amorphous silica. The remaining two peaks found within the glow curves for the cylindrical and flat fibre, with energies up to 2.6 eV, are suggested to be due to Ge nano-clusters or ion defects in the fibre [105], or to strain generation.

Table 5.5: Trap parameters for: (a) Ge-doped cylindrical fibre; (b) Ge-doped capillary fibre, and; (c) Ge-doped flat fibre. The glow curve deconvolution was performed based on the second order kinetics model of relation 3.3.

	Left to Right	Peak 1	Peak 2	Peak 3	Peak 4	Peak 5
(a) Cylindrical	E_a (eV)	0.68	1.00	1.19	1.75	2.54
	s	2.95E+02	1.61E+05	1.41E+06	1.92E+10	6.67E+15
	n_0	47553	48973	42877	27791	18380
	T-max	195	235	283	330	375
	FWHM	87	69	72	57	42
	Emission (nm)	1821	1240	1046	710	488
(b) Capillary	E_a (eV)	0.80	1.15	1.38		
	s	2.30E+04	5.59E+06	8.22E+07		
	n_0	25926	43030	24692		
	T-max	185	235	283		
	FWHM	70	60	62		
	Emission (nm)	1547	1078	901		
(c) Flat	E_a (eV)	0.71	0.96	1.37	1.35	1.76
	s	6.46E+02	1.92E+04	4.92E+07	2.07E+06	3.97E+08
	n_0	99219	127066	109376	98402	101067
	T-max	185	235	283	330	380
	FWHM	78	74	62	75	47
	Emission (nm)	1740	1295	904	919	703

At the end, the TL glow curves reveal generation of additional new defects induced due to collapsing of the Ge-doped layer, the deeper traps contributions being greater in the flat fibre. By using CGCD analysis, the original or main peak in all three fibre types is deconvolved into three peaks that are associated with silicon oxygen defect centres (Si-ODCs), Si^{-} and GeO_2 and Si and Ge nano-clusters [86, 105], the numbers of such defects in the flat fibre being significantly greater than that in the cylindrical followed by the capillary fibre. Deconvolution of the newly generated defect peak has pointed to the higher activation energy of these, clearly being of a different nature of defects.

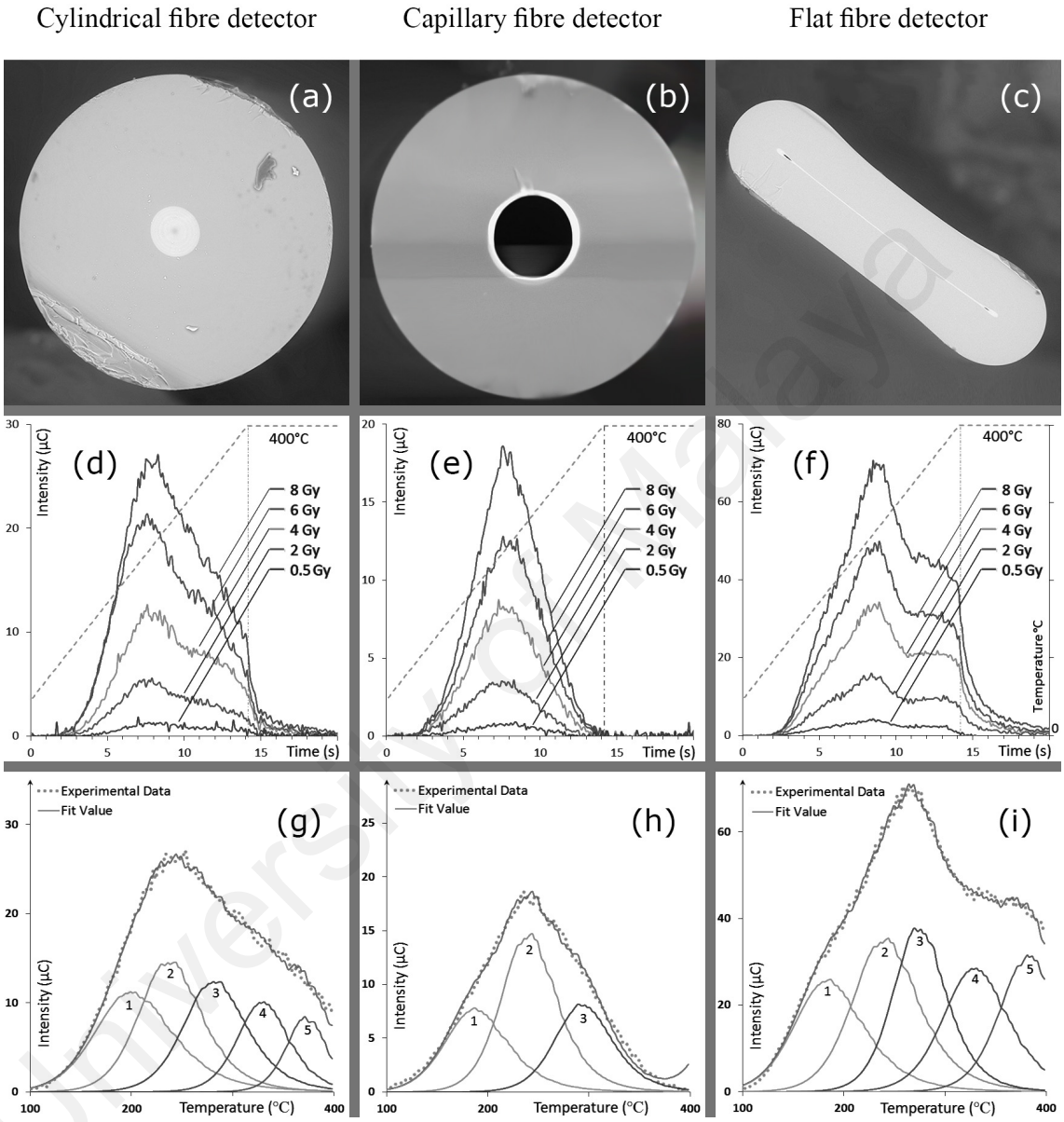

Figure 5.11: Glow curve analysis. The sub-panels (a), (b) and (c) are SEM cross-sectional images for the cylindrical, capillary and flat fibre, respectively; sub-panels (d), (e) and (f) are the respective glow curves obtained using five different doses, provided in the form of TL intensity versus acquisition time, with temperature represented on the right-hand y-axis, and finally; sub-panels, (g), (h) and (i) show the results of glow curve deconvolution calculated according to second-order kinetics modelling for the cylindrical, capillary and flat fibre respectively.

5.4 Chapter summary

Three forms of undoped optical fibres, capillary fibre, flat fibre and PCF have been fabricated and tested for sensitivity towards ionising radiation dose detection. By collapsing the undoped capillary fibre wall so that the internal surfaces fuse, the arrangement forming a flat fibre, it is shown that its TL response increases by some 12 times over that of the undoped capillary fibre. Similar results are observed for the PCF, in which the capillary outer wall surfaces are made to fuse. The PCF is fabricated by stacking an array of capillaries inside a glass tube. In this particular instance, the PCF was formed from 168 stacked capillaries, the TL response of the PCF being some 17 times that of a single capillary optical fibre. These results suggest that by collapsing capillary fibres until their outer surfaces fuse, strained surface defects are generated, the dose detection sensitivity of the product fibre increasing in a commensurate fashion.

In the second part, TL characteristics of three different types of Ge-doped optical fibres i.e., cylindrical, capillary, and flat fibre, all fabricated, using a single preform, have been demonstrated. The TL response of the flat fibre is far superior to that of the cylindrical and capillary fibres, offering greater sensitivity and uniform response throughout the dose range investigated. The results address to additional defect centres produced in the flat fibre, mainly being due to the fusing of the surface of the interior walls of the capillary fibre. These additional defects in the flat fibre are the basis of the improved TL response.

The findings of this study are anticipated to be helpful in the design and fabrication of high sensitivity dosimeter sensors based on optical fibre.

CHAPTER 6: EFFECT OF FIBRE SIZE ON TL RESPONSE

This chapter has shown the effect of size of optical fibres according to their TL responses. Challenges on the effect of methods used for fabrication and normalisation on the TL response are also discussed.

6.1 Introduction

In recent years, study on the fibre dosimetry has started to experimentally grow and the results were incredibly interesting [77]. Generally fibre dosimeters are examined as either thermoluminescence dosimeters (TLD) or optical stimulation luminescence (OSL) dosimetry [79, 88]. Due to the easy accessibility of commercial fibres, most of the studies reported are the response of these fibres with respect to different doses or source [37, 92, 101]. In this way, some also had experiments of optical fibres which they doped by different elements and germanium (Ge) was more interesting dopant among them [37, 92, 98, 101].

Defect structure of optical fibres that rise the TL are mainly because of the dopant inside them [137], however, there might be some extra defects in the fibres with various sizes, which influence their thermoluminescence response and sensitivity. Some sorts of studies about fibre dosimeters with different core-size are done in the range of UVA radiation [175]. In spite of everything, the result is not expandable to all the other range of radiation, exclusively, the smaller core size has shown a better response.

In this study, two types of optical fibres in five sizes are examined for their TL response. The Ge-doped preforms are drawn in the fibre pulling facility to five sizes of cylindrical (SEM images were shown in Figure 3.14) and flat fibres (SEM image in Figure 3.15) with core and cladding to guide the waves. Hence, the experiments are done to clarify the effect of fibre size in the TL response.

6.2 Results and discussions

This study is investigating the effective parameter on enhancing the TL response to optical fibre base on dosimeters, which are subjected to their size. Glow curve of different fibre sizes for both Ge-doped cylindrical and flat fibre are shown in Figure 6.1b and 6.1d. Also, the effect of different doses on the glow curve of the samples are shown in Figure 6.1a (for 604 μm cylindrical fibre) and 6.1c (for 620 μ $\times$ 170 μm flat fibre). As it found out in Figure 6.1, there is no significant deference in the shape of the glow curves for various sizes and doses, but, the intensity of them is increased by enlarging the size and increasing the dose as they were expected. The same shape of the glow curves ensures that the comparison between the sizes are done in uniform conditions.

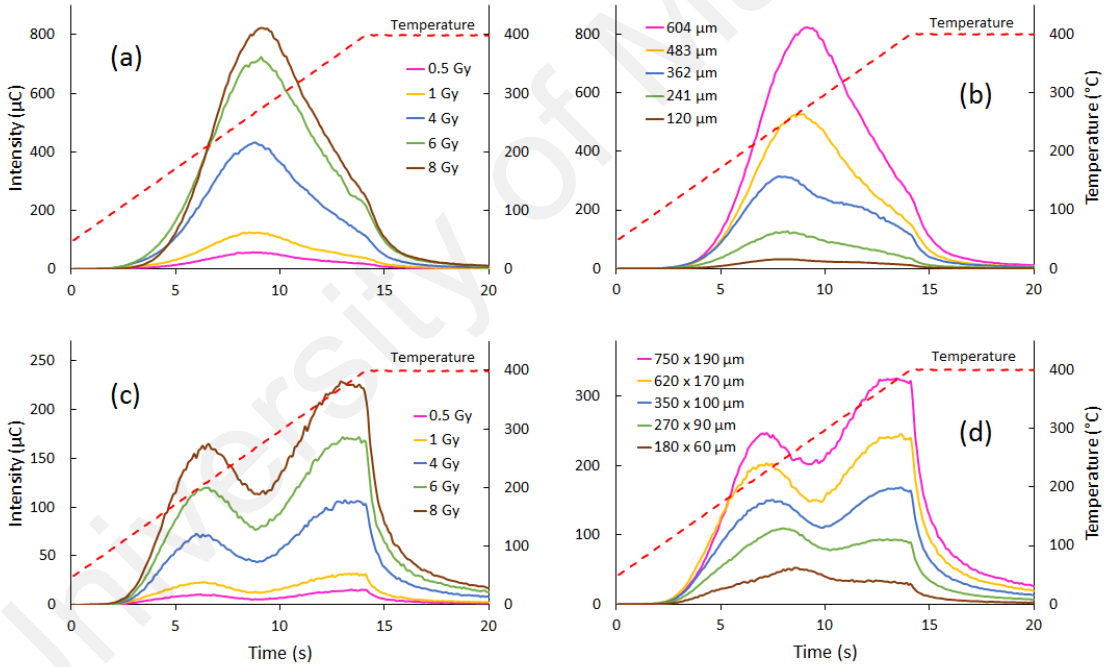

Figure 6.1: Glow curves of cylindrical fibre samples a) the thickest size (604 μm) in five doses b) all sizes in 8 Gy; Glow curve of flat fibre samples a) the thickest size (620 $\times$ 170 μm) in five doses b) all sizes in 8 Gy.

In the Figure 6.2 thermoluminescence response of the cylindrical fibre are shown for all the sizes before normalisation. Increase in the response of the samples has mostly a direct relation with the cross-section diameter of the fibres. Since the density of all the sizes with same percentage of dopant is same, it is concluded the TL response, which has a direct relation with root square of mass of the samples.

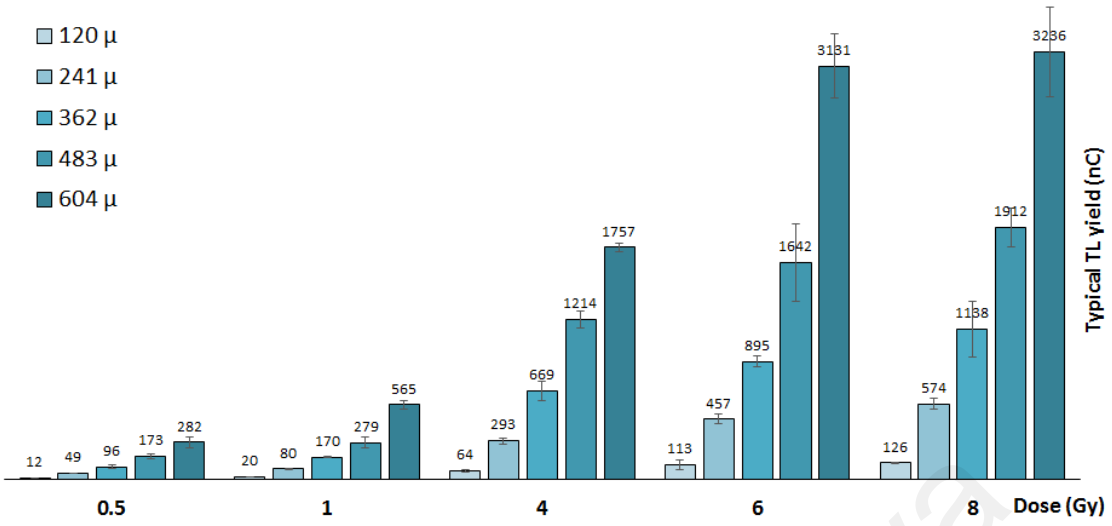

Figure 6.2: Typical TL absorbance of the samples with different sizes with different doses for Ge-doped cylindrical fibre.

This pattern is repeated in all the doses from 0.5 Gy to 8 Gy. Although, there are some deviations from the pattern, they could be due to errors during the experiment and/or sample preparation. The error bars provide evidence of these errors and are calculated with standard deviation formula according to the many tested samples.

After all, the response of the cylindrical fibre samples were normalised to their weight as shown in Figure 6.3. Considering the errors in the sample preparation and measurements, the normalised response of doses are drown from same preform are almost same. This can be supported by the finding of Lyytikainen et.al. [137]. They found that the diameter of preform had no magnificent effect on the diffusion of dopant during the fabrication, which is the main cause of TL activity inside the doped fibres. The variation in the biggest size samples (483 & 604 μm) is mainly due to the cutting process during the preparation of them. It is widely happen the edge of those samples with big diameters breaks and cause error in scale measurement.

Table 6.1: Correlation of dose dependency of the response of each cylindrical fibre sample.

	604 μm	483 μm	362 μm	241 μm	120 μm
dose dependency correlation	0.9848	0.9917	0.9971	0.9992	0.9998

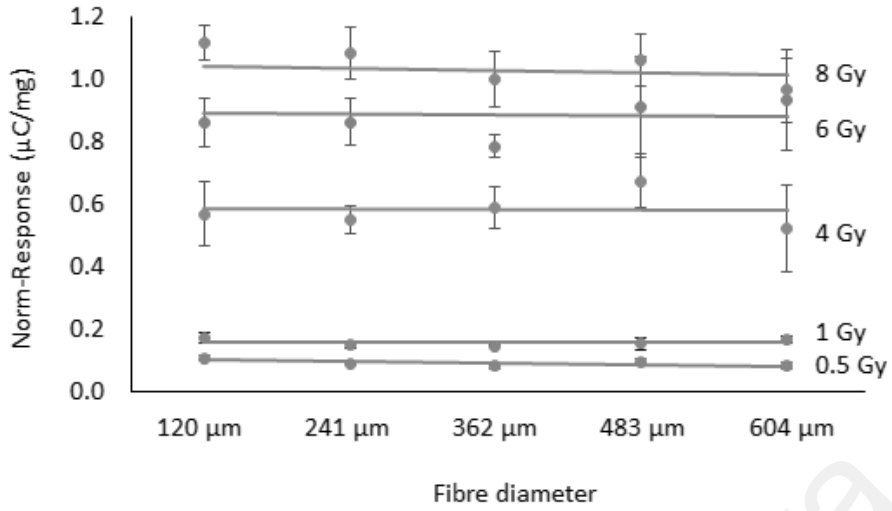

Figure 6.3: Normalized response against fibre size for cylindrical fibre.

Dose dependency correlation for each samples is calculated and results are reflected in Table 6.1. A linear relationship between dependent variable (response) and independent variable (dose) will be indicated, once the correlation is greater than 0.8. Fortunately for all the samples, the correlation value is higher than 0.9800 and it means the samples are depending upon the dose in the experimented interval can be surely linear.

In Figure 6.4 the trendline for each sample data is plotted linear as it discussed in Table 6.1. In these figures the response of each sample is normalised to its weight. It makes possible more convenient comparison between sizes. However, it is seen that the normalised response of the samples is not depends on the size.

Further work is done to figure out the effective parameter in the doped optical fibres subject to their TL response related to fibre size by examining a fibre with constant core size but different cladding diameters. The purpose of this experiment is to find out how cladding can impact on the TL response of optical fibres. The fibre is chosen were 604 μm cylindrical Ge-doped fibre and etching method is used to reduce the cladding thickness. Five pieces of the fibre are kept inside the HF acid and each removed after a fixed period. To make sure about uniform solvation of cladding material in to the acid, the fibres were rotated and regularly moved. The relation between the etching duration and remained mass is given in Figure 6.5a – inset. This linear decrease of weight according to the etching duration is important

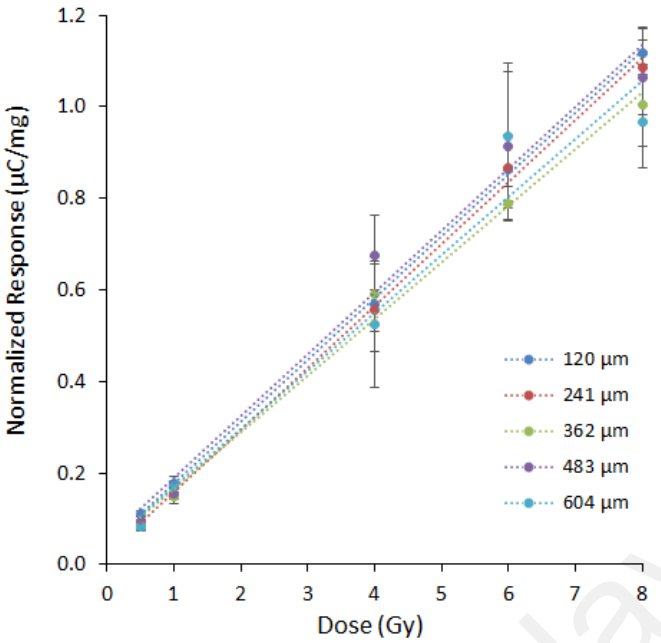

Figure 6.4: Normalized TL response for Ge doped cylindrical fibre in five different sizes.

for comparison of the yielded samples in following steps. In Figure 6.5a, it is shown that by removing the cladding of the doped fibre, the TL response of the fibre is not changing. After normalising the same result to their weights (Figure 6.5b), the results follow the second order polynomial, which support the diminished surface size (πr^2) for circular cross section fibre.

After examining the cylindrical fibre over different sizes, these tests were repeated for another types of fibre which were flat fibre. Again five sets of flat fibre size were chosen and irradiated to doses from 0.5 Gy up to 8 Gy. The typical response is

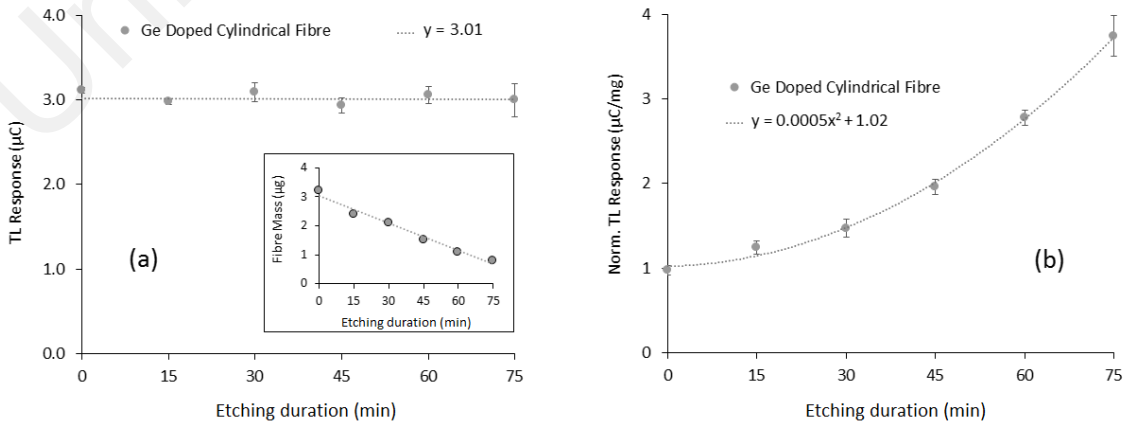

Figure 6.5: Etching results for cylindrical fibre, a) not normalised results – inset: amount of etching - etching duration, b) normalised results for 5 etched samples and one not etched.

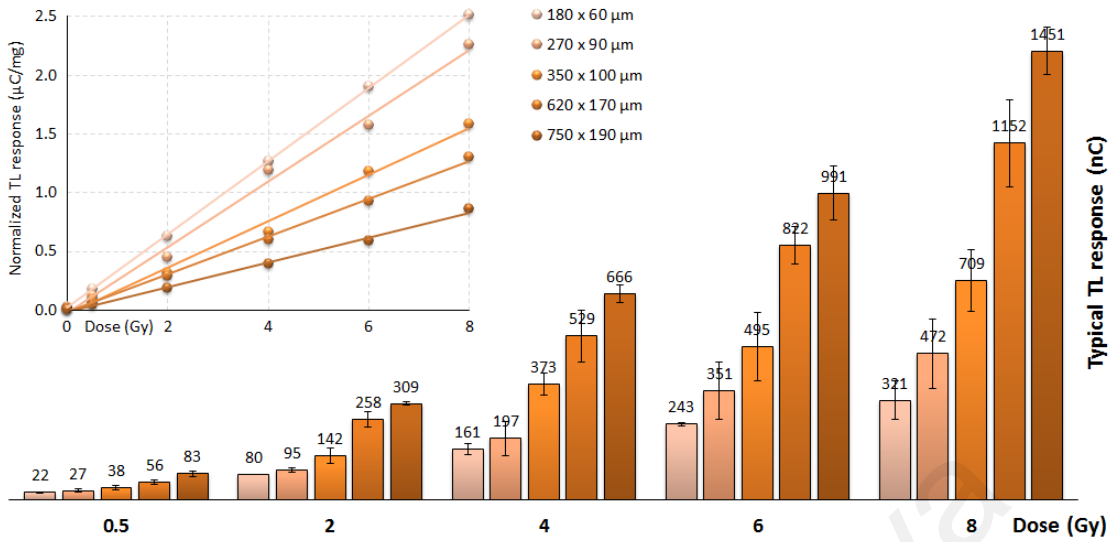

Figure 6.6: Typical absorbance of the samples in different doses for Ge-doped Flat fibre – inset: Normalized TL response for Ge doped flat fibre in five different sizes.

shown in Figure 6.6 for all sizes and doses. The inset indicates the normalised results over sample mass, which can be still linear. Despite the cylindrical fibre, in the discussed flat fibre, by increasing the fibre size, the TL response slightly decreases (Figure 6.6-inset). Because of the same material, it could be explained by considering fabrication induced defects, which were appeared inside the core or cladding due to mechanical stress and quenching. Improving or weakening the defects in sensitivity of fibre dosimeter, which is out of the scope of this study. However, it is necessary to find how cladding is influencing on TL response of flat fibre. For this purpose, the 750×190 μm flat fibre is etched five times and each time for eight minutes. Soon after, each etched sample is irradiated to 8 Gy, 6 MV photon source and the TL response is plotted in Figure 6.7a. The co-relationship between the duration of etching and level of corrosion of cladding is extremely linear, which has been illustrated in inset. In Figure 6.7.b the TL results are normalised to the samples' weights. The growing normalised responses over increasing etch duration shows the high offset to second order polynomial. According to Figure 6.7, cladding is also not responsible for the TL response of the flat fibre.

As a final point the sensitivity of different fibre sizes were calculated for each batch of samples. The sensitivity of the samples are calculated and the results are shown in Figure 6.8 for both cylindrical and flat fibres.

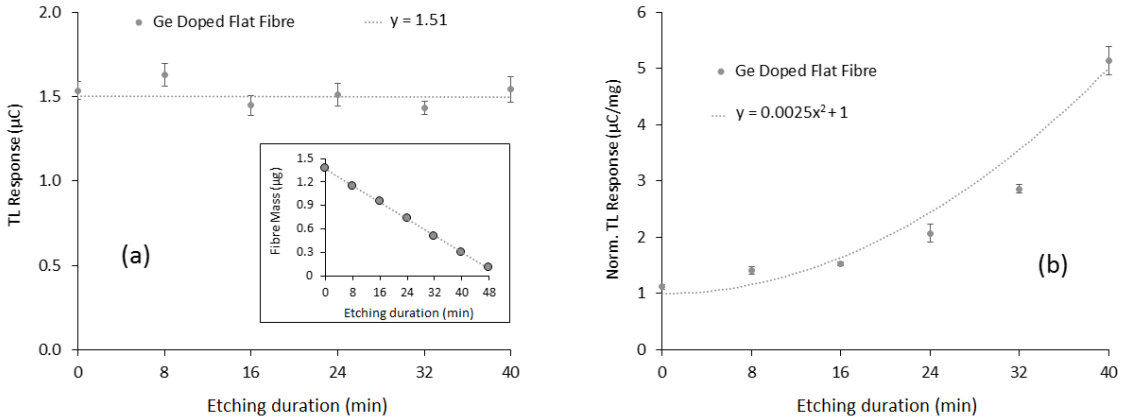

Figure 6.7: Etching results for flat fibre, a) not normalised results – inset: amount of etching - etching duration, b) normalised results of 5 etched samples a not etched.

As it is expected, for cylindrical fibre in different sizes, the sensitivity is similar over variety of fibre size, however, by increasing the irradiated dose, the sensitivity is reduced by a moderate slop (Figure 6.8a). On the other hand, flat fibre sensitivity is very much flat over different doses (figure 6.8b), however, as it was discussed earlier, they are size dependent, which can be achieved the opportunity to choose the appropriate detector for desired application by changing the size of flat fibres.

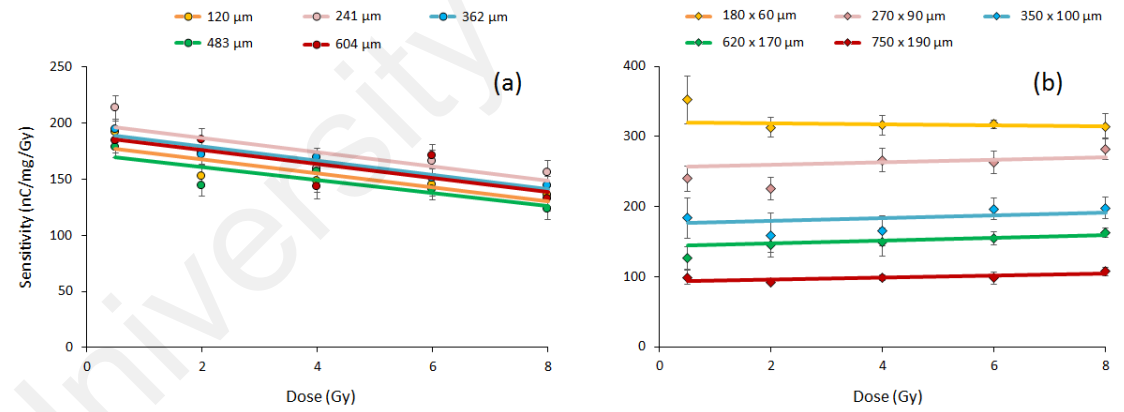

Figure 6.8: sensitivity of: a) cylindrical fibre, b) FF, subject to fibre size.

Normalisation via volume instead of weight

In addition to the above results, three extra studies have been done which are related to this result. The first was to find the accuracy of normalisation to weight. Since the mass of fibre segments are less than 400 μg, there can be some errors in the weight measurements that accordingly affect our results. Therefore, two sets of Ge-doped fibres were chosen to be normalised by their volume in which their lengths

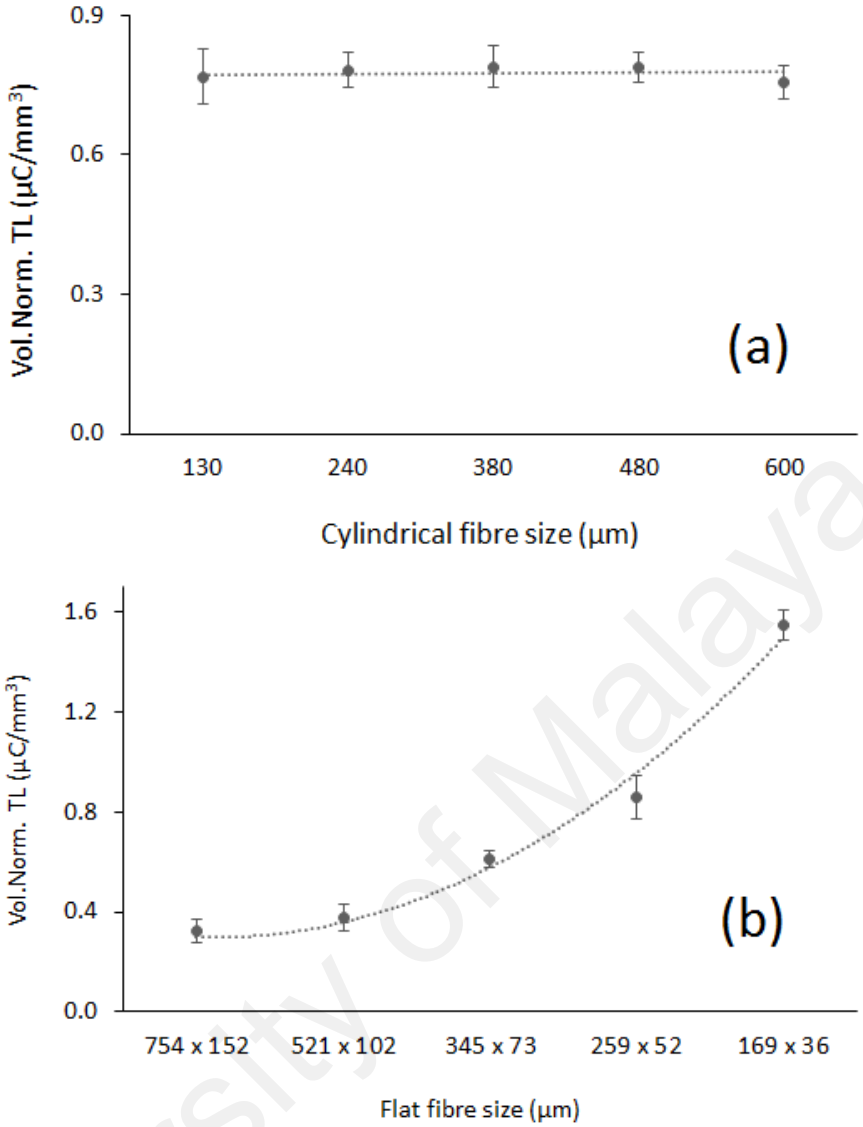

Figure 6.9: TL response of different fibre sizes normalised by their volume; (a) cylindrical fibres (b) flat fibres.

and surface dimensions were individually measured under the electronic microscope. The first set consists in five different sizes of cylindrical fibres (Figure 6.9a) and the second set in five different sizes of flat fibres (Figure 6.9b). Since the density of the fibres in different sizes is constant, it can be assumed that normalisation to their volume should show the same behaviour as normalised result to weight.

The results observed in this highly-precise measurement is in agreement with the observations using sample-mass for normalisation. Figure 6.9a shows that fabricating different sizes of optical fibres from a preform with the same core-to-cladding ratio, results in the similar TL response. Furthermore, for the case of FF, different sizes of FFs fabricated from the same preform provide different TL responses. The

smaller fibre, provides larger TL response. It should be noted that the detail of this behaviour is still under the study with the group for carefully addressing the reasons behind. Based on the preliminary observation, this effect is expected to be due to the collapsing method, the area of collapsing region, and the fusing condition. For better understanding, few other experiments are performed on FF fabrication methods as presented in the following.

Influence of collapsing condition and uniformity in fabricating FF on TL response

Since all the FF samples presented above were fabricated directly from a hollow preform/capillary into flat shape, there is some probability that the collapsing condition in fabricating different sizes might not be exactly the same. To study this probability, a greater FF cane ($\sim$ 1 mm $\times$ $\sim$ 3 mm), is fabricated directly from the preform. This FF cane is then used to redrawn five fibres with different smaller sizes. By this experiment, the probability of having different fusing condition for different size of FF is reduced.

Figure 6.10 shows the TL response of these five sizes of the FFs. As the result implies, the effect of FF size on TL response is still obvious. As observed earlier, the smaller FF can contribute higher TL compared to the greater size.

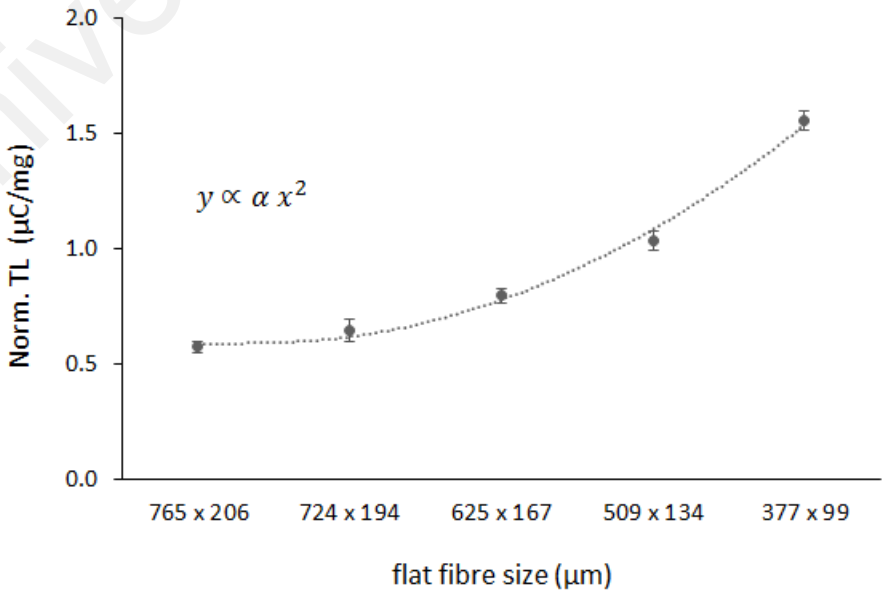

Figure 6.10: Five sizes of flat fibre fabricated using the same FF.

Effect of different collapsing methods for making flat fibre on TL response

To finalise this chapter, the effect of collapsing method for making flat fibre samples was investigated according to their TL yields. Flat fibre samples were made in three different ways.

The first method (which is the main method used in this study for fabricating all FFs presented in previous sections, unless the FFs in this section and in Figure 6.10) is based on capillary-into-flat (labelled as "*cap to ff*") fibre, which a greater capillary or hollow preform is used for direct pulling down into flat shape fibres.

In the second method, a capillary cane ($\sim$ 2 mm diameter) is utilised to convert into flat fibre without the fibre undergo any drawing process. Instead, the capillary cane converted into flat shape by applying a vacuum pressure form the top of the capillary, while, it was annealed in the furnace at high temperature, $\sim$ 2100 °C, and very slowly moved towards down in the furnace, labelled here as "*FF*".

In the third method, the same flat fibre that its result shown in Figure 6.10 is utilised, where a smaller size "*FF*" is fabricated from a great FF cane, labelled here as "*FF to ff*".

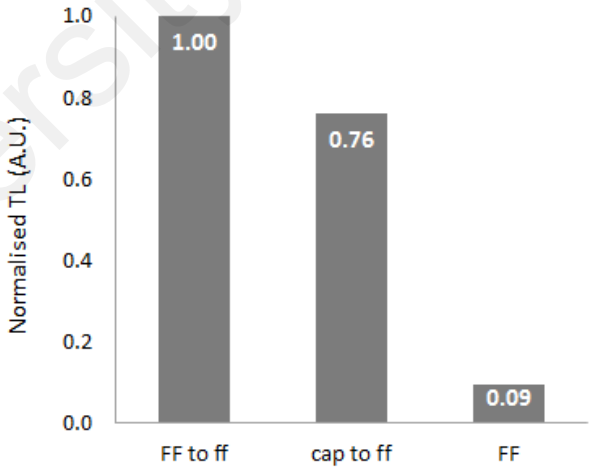

Figure 6.11: Comparison of three different flat fibres according to collapsing method during the fabrication.

As it is shown in Figure 6.11, among these three types of flat fibre, *FF to ff* had the best TL response with less than 1.2% variations. While, the response of *cap to ff* with 3.8% variations is not too far from the *FF to ff*, the TL response of *FF* with 2.4% variation is way far from the other two samples.

6.3 Chapter summary

The impact of fibre size on the thermoluminescence response is discussed in this paper. As the point has been reached to clinical dose range of photon irradiation, so the cylindrical fibre TL dosimeters are not size dependent. To use of bigger size can offer an easier handling and managing, merely, can exhaust more material to fabricate. On the other hand, the use of small samples are sometimes advise when it is necessary to measure the sensitive and narrow area – like the facial area under irradiation treatment. Likewise, regardless of the material of fibres the response will increase related to the square of fibre diameter. The results were proved by statistical tests.

Unlike cylindrical fibres, flat fibres are shown to be size dependent, where a smaller size can contribute to higher TL yield compared to greater size. Furthermore, FFs offer more uniform and flat sensitivity over different doses compared to cylindrical fibres.

Different methods for fabricating FF show that more TL can be obtained with a FF that is fabricated from a FF cane. Overall, the results related to FFs open a new window for further study and development of new types of dosimeters with higher sensitivity by optimising the fibre size and the method of fabrication.

CHAPTER 7: GE-DOPING CONCENTRATION VERSUS TL RESPONSE

In this chapter the effect of different concentrations of germanium, which is doped inside the fibre core are investigated to find the optimum concentration for higher TL generation among the available Ge-doped fibres.

7.1 Introduction

As the interest in fibre optic thermoluminescence dosimeters arising in worldwide, a deep study on optical fibres are getting important to achieve more goals about dosimetry aspects. Effect of different dopant material have been discussed and optical fibre with various cross sectional shape and size were studied in previous chapters. Since, Ge has been shown to be amongst the best elements for improving TL response of optical fibres since recent years, in this chapter, it has been attempted to find the optimum Ge concentrations by evaluating ten Ge-doped fibres doped with different concentrations (whereas, eight of them are fabricated in association with this study in the lab, while the other two were from commercial SMFs). To the best of our knowledge, such investigation showing the optimum Ge concentration for generating higher luminescence is never reported.

7.2 Results and discussions

The concentration study were done on 10 available concentration of germanium doped fibres. All the samples were exposed to 6 MV photon irradiation at 8 Gy dose with completely the same procedure. The TL response of each fibre is then normalised considering both weight and the effect of core size.

The effect of core size is considered in the normalisation by assuming the main TL generated from fibre core, where Ge is incorporated. Table 7.1 shows the detail of TL response and normalisation per fibre. Figure 7.1 shows the TL response of optical fibres with different Ge concentration, normalised to both mass and fibre

Table 7.1: Analysis of different concentrations of Ge-doped fibres by considering core size correction factor.

Attribute	Germanium Weight%	Norm. TL (μC/mg)	Size correction (core : cladding)	Homogenised TL after correction
Ge01	0.7	0.20	0.004	45
Ge02	3.1	3.68	0.067	55
Ge03	3.8	3.04	0.038	79
Ge04	4.3	2.01	0.004	542
Ge05	4.9	14.15	0.005	2658
Ge06	6.3	0.45	0.003	148
Ge07	7.0	2.51	0.049	52
Ge08	8.2	1.05	0.025	42
Ge09	12.1	0.77	0.024	32
Ge10	16.7	0.64	0.021	30

core-to-cladding ration. As it comes to the sight, the best responses have been taken in the range of 4 - 6 weight percent of germanium. The peak at 4.9 belongs to the fibre, which was discussed in Chapter 4 (labeled as SMF-1) and introduced as a fibre which its response could beat the TLD-100. As the detail of material concentration measurements are presented in Chapter 3, the concentration of each fibre were measured several times from different fibre samples and different segments from each fibre core, where the average concentration is used in the optimum concentration analysis.

Figure 7.1 illustrates both home-made and commercial Ge-doped optical fibres. However, the two fibres with highest responses were both commercial fibres. Since though, another comparison were done, but this time with only the fibres which were fabricated at our fibre pulling laboratory. This comparison is plotted in Figure 7.2. As it can be seen, still the best response belongs to the range of 4 - 7 weight percentage of Ge-doped fibres, which supports the results presented in Figure 7.1.

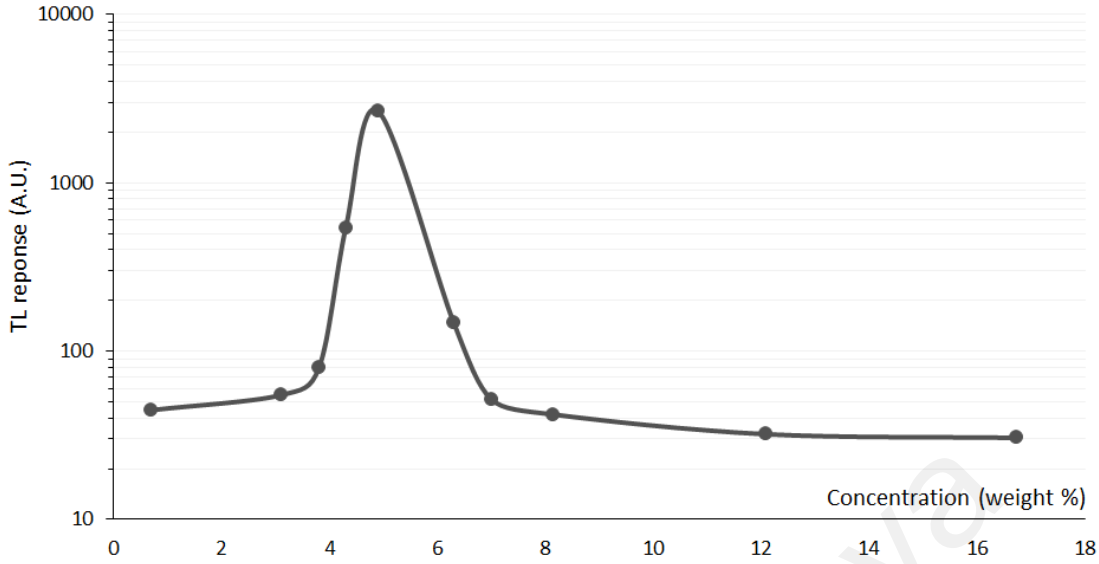

Figure 7.1: Normalised TL response after core size correction.

Since almost all the TL responses emerge from the doped area, which is core in the case of silica based optical fibres, the effect of core size need to be taken into consideration. For this purpose, after reading the raw TL data from the reader and normalising them to their weights, the relation of core area in comparison with the cladding area were calculated (as it has been brought to Table 7.1) and the normalised TL responses were divided by this correction factor.

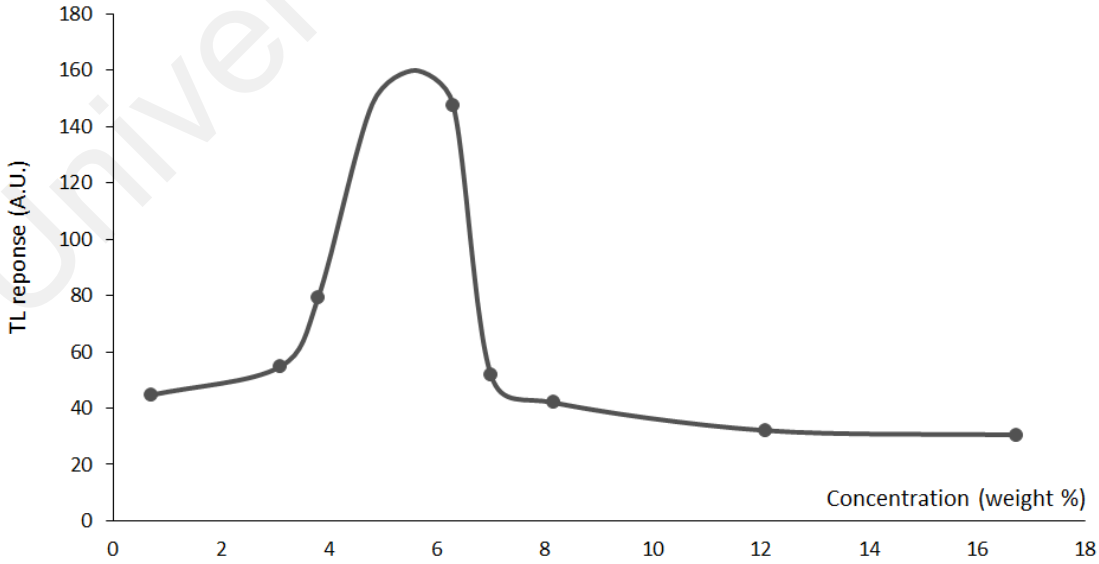

Figure 7.2: Normalised TL response after core size correction in absence of commercial Ge-doped optical fibres.

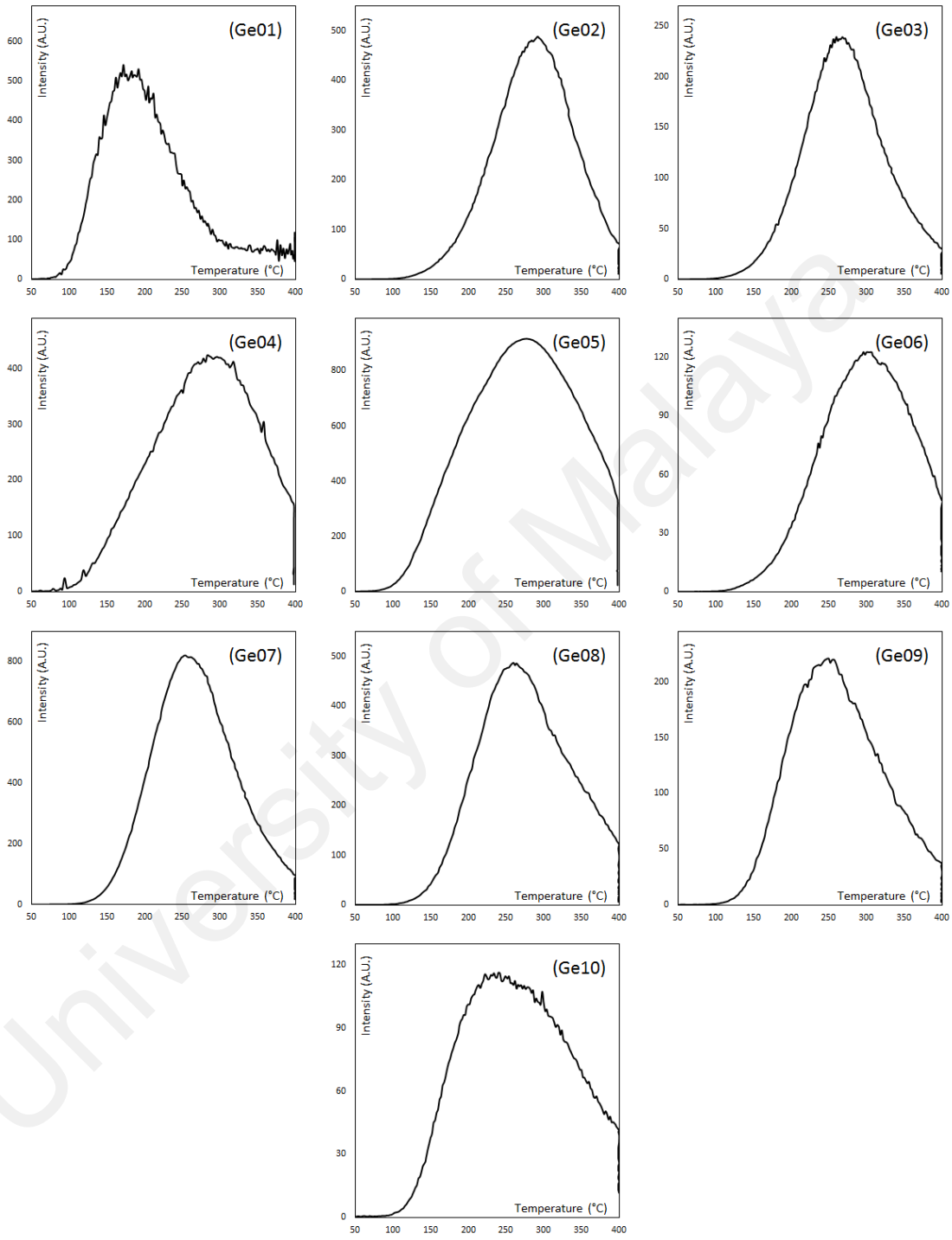

Figure 7.3: Glow curve of different concentrations of Ge-doped fibres starting from Ge01 with about 0.7% of germanium up to Ge10 with more than 16% germanium at the core of the fibre.

Figure 7.3 shows the glow curves of each fibres used in concentration study. The uniform shapes of glow curves for different fibres offer the correct choice as different glow curve shapes may state that other parameters such as additional dopant, fabrication enhancement or impurity may involve in the study and the specific fibre without uniform glow curve should be removed from the comparison. As shown in Figure 7.3, a wide single peak can be a similar characteristics of each glow curve.

7.3 Chapter summary

By comparing ten different Ge-doped silica based optical fibres in which their germanium concentration varies from as low as 0.7 % in weight up to about 16 % in weight, the best fibre is chosen as it was carried 4.9 % of germanium in weight. It seems that the range of 4 % to 6 % germanium in weight offer the highest TL response as a TLD. Possessing these results for the first time, will lead the researches to optimise the intensity of TL response of fibre TLDs and designing at high sensitive TLD considering flat fibre structure with this optimum Ge concentration.

CHAPTER 8: CONCLUSIONS

This study is performed with the main aim of investigating the effect of optical fibre physical parameters such as shape and size, the effect of doping concentration and different dopants on performance of TL response. These objectives are managed and achieved by developing several classical approaches as presented in previous chapters. A summary of the findings and contributions of this study are highlighted in the following in respect to the objectives.

The study has been started by characterising a couple of standard SMFs in comparison with a commercially available dosimeter material (here TLD-100) to understand their dosimetric properties and behaviours. Through that study, it is shown that

1. with the optical fibre technology, going beyond sensitivity of commercial dosimeter sensors is feasible even with a commercially available optical fibre;

2. two closely similar conventional SMFs might have very different dosimetric behaviours, which gives the warning of low trust-ability to derive an investigation reliance to the commercial fibres fabricated from different manufacturers, and emphasising the necessity of developing a classical approaches to understand the behaviour of optical fibres versus variation of different physical/fabrication parameters.

In another study, the optical fibres with different structures including undoped and doped fibres have been used. The findings of that study can be listed as following:

1. Fusing/collapsing of optical fibre surfaces during the fabrication process can significantly increase dose detection sensitivity of optical fibres, especially if there exist some impurity/dopant element in the collapsing region.

2. According the term of value of sensitivity, the detected dose by PCF can be

reached to multiple times of a capillary, mainly due to the fusing of capillary's outer surfaces in PCF.

3. This is confirmed by developing a novel shape flat optical fibre, which consists of only one capillary fibre collapsed in the form of flat shape but with multiple times more sensitivity than a capillary. In fact, development of flat fibre as a potential radiation dosimeter is one of the main contribution of this study.

4. The TL response of a FF can be increased tremendously if some doping element exist in the collapsing region, compared to the undoped FF. However, the level of improvement of TL response in a Ge-doped capillary compared to undoped capillary is minor.

5. To compare among the Ge-doped capillary, cylindrical and FF fabricated from the same preform, FF has shown the highest level of sensitivity.

6. In terms of dosimeter characteristics; including linearity, sensitivity, fading, repeatability, minimum dose detection, energy dependency, and dose dependency, FF behaves better than the rest, therefore, suitability of FF as a potential radiation dosimeter has confirmed.

7. By the aid of glow curve deconvolution, it has been shown that FF has been provided an additional glow peaks at the higher temperature has been suggested new structural defects with the higher activation energy, where such glow peak was not originally observed in the capillary fibre.

8. Referring to kinetics parameters of cylindrical and flat fibres, it is shown that although the two extra glow peaks in cylindrical and flat fibres, which are the issue of collapsing either to the flat or conventional cylindrical shape, however, they have different kinetics and they are developed by O^{-}/OH contents followed by strain stress structural defects. Besides, the first three peaks of them have been found in capillary fibre, the reason can be Si-O and Ge-O centres (nano-clusters).

The effect of optical fibre size for both cylindrical and flat fibres on TL response of optical fibres are investigated. The outcome of the study can be listed as following:

1. By fabricating and evaluating performance of five different sizes of cylindrical fibres, it is found that the fibre size does not have significant effect on TL response of optical fibre if the core-to-cladding ratio of the fibres are the same.

2. Unlike the cylindrical fibres, the effect of size in flat fibre is shown to be significant, where the smallest fibre contributes higher luminescence compared to the greater one. Similar property is observed in FFs fabricated with different collapsing methods.

3. The effect of different methods of flat fibre fabrications, i.e., the method of collapsing, is investigated and confirms that a higher-sensitive radiation dose detection fibre would be the one that collapsed during the fibre drawing process, instead of collapsed in the furnace without experiences any strain stress.

4. By removing the cladding of an optical fibre using HF acid, it has been shown that the main source of TL is from the fibre core.

5. A fibre with larger core-to-cladding ratio contributes higher TL response normalised to the unit mass.

Further investigation is performed by fabricating few doped optical fibres and examining their TL response and glow curve analysis. The finding of the study is that:

1. The highest dose detection sensitivity is observed using Ge-doped fibres compared to the other tested dopants in this study.

2. Those co-doped fibres with the element of Tm exhibit significantly lower sensitivity to therapeutical dose range radiation, suggesting potentially suitable fibres for higher radiation doses.

3. The Tm-Al co-doped fibre shows a meaningful sensitivity at high dose up to 100 kGy which can suggest a suitable dopant to design a fibre dosimeter for high dose radiation.

Investigation on the effect of Ge-doped fibres with ten different concentrations is demonstrated from 0.7 to 16 wt.% showing that:

1. The optimum Ge concentration for highest dose detection sensitivity without considering the commercial SMFs is observed to be around 4 - 7 wt.%.

2. With considering the commercial optical fibres, this optimum concentration is observed around 4 - 6 wt.%.

Overall, the findings of current study can be useful for designing a suitable optical fibre dosimeter for different range of dose detection, specially higher-sensitive radiation dose detection (or insensitive optical fibres) considering the effect of fibre shape, size, doped elements, and Ge-concentration. The dosimetric characterisation of optical fibres strongly suggests optical fibre technology to provide a promising basis for developing the next generation at high sensitivity (or insensitive) irradiation dosimeters for wide range of ionising radiation doses.

Future Research Directions

This study mainly focused on the fabrication and evaluation of the tailor made optical fibres with different shape, size, elements, and concentrations. However, due to the limitation of accessing to microscopic measurements, some fundamental elemental/chemical analysis such as defect centre analysis, the applied stress-analysis in collapsed fibres, the spectrum range of luminescence for different types/structures of optical fibres specially doped with rare elements are the potential area to be studied in the future.

In addition, the optical fibres tested in this study are examined over a fixed range of doses with three radiation sources; thus, the study of wider range of doses and other radiation sources can be the potential topics for future studies.

REFERENCES

[1] G. Amouzad Mahdiraji, E. Dermosesian, M. Safari, F. R. Mahamd Adikan, and D. Bradley, "Collapsed-hole Ge-doped photonic crystal fiber as a diagnostic radiation dosimeter," *Journal of Lightwave Technology*, 2015. xv

[2] J. L. Anderson, R. D. Daniels, D. A. Fleming, and C. Y. Tseng, "Exposure assessment for a cohort of workers at a former uranium processing facility," *J Expo Sci Environ Epidemiol*, vol. 22, no. 4, pp. 324–30, 2012. 1

[3] X. Deng, E. R. Hofmann, A. Villanueva, O. Hobert, P. Capodieci, D. R. Veach, X. Yin, L. Campodonico, A. Glekas, C. Cordon-Cardo, B. Clarkson, W. G. Bornmann, Z. Fuks, M. O. Hengartner, and R. Kolesnick, "Caenorhabditis elegans ABL-1 antagonizes p53-mediated germline apoptosis after ionizing irradiation," *Nat Genet*, vol. 36, no. 8, pp. 906–12, 2004. 1

[4] M. Drouet, F. Mourcin, N. Grenier, C. Delaunay, J. F. Mayol, J. J. Lataillade, A. Peinnequin, and F. Herodin, "Mesenchymal stem cells rescue cd34+ cells from radiation-induced apoptosis and sustain hematopoietic reconstitution after coculture and cografting in lethally irradiated baboons: is autologous stem cell therapy in nuclear accident settings hype or reality?" *Bone Marrow Transplant*, vol. 35, no. 12, pp. 1201–9, 2005. 1

[5] C. L. White, T. Menghistu, K. R. Twigger, P. F. Searle, S. A. Bhide, R. G. Vile, A. A. Melcher, H. S. Pandha, and K. J. Harrington, "Escherichia coli nitroreductase plus CB1954 enhances the effect of radiotherapy in vitro and in vivo," *Gene Ther*, vol. 15, no. 6, pp. 424–33, 2008. 1

[6] S. Aravindan, M. Natarajan, S. K. Ramraj, V. Pandian, F. H. Khan, T. S. Herman, and N. Aravindan, "Abscopal effect of low-LET gamma-radiation mediated through Rel protein signal transduction in a mouse model of non-targeted radiation response," *Cancer Gene Ther*, vol. 21, no. 2, pp. 54–9, 2014. 1

[7] M. Drouet, P. Garrigou, A. Peinnequin, and F. Herodin, "Short-term sonic-hedgehog gene therapy to mitigate myelosuppression in highly irradiated monkeys: hype or reality?" *Bone Marrow Transplant*, vol. 49, no. 2, pp. 304–9, 2014.

[8] A. Schlegel, C. Buhler, F. Devun, C. Agrario, S. Urien, F. Lokiec, J. S. Sun, and M. Dutreix, "Pharmacokinetics and toxicity in rats and monkeys of cod-bait: A therapeutic double-stranded dna oligonucleotide conjugated to cholesterol," *Mol Ther Nucleic Acids*, vol. 1, p. e33, 2012.

[9] M. W. Xie, R. Gorodetsky, E. D. Micewicz, N. C. Mackenzie, E. Gaberman, L. Levdansky, and W. H. McBride, "Marrow-derived stromal cell delivery on fibrin microbeads can correct radiation-induced wound-healing deficits," *J Invest Dermatol*, vol. 133, no. 2, pp. 553–61, 2013. 1

[10] S. A. Carruthers and M. M. Wallington, "Total body irradiation and pneumonitis risk: a review of outcomes," *Br J Cancer*, vol. 90, no. 11, pp. 2080–4, 2004. 1

[11] F. Gijbels, G. Sanderink, C. Bou Serhal, H. Pauwels, and R. Jacobs, "Organ doses and subjective image quality of indirect digital panoramic radiography," *Dentomaxillofacial Radiology*, vol. 30, no. 6, pp. 308–313, 2001. 1

[12] A. Lecomber, S. Downes, M. Mokhtari, and K. Faulkner, "Optimisation of patient doses in programmable dental panoramic radiography," *Dentomaxillofacial Radiology*, vol. 29, no. 2, pp. 107–112, 2000. 1

[13] M. Benabdesselam, F. Mady, and S. Girard, "Assessment of Ge-doped optical fibre as a TL-mode detector," *Journal of Non-Crystalline Solids*, vol. 360, no. 0, pp. 9–12, 2013. 1, 2

[14] N. M. Noor, M. Hussein, D. A. Bradley, and A. Nisbet, "Investigation of the use of Ge-doped optical fibre for in vitro IMRT prostate dosimetry," *Nuclear Instruments and Methods in Physics Research Section A: Accelerators, Spectrometers, Detectors and Associated Equipment*, vol. 652, no. 1, pp. 819–823, 2011. 2, 22

[15] S. Devic, "Radiochromic film dosimetry: past, present, and future," *Physica Medica*, vol. 27, no. 3, pp. 122–134, 2011. [Online]. Available: http://www.ncbi.nlm.nih.gov/pubmed/21050785 2, 9

[16] D. A. Bradley, R. P. Hugtenburg, A. Nisbet, A. T. Abdul Rahman, F. Issa, N. Mohd Noor, and A. Alalawi, "Review of doped silica glass optical fibre: their TL properties and potential applications in radiation therapy dosimetry," *Appl Radiat Isot*, vol. 71 Suppl, pp. 2–11, 2012. 2, 20, 56

[17] F. Issa, A. T. Abdul Rahman, R. P. Hugtenburg, D. A. Bradley, and A. Nisbet, "Establishment of Ge-doped optical fibres as thermoluminescence dosimeters for brachytherapy," *Applied Radiation and Isotopes*, vol. 70, no. 7, pp. 1158–1161, 2012.

[18] N. H. Yaakob, H. Wagiran, M. I. Hossain, A. T. Ramli, D. A. Bradley, S. Hashim, and H. Ali, "Thermoluminescence response of Ge-and Al-doped optical fibers subjected to low-dose electron irradiation," *Journal of nuclear science and technology*, vol. 48, no. 7, pp. 1115–1117, 2011. 2, 23

[19] A. Timar-Gabor, C. Ivascu, S. Vasiliniuc, L. Daraban, I. Ardelean, C. Cosma, and O. Cozar, "Thermoluminescence and optically stimulated luminescence properties of the 0.5P 2O 5-xBaO-(0.5-x)Li 2O glass systems," *Applied Radiation and Isotopes*, vol. 69, no. 5, pp. 780–784, 2011. 2

[20] N. Salah, S. S. Habib, Z. H. Khan, and F. Djouider, "Thermoluminescence and photoluminescence of ZrO2 nanoparticles," *Radiation Physics and Chemistry*, vol. 80, no. 9, pp. 923–928, 2011. 2

[21] M. Erfani Haghiri, E. Saion, W. S. wan Abdullah, N. Soltani, M. Hashim, M. Navasery, and M. A. Shafaei, "Thermoluminescence studies of manganese doped calcium tetraborate (CaB4O7:Mn) nanocrystal synthesized by co-precipitation method," *Radiation Physics and Chemistry*, vol. 90, no. 0, pp. 1–5, 2013. 2

[22] Y. S. M. Alajerami, S. Hashim, S. K. Ghoshal, M. A. Saleh, T. Kadni, M. I. Saripan, K. Alzimami, Z. Ibrahim, and D. A. Bradley, "The effect of TiO2 and MgO on the thermoluminescence properties of lithium potassium borate glass system," *Journal of Physics and Chemistry of Solids*, vol. 74, no. 12, pp. 1816–1822, 2013. 2

[23] S. Girard, J. Kuhnhenn, A. Gusarov, B. Brichard, M. Van Uffelen, Y. Ouerdane, A. Boukenter, and C. Marcandella, "Radiation effects on silica-based optical fibers: Recent advances and future challenges," *IEEE Transactions on Nuclear Science*, vol. 60, pp. 2015–2036, 2013. 2, 21

[24] M. Benabdesselam, F. Mady, S. Girard, Y. Mebrouk, J. B. Duchez, M. Gaillardin, and P. Paillet, "Performance of Ge-doped optical fiber as a thermoluminescent dosimeter," 2013. 2, 21, 57

[25] S. Girard, D. Griscom, J. Baggio, B. Brichard, and F. Berghmans, "Transient optical absorption in pulsed-x-ray-irradiated pure-silica-core optical fibers: Influence of self-trapped holes," *Journal of non-crystalline solids*, vol. 352, no. 23, pp. 2637–2642, 2006. 2, 3, 25

[26] M. C. Paul, D. Bohra, A. Dhar, R. Sen, P. Bhatnagar, and K. Dasgupta, "Radiation response behavior of high phosphorous doped step-index multimode optical fibers under low dose gamma irradiation," *Journal of Non-Crystalline Solids*, vol. 355, no. 28, pp. 1496–1507, 2009.

[27] S. Ghosh, S. Das, M. C. Paul, K. Dasgupta, D. Bohra, H. S. Chaudhary, L. Panwar, P. K. Bhatnagar, and S. G. Vaijapurkar, "Evaluation of the performance of high phosphorous with germanium codoped multimode optical fiber for use as a radiation sensor at low dose rates," *Applied Optics*, vol. 50, no. 25, pp. E80–E85, 2011.

[28] P. Lu, X. Bao, K. Brown, and N. Kulkarni, "Gamma-induced attenuation in normal single-mode and multimode, Ge-doped and p-doped optical fibers: A fiber optic dosimeter for low dose levels," *Canadian Journal of Physics*, vol. 78, no. 2, pp. 89–97, 2000. 2

[29] J. Polf, E. Yukihara, M. Akselrod, and S. McKeever, "Real-time luminescence from Al2O3 fiber dosimeters," *Radiation measurements*, vol. 38, no. 2, pp. 227–240, 2004. 2

[30] A. Alessi, S. Girard, M. Cannas, S. Agnello, A. Boukenter, and Y. Ouerdane, "Influence of drawing conditions on the properties and radiation sensitivities of pure-silica-core optical fibers," *Journal of Lightwave Technology*, vol. 30, no. 11, pp. 1726–1732, 2012. 2, 3

[31] N. A. Zahaimi, M. H. R. Ooi Abdullah, H. Zin, A. L. Abdul Rahman, S. Hashim, M. I. Saripan, M. C. Paul, D. A. Bradley, and A. T. Abdul Rahman, "Dopant concentration and thermoluminescence (TL) properties of tailor-made Ge-doped SiO2 fibres," *Radiation Physics and Chemistry*, no. 0, 2014. 2, 56, 57

[32] J.-W. Lee, G. Sigel Jr, and J. Li, "Processing-induced defects in optical waveguide materials," *Journal of non-crystalline solids*, vol. 239, no. 1, pp. 57–65, 1998. 3, 26, 27

[33] Y. Hibino and H. Hanafusa, "Defect structure and formation mechanism of drawing induced absorption at 630 nm in silica optical fibers," *Journal of applied physics*, vol. 60, no. 5, pp. 1797–1801, 1986. 3, 25, 78

[34] H. Hanafusa, Y. Hibino, and F. Yamamoto, "Formation mechanism of drawing-induced defects in optical fibers," *Journal of Non-Crystalline Solids*, vol. 95, pp. 655–661, 1987. 3, 26

[35] S. Sakaguchi, H. Itoh, F. Hanawa, and T. Kimura, "Drawing induced 1.53 um wavelength optical loss in single mode fibers drawn at high speeds," *Applied Physics Letters*, vol. 47, no. 4, pp. 344–346, 1985. 3

[36] Y. Hibino, F. Hanawa, and M. Horiguchi, "Drawing induced residual stress effects on optical characteristics in pure silica core single mode fibers," *Journal of Applied Physics*, vol. 65, no. 1, pp. 30–34, 1989. 3, 26

[37] A. Alessi, S. Girard, C. Marcandella, S. Agnello, M. Cannas, A. Boukenter, and Y. Ouerdane, "X-ray irradiation effects on a multistep Ge-doped silica fiber produced using different drawing conditions," *Journal of Non-Crystalline Solids*, vol. 357, no. 8-9, pp. 1966–1970, 2011. 3, 95

[38] S. Girard, C. Marcandella, A. Alessi, A. Boukenter, Y. Ouerdane, N. Richard, P. Paillet, M. Gaillardin, and M. Raine, "Transient radiation responses of optical fibers: influence of mcvd process parameters," *Nuclear Science, IEEE Transactions on*, vol. 59, no. 6, pp. 2894–2901, 2012. 3

[39] S. Girard, J. Baggio, and J. Leray, "Radiation-induced effects in a new class of optical waveguides: the air-guiding photonic crystal fibers," *Nuclear Science, IEEE Transactions on*, vol. 52, no. 6, pp. 2683–2688, 2005. 4

[40] N. J. Florous, K. Saitoh, T. Murao, and M. Koshiba, "Radiation dose enhancement in photonic crystal fiber bragg gratings: towards photo-ionization monitoring of irradiation sources in harsh nuclear power reactors," in *Quantum Electronics and Laser Science Conference*. Optical Society of America, Conference Proceedings, p. JTuA59.

[41] S. DeHaven, S. Albin, and W. Kelliher, "Liquid filled microstructured optical fiber for x-ray detection," *Optics Express*, vol. 18, no. 13, pp. 13 754–13 760, 2010.

[42] H. El Hamzaoui, Y. Ouerdane, L. Bigot, G. Bouwmans, B. Capoen, A. Boukenter, S. Girard, and M. Bouazaoui, "Sol-gel derived ionic copper-doped microstructured optical fiber: a potential selective ultraviolet radiation dosimeter," *Optics express*, vol. 20, no. 28, pp. 29 751–29 760, 2012. 4

[43] G. F. Knoll, *Radiation detection and measurement*. Wiley. com, 2010. 8, 9

[44] J. Izewska and G. Rajan, *Radiation dosimeters*, 2005. 8, 9, 10, 11, 20

[45] F. M. Khan, *The physics of radiation therapy*, 3rd ed. Lippincott Williams and Wilkins Philadelphia, 2003, vol. 3.

[46] G. Shani, *Radiation dosimetry: instrumentation and methods*. CRC Press, 2001. 8, 20

[47] S. McKeever, M. Moscovitch, and P. Townsend, *Thermoluminescence dosimetry materials: properties and uses*. Nuclear Technology Pub., 1995. 8, 10, 11, 12, 14, 17, 19

[48] M. Oberhofer and A. Scharmann, *Applied thermoluminescence dosimetry*, 1981. 8

[49] A. Niroomand-Rad, C. R. Blackwell, B. M. Coursey, K. P. Gall, J. M. Galvin, W. L. McLaughlin, A. S. Meigooni, R. Nath, J. E. Rodgers, and C. G. Soares, "Radiochromic film dosimetry: recommendations of aapm radiation therapy

committee task group 55," *Medical physics*, vol. 25, no. 11, pp. 2093–2115, 1998. 9

[50] W. L. Mclaughlin and M. F. Desrosiers, "Dosimetry systems for radiation processing," *Radiation Physics and Chemistry*, vol. 46, no. 4, pp. 1163–1174, 1995. 9

[51] C. Oliveira, J. Salgado, M. L. Botelho, and L. Ferreira, "Dose determination by monte carlo-a useful tool in gamma radiation process," *Radiation Physics and Chemistry*, vol. 57, no. 3, pp. 667–670, 2000. 9

[52] S. Bernal and J. Bogard, *Protocols for Thermoluninescence and Optically Stimulated Luminescence Research at DOSAR*. United States. Department of Energy, 2004. 10

[53] M. Martini and F. Meinardi, "Thermally stimulated luminescence: new perspectives in the study of defects in solids," *La Rivista del Nuovo Cimento*, vol. 20, no. 8, pp. 1–71, 1997. 11, 12, 13, 28

[54] C. Furetta, *Handbook of thermoluminescence*. World Scientific, 2003. 12, 13, 14, 15, 16, 17, 28, 30, 31, 32, 33, 44, 78

[55] E. Hodgson, A. Delgado, and J. A. Rivas, "In-beam studies of m-centre production processes in nacl," *Journal of Physics C: Solid State Physics*, vol. 12, no. 7, p. 1239, 1979.

[56] F. Sagastibelza and J. A. Rivas, "Thermoluminescence in LiF (TLD-100) and LiF crystals irradiated at room temperature," *Journal of Physics C: Solid State Physics*, vol. 14, no. 13, p. 1873, 1981.

[57] K. Tanimura and T. Okada, "Formation of the self-trapped exciton via thermally induced defect reactions in alkali halides," *Physical Review B*, vol. 21, no. 4, p. 1690, 1980. 12

[58] T. Kron, "Thermoluminescence dosimetry and its applications in medicine–part 1: Physics, materials and equipment," *Australasian physical and engineering sciences in medicine*, vol. 17, no. 4, pp. 175–199, 1994. 13

[59] V. Manjunathaguru and T. K. Umesh, "Effective atomic numbers and electron densities of some biologically important compounds containing h, c, n and o in the energy range 145-1330 kev," *Journal of Physics B: Atomic, Molecular and Optical Physics*, vol. 39, no. 18, pp. 3969–3981, 2006. 16

[60] S. R. Manohara, S. M. Hanagodimath, K. S. Thind, and L. Gerward, "On the

effective atomic number and electron density: A comprehensive set of formulas for all types of materials and energies above 1kev," *Nuclear Instruments and Methods in Physics Research Section B: Beam Interactions with Materials and Atoms*, vol. 266, no. 18, pp. 3906–3912, 2008.

[61] V. Ramprasath, "Effective atomic numbers for photon energy absorption and energy dependence of some thermoluminescent dosimetric compounds," *Nuclear Instruments and Methods in Physics Research Section B: Beam Interactions with Materials and Atoms*, vol. 168, no. 3, pp. 294–304, 2000.

[62] F. Spiers, "Effective atomic number and energy absorption in tissues," *British Journal of Radiology*, vol. 19, no. 218, pp. 52–63, 1946. 16

[63] C. Jayachandran, "Calculated effective atomic number and kerma values for tissue-equivalent and dosimetry materials," *Physics in medicine and biology*, vol. 16, no. 4, p. 617, 1971. 17

[64] I. Olarinoye, "Variation of effective atomic numbers of some thermoluminescence and phantom materials with photon energies," *Research Journal of Chemical Sciences*, vol. 1, p. 2, 2011.

[65] M. Taylor, R. Franich, J. Trapp, and P. Johnston, "The effective atomic number of dosimetric gels," *Australasian Physics and Engineering Sciences in Medicine*, vol. 31, no. 2, pp. 131–138, 2008. 17

[66] C. Furetta, M. Prokic, R. Salamon, V. Prokic, and G. Kitis, "Dosimetric characteristics of tissue equivalent thermoluminescent solid TL detectors based on lithium borate," *Nuclear Instruments and Methods in Physics Research Section A: Accelerators, Spectrometers, Detectors and Associated Equipment*, vol. 456, no. 3, pp. 411–417, 2001. 17

[67] S. Gowda, S. Krishnaveni, T. Yashoda, T. Umesh, and R. Gowda, "Photon mass attenuation coefficients, effective atomic numbers and electron densities of some thermoluminescent dosimetric compounds," *Pramana*, vol. 63, no. 3, pp. 529–541, 2004.

[68] S. Miljanic, M. Ranogajec-Komor, and B. Vekic, "Main dosimetric characteristics of some tissue-equivalent TL detectors," *Radiation protection dosimetry*, vol. 100, no. 1-4, pp. 437–442, 2002.

[69] V. Vasiliev, V. Kostjuchenko, O. Riazantsev, V. Khaybullin, S. Samarin, and A. Uglov, "Tissue equivalence of some phantom materials for proton beams," *arXiv preprint arXiv:1005.4389*, 2010. 17

[70] R. Visocekas, T. Ceva, C. Marti, F. Lefaucheux, and M. Robert, "Tunneling

processes in afterflow ot calcite," *Phys. Slat. Solidi (a)*, vol. 35, no. 1, pp. 315–327, 1976. 17

[71] R. Templer, "The localised transition model of anomalous fading," *Radiation Protection Dosimetry*, vol. 17, no. 1-4, pp. 493–497, 1986. 17

[72] R. Chen, W. Hornyak, and V. Mathur, "Competition between excitation and bleaching of thermoluminescence," *Journal of Physics D: Applied Physics*, vol. 23, no. 6, p. 724, 1990. 17

[73] T. Kron, "Applications of thermoluminescence dosimetry in medicine," *Radiation protection dosimetry*, vol. 85, no. 1-4, pp. 333–340, 1999. 19

[74] R. Hille, H. Bueker, and F. Haesing, "Glass fibers as radiation detectors," *Nuclear Instruments and Methods in Physics Research Section A: Accelerators, Spectrometers, Detectors and Associated Equipment*, vol. 299, no. 1, pp. 217–221, 1990. 20

[75] F. Berghmans, B. Brichard, A. F. Fernandez, A. Gusarov, M. Van Uffelen, and S. Girard, *An introduction to radiation effects on optical components and fiber optic sensors*. Springer, 2008, pp. 127–165. 20

[76] R. A. Clark, "Intrinsic dosimetry: properties and mechanisms of thermoluminescence in commercial borosilicate glass," Thesis, 2012.

[77] A. Daricova and M. Vaickova, "Utilization of optical fibers in dosimetry," *Applied radiation and isotopes*, vol. 46, no. 6, pp. 471–472, 1995. 20, 95

[78] E. BADITA, E. STANCU, F. SCARLAT, C. VANCEA, and A. SCARISOREANU, "Study of optical fiber as new radiation dosimeter," *Romanian Reports in Physics*, vol. 65, no. 4, pp. 1438–1442, 2013. 20

[79] G. Bartesaghi, V. Conti, D. Bolognini, S. Grigioni, V. Mascagna, M. Prest, S. Scazzi, A. Mozzanica, P. Cappelletti, M. Frigerio, S. Gelosa, A. Monti, A. Ostinelli, G. Giannini, and E. Vallazza, "A scintillating fiber dosimeter for radiotherapy," *Nuclear Instruments and Methods in Physics Research Section A: Accelerators, Spectrometers, Detectors and Associated Equipment*, vol. 581, no. 1-2, pp. 80–83, 2007. 95

[80] B. Medved Rogina and B. Vojnovic, "Application of optical fibre sensors for radiation dosimetry," *Radiation measurements*, vol. 26, no. 4, pp. 599–602, 1996.

[81] M. N. Ott, "Radiation effects data on commercially available optical fiber:

database summary," in *Radiation Effects Data Workshop, 2002 IEEE.* IEEE, Conference Proceedings, pp. 24–31.

[82] A. L. Yusoff, R. P. Hugtenburg, and D. A. Bradley, "Review of development of a silica-based thermoluminescence dosimeter," *Radiation Physics and Chemistry*, vol. 74, no. 6, pp. 459–481, 2005. 20, 21, 35, 56

[83] S. McKeever, "Thermoluminescence in quartz and silica," *Radiation Protection Dosimetry*, vol. 8, no. 1-2, pp. 81–98, 1984. 20

[84] R. Chen, Y. Kirsh, and P. Townsend, "Models for the sensitization of thermoluminescence in silica fibres," *International Journal of Radiation Applications and Instrumentation. Part D. Nuclear Tracks and Radiation Measurements*, vol. 18, no. 1, pp. 13–17, 1991. 20

[85] K. Nakahashi, K. Watanabe, A. Uritani, A. Yamazaki, and E. Ariga, "Feasibility study on a micro-size dosimeter using an optical fiber probe based on a photostimulable phosphorescence," *Radiation Measurements*, vol. 46, no. 12, pp. 1547–1550, 2011.

[86] N. M. Noor, M. Hussein, D. A. Bradley, and A. Nisbet, "The potential of Ge-doped optical fibre TL dosimetry for 3D verification of high energy IMRT photon beams," *Nuclear Instruments and Methods in Physics Research Section A: Accelerators, Spectrometers, Detectors and Associated Equipment*, vol. 619, no. 1-3, pp. 157–162, 2010. 20, 92

[87] Z. Zheng, D. Hong-Gui, H. Shang-Ze, L. Jian, and F. Jie, "An optical fibre-type silicate glass thermoluminescent detector," *Nuclear Instruments and Methods in Physics Research Section A: Accelerators, Spectrometers, Detectors and Associated Equipment*, vol. 301, no. 2, pp. 337–340, 1991. 20

[88] A. Huston, B. Justus, P. Falkenstein, R. Miller, H. Ning, and R. Altemus, "Remote optical fiber dosimetry," *Nuclear Instruments and Methods in Physics Research Section B: Beam Interactions with Materials and Atoms*, vol. 184, no. 1, pp. 55–67, 2001. 20, 95

[89] Y. A. Abdulla, Y. Amin, and D. Bradley, "The thermoluminescence response of Ge-doped optical fibre subjected to photon irradiation," *Radiation Physics and Chemistry*, vol. 61, no. 3, pp. 409–410, 2001. 21

[90] S. Hashim, S. Al-Ahbabi, D. A. Bradley, M. Webb, C. Jeynes, A. T. Ramli, and H. Wagiran, "The thermoluminescence response of doped SiO2 optical fibres subjected to photon and electron irradiations," *Applied radiation and isotopes*, vol. 67, no. 3, pp. 423–427, 2009. 21, 57

[91] H. Wagiran, I. Hossain, D. Bradley, A. N. H. Yaakob, and T. Ramli, "Thermoluminescence responses of photon and electron irradiated Ge- and Al-Doped SiO2 optical fibres," *Chinese Physics Letters*, vol. 29, no. 2, p. 027802, 2012. 21, 22

[92] S. Hashim, D. A. Bradley, N. Peng, A. T. Ramli, and H. Wagiran, "The thermoluminescence response of oxygen-doped optical fibres subjected to photon and electron irradiations," *Nuclear Instruments and Methods in Physics Research Section A: Accelerators, Spectrometers, Detectors and Associated Equipment*, vol. 619, no. 1-3, pp. 291–294, 2010. 21, 95

[93] S. Girard, Y. Ouerdane, C. Marcandella, A. Boukenter, S. Quenard, and N. Authier, "Feasibility of radiation dosimetry with phosphorus-doped optical fibers in the ultraviolet and visible domain," *Journal of Non-Crystalline Solids*, vol. 357, no. 8-9, pp. 1871–1874, 2011. 21

[94] A. T. Abdul Rahman, A. Nisbet, and D. A. Bradley, "Dose-rate and the reciprocity law: TL response of Ge-doped SiO2 optical fibers at therapeutic radiation doses," *Nuclear Instruments and Methods in Physics Research Section A: Accelerators, Spectrometers, Detectors and Associated Equipment*, vol. 652, no. 1, pp. 891–895, 2011. 21

[95] C. L. Ong, S. Kandaiya, H. T. Kho, and M. T. Chong, "Segments of a commercial Ge-doped optical fiber as a thermoluminescent dosimeter in radiotherapy," *Radiation Measurements*, vol. 44, no. 2, pp. 158–162, 2009.

[96] N. H. Yaakob, H. Wagiran, M. I. Hossain, A. T. Ramli, D. A. Bradley, and H. Ali, "Low-dose photon irradiation response of Ge and Al-doped SiO2 optical fibres," *Appl Radiat Isot*, vol. 69, no. 9, pp. 1189–92, 2011. 21, 23

[97] A. T. Abdul Rahman, D. A. Bradley, S. J. Doran, B. Thierry, E. Brauer-Krisch, and A. Bravin, "The thermoluminescence response of Ge-doped silica fibres for synchrotron microbeam radiation therapy dosimetry," *Nuclear Instruments and Methods in Physics Research Section A: Accelerators, Spectrometers, Detectors and Associated Equipment*, vol. 619, no. 1-3, pp. 167–170, 2010. 21, 22

[98] F. Issa, N. A. A. Latip, D. A. Bradley, and A. Nisbet, "Ge-doped optical fibres as thermoluminescence dosimeters for kilovoltage x-ray therapy irradiations," *Nuclear Instruments and Methods in Physics Research Section A: Accelerators, Spectrometers, Detectors and Associated Equipment*, vol. 652, no. 1, pp. 834–837, 2011. 22, 95

[99] A. T. Abdul Rahman, R. P. Hugtenburg, S. F. Abdul Sani, A. I. Alalawi, F. Issa, R. Thomas, M. A. Barry, A. Nisbet, and D. A. Bradley, "An investigation of the thermoluminescence of Ge-doped SiO2 optical fibres for application

in interface radiation dosimetry," *Appl Radiat Isot*, vol. 70, no. 7, pp. 1436–41, 2012. 22

[100] A. T. Ramli, D. A. Bradley, S. Hashim, and H. Wagiran, "The thermoluminescence response of doped SiO2 optical fibres subjected to alpha-particle irradiation," *Appl Radiat Isot*, vol. 67, no. 3, pp. 428–32, 2009. 22

[101] S. Hashim, D. A. Bradley, M. I. Saripan, A. T. Ramli, and H. Wagiran, "The thermoluminescence response of doped SiO2 optical fibres subjected to fast neutrons," *Appl Radiat Isot*, vol. 68, no. 4-5, pp. 700–3, 2010. 22, 95

[102] N. H. Yaakob, H. Wagiran, I. Hossain, A. T. Ramli, D. A. Bradley, S. Hashim, and H. Ali, "Electron irradiation response on Ge and Al-doped SiO2 optical fibres," *Nuclear Instruments and Methods in Physics Research Section A: Accelerators, Spectrometers, Detectors and Associated Equipment*, vol. 637, no. 1, pp. 185–189, 2011. 22, 57

[103] N. M. Noor, N. A. Shukor, M. Hussein, A. Nisbet, and D. A. Bradley, "Comparison of the TL fading characteristics of Ge-doped optical fibres and LiF dosimeters," *Applied Radiation and Isotopes*, vol. 70, no. 7, pp. 1384–1387, 2012. 23, 65

[104] T. Bakos, "Defects in amorphous SiO2: Reactions, dynamics and optical properties," Thesis, 2003. 23, 24

[105] R. Salh, *Defect related luminescence in silicon dioxide network: a review.* InTech, 2011, book section 8, pp. 135–172. 23, 24, 25, 62, 66, 91, 92

[106] M. Cannas, "Luminescence properties of point defects in silica," *Gnsr 2001: State of Art and Future Development in Raman Spectroscopy and Related Techniques*, p. 91, 2002. 23, 24

[107] A. Cannizzo, "Optical properties of point defects in silica: Role of the local dynamics of the host matrix," Thesis, 2005. 24

[108] Z.-Y. Lu, C. Nicklaw, D. Fleetwood, R. Schrimpf, and S. Pantelides, "The structure, properties, and dynamics of oxygen vacancies in amorphous SiO2," *Physical review letters*, vol. 89, no. 28, p. 285505, 2002. 24

[109] K. Kajihara, Y. Ikuta, M. Hirano, and H. Hosono, "Effect of F2 laser power on defect formation in high-purity SiO2 glass," *Journal of Non-Crystalline Solids*, vol. 322, no. 1, pp. 73–77, 2003. 24

[110] G. Pacchioni, G. Ierano, and A. M. Marquez, "Optical absorption and nonra-

diative decay mechanism of E' center in silica," *Physical review letters*, vol. 81, no. 2, p. 377, 1998.

[111] L. Skuja, "Optically active oxygen-deficiency-related centers in amorphous silicon dioxide," *Journal of NON-crystalline Solids*, vol. 239, no. 1, pp. 16–48, 1998. 24

[112] C. Brinker, R. Kirkpatrick, D. Tallant, B. Bunker, and B. Montez, "Nmr confirmation of strained "defects" in amorphous silica," *Journal of non-crystalline solids*, vol. 99, no. 2, pp. 418–428, 1988. 24

[113] D. L. Griscom, "Optical properties and structure of defects in silica glass," *J. Cerm. Soc. Jpn.*, vol. 99, no. 10, pp. 923–942, 1991. 25, 26

[114] A. Song and R. Williams, "Self-trapped excitons," 1996. 25

[115] W. Carvalho, P. Dumas, J. Corset, and V. Neuman, "Raman spectra and oxygen-related absorption bands in pure silica core fibres," *Journal of Raman spectroscopy*, vol. 16, no. 5, pp. 330–331, 1985. 25

[116] K. Arai, H. Imai, J. Isoya, H. Hosono, Y. Abe, and H. Imagawa, "Evidence for pair generation of an E'center and a nonbridging oxygen-hole center in gamma-ray-irradiated fluorine-doped low-OH synthetic silica glasses," *Physical Review B*, vol. 45, no. 18, p. 10818, 1992. 25

[117] M. Guzzi, M. Martini, A. Paleari, F. Pio, A. Vedda, and C. Azzoni, "Neutron irradiation effects in amorphous SiO2: optical absorption and electron paramagnetic resonance," *Journal of Physics: Condensed Matter*, vol. 5, no. 43, p. 8105, 1993.

[118] H. Imai, K. Arai, H. Hosono, Y. Abe, T. Arai, and H. Imagawa, "Dependence of defects induced by excimer laser on intrinsic structural defects in synthetic silica glasses," *Physical Review B*, vol. 44, no. 10, p. 4812, 1991.

[119] C. D. Marshall, J. A. Speth, and S. A. Payne, "Induced optical absorption in gamma, neutron and ultraviolet irradiated fused quartz and silica," *Journal of non-crystalline solids*, vol. 212, no. 1, pp. 59–73, 1997.

[120] R. Weeks, R. Magruder III, and P. Wang, "Some effects of 5 eV photons on defects in SiO2," *Journal of non-crystalline solids*, vol. 149, no. 1, pp. 122–136, 1992.

[121] R. A. Weeks, "The many varieties of E' centers: A review," *Journal of non-crystalline solids*, vol. 179, pp. 1–9, 1994. 25

[122] G. Origlio, M. Cannas, S. Girard, R. Boscaino, A. Boukenter, and Y. Ouerdane, "Influence of the drawing process on the defect generation in multistep-index germanium-doped optical fibers," *Optics letters*, vol. 34, no. 15, pp. 2282–2284, 2009. 25, 27

[123] Y. Hibino and H. Hanafusa, "Formation mechanism of drawing induced peroxy radicals in pure silica optical fibers," *Journal of applied physics*, vol. 62, no. 4, pp. 1433–1436, 1987. 25

[124] E. Friebele, G. Sigel, and D. Griscom, "Drawing induced defect centers in a fused silica core fiber," *Applied Physics Letters*, vol. 28, no. 9, pp. 516–518, 1976. 26

[125] Y. Hibino, H. Hanafusa, and S. Sakaguchi, "Formation of drawing induced E'-centers in silica optical fibers," *Jpn. J. Appl. Phys. 1*, vol. 24, no. 9, pp. 1117–1121, 1985. 26

[126] H. Huang, R. M. Miura, and J. J. Wylie, "Optical fiber drawing and dopant transport," *SIAM Journal on Applied Mathematics*, vol. 69, no. 2, pp. 330–347, 2008. 26

[127] Y. Hibino and H. Hanafusa, "Drawing induced hydrogen associated defect centers at the silica optical fiber surface," *Applied Physics Letters*, vol. 45, p. 614, 1984. 26

[128] ——, "Esr study on e centers induced by optical fiber drawing process," *Jpn. J. Appl. Phys*, vol. 22, no. 12, pp. L766–L768, 1983. 26

[129] N. H. Ky, H. G. Limberger, R. P. Salathé, and F. Cochet, "Effects of drawing tension on the photosensitivity of Sn–Ge-and B–Ge-codoped core fibers," *Optics letters*, vol. 23, no. 17, pp. 1402–1404, 1998. 26

[130] Y. Hibino and H. Hanafusa, "Formation mechanism of hydrogen associated defect centers at silica optical fiber surfaces," *Journal of applied physics*, vol. 61, no. 5, pp. 1806–1810, 1987. 27

[131] E. J. Friebele, "Defect centers in a germanium-doped silica-core optical fiber," *Journal of Applied Physics*, vol. 45, no. 8, p. 3424, 1974. 27

[132] F. Messina, S. Agnello, R. Boscaino, M. Cannas, S. Grandi, and E. Quartarone, "Optical properties of Ge-oxygen deficient centers embedded in silica films," *Journal of Non-Crystalline Solids*, vol. 353, no. 5, pp. 670–673, 2007. 27

[133] Y. Watanabe, H. Kawazoe, K. Shibuya, and K.-i. Muta, "Structure and mechanism of formation of drawing-or radiation-induced defects in SiO2:GeO2 optical fiber," *Jpn. J. Appl. Phys*, vol. 25, pp. 425–431, 1986. 27

[134] B. Fox, Z. Schneider, K. Simmons-Potter, W. Thomes Jr, D. Meister, R. Bambha, D. Kliner, and M. Soderlund, "Gamma radiation effects in yb-doped optical fiber," *Fiber Lasers IV: Technology, Systems, and Applications, Proc. SPIE*, vol. 6453, p. 645328, 2007. 28

[135] V. Singh, S. Watanabe, T. K. Gundu Rao, J. F. D. Chubaci, I. Ledoux Rak, and H. Y. Kwak, "Infrared luminescence, thermoluminescence and defect centres in er and yb co-doped znal2o4 phosphor," *Applied Physics B*, vol. 98, no. 1, pp. 165–172, 2009. 28

[136] A. Pugh, R. Stratton, and D. Lewis, "Investigation of elemental diffusion during the drawing and heat treatment of glass optical fibres," *Journal of materials science*, vol. 29, no. 4, pp. 1036–1040, 1994. 28

[137] K. Lyytikainen, S. Huntington, A. Carter, P. McNamara, S. Fleming, J. Abramczyk, I. Kaplin, and G. Schotz, "Dopant diffusion during optical fibre drawing," *Opt. Express*, vol. 12, no. 6, pp. 972–977, 2004. 28, 95, 97

[138] K. Lyytikainen, P. Raback, and J. Ruokolainen, "Numerical simulation of a specialty optical fibre drawing process," in *ASME Pressure Vessels and Piping*, Conference Proceedings, pp. 267–276. 28

[139] E. A. Raja, B. Dhabekar, S. Menon, S. More, T. G. Rao, and R. Kher, "Role of defect centres in thermoluminescence mechanism of Tb3+ doped MgAl2O4," *Indian Journal of Pure and Applied Physics*, vol. 47, no. 6, p. 420, 2009. 28

[140] F. A. Soliman, "Radiation testing of fiber optic systems," *Applied radiation and isotopes*, vol. 47, no. 2, pp. 175–183, 1996. 28

[141] A. I. Gusarov, D. Doyle, A. Hermanne, F. Berghmans, M. Fruit, G. Ulbrich, and M. Blondel, "Refractive-index changes caused by proton radiation in silicate optical glasses," *Applied optics*, vol. 41, no. 4, pp. 678–684, 2002. 28

[142] B. Brichard, P. Borgermans, A. F. Fernandez, K. Lammens, and A. Decreton, "Radiation effect in silica optical fiber exposed to intense mixed neutron-gamma radiation field," *Nuclear Science, IEEE Transactions on*, vol. 48, no. 6, pp. 2069–2073, 2001.

[143] A. Gusarov, D. Doyle, A. Hermanne, and F. Berghmans, "Index and density changes induced by proton radiation in lanthanum crown glass," *Applied Physics Letters*, vol. 78, no. 21, p. 3196, 2001.

[144] F. Liu, Y. An, P. Wang, B. Shao, and S. Chen, "Effects of radiation on optical fibers," *Recent Progress in Optical Fiber Research*, pp. 978–953, 2007. 28

[145] T. K. Gundu Rao, B. C. Bhatt, and P. S. Page, "Defect centers and thermoluminescence in al2o3:si,ti," *Radiation Measurements*, vol. 43, no. 2-6, pp. 295–299, 2008. 29

[146] P. Townsend and A. Rowlands, "Extended defect models for thermoluminescence," *Radiation protection dosimetry*, vol. 84, no. 1-4, pp. 7–12, 1999. 29

[147] N. Kucuk and I. Kucuk, "Computational modeling of thermoluminescence glow curves of zinc borate crystals," *Journal of Inequalities and Applications*, vol. 2013, no. 1, pp. 1–7, 2013. 29

[148] A. A. El-Hafez and A. M. N. El-Faramawy, "In defense of thermoluminescence dosimeter zero dose readouts," *Journal of American Science*, vol. 7, no. 3, 2011. 30

[149] R. Chen and S. McKeever, *Theory of Thermoluminescence and Related Phenomena*. World Scientific, 1997. 31

[150] R. Chen and G. Haber, "Calculation of glow curves activation energies by numerical initial rise method," *Chemical Physics Letters*, vol. 2, no. 7, pp. 483–485, 1968. 32

[151] Y. S. Horowitz and M. Moscovitch, "Highlights and pitfalls of 20 years of application of computerised glow curve analysis to thermoluminescence research and dosimetry," *Radiat. Prot. Dosimetry*, vol. 153, no. 1, pp. 1–22, 2013. 33, 35

[152] V. Pagonis, G. Kitis, and C. Furetta, *Numerical and Practical Exercises in Thermoluminescence*. Springer, 2006. 33

[153] R. Chen, "On the order of kinetics in the study of thermoluminescence," *Journal of Physics D: Applied Physics*, no. 16, pp. L107–L114, 1983. 33

[154] S. Basun, G. F. Imbusch, D. D. Jia, and W. M. Yen, "The analysis of thermoluminescence glow curves," *Journal of Luminescence*, vol. 104, no. 4, pp. 283–294, 2003. 34, 35

[155] M. Shah Alam and S. Bauk, "Analysis of thermoluminescence glow-curves for general order kinetics using mathematica," *Advanced Studies in Theoretical Physics*, vol. 4, no. 17, pp. 837 – 853, 2010. 34

[156] J. Prakash, P. Singh, and D. Dwivedi, "Thermally stimulated processes: I-mechanisms involved in the appearance of a thermoluminescence glow curve," *Indian Journal of Pure and Applied Physics*, vol. 44, no. 7, p. 532, 2006.

[157] M. S. Rasheedy, "A modification of the kinetic equations used for describing the thermoluminescence phenomenon," *J Fluoresc*, vol. 15, no. 4, pp. 485–91, 2005. 56

[158] A. N. Yazici and M. Y. Haciibrahimoglu, "Determination of the trapping parameters of glow peaks of CaF2Dy (TLD-200) by using computer glow curve deconvolution method," *Turkish Journal of Physics*, vol. 25, pp. 249–255, 2001. 34

[159] J. A. Harvey, M. L. Rodrigues, and K. J. Kearfott, "A computerized glow curve analysis (GCA) method for WinREMS thermoluminescent dosimeter data using MATLAB," *Appl Radiat Isot*, vol. 69, no. 9, pp. 1282–6, 2011. 34

[160] M. Puchalska and P. Bilski, "Glowfit-a new tool for thermoluminescence glow-curve deconvolution," *Radiation Measurements*, vol. 41, no. 6, pp. 659–664, 2006. 34

[161] K. S. Chung, C. Y. Park, J. I. Lee, and J. L. Kim, "Thermoluminescence glow curve deconvolution of LiF:Mg,Cu,Si with more realistic kinetic models," *Radiation Measurements*, vol. 59, pp. 151–154, 2013. 35

[162] P. R. Gonzalez, C. Gutierrez-Tapia, and H. Flores-Llamas, "Kinetics of the TL phenomenon in LiF:Mg irradiated to different dose of gamma radiation of (60)Co using two different programs of deconvolution," *Appl Radiat Isot*, vol. 83 Pt C, pp. 200–3, 2014. 35

[163] R. K. Gartia and L. L. Singh, "Evaluation of trapping parameter of quartz by deconvolution of the glow curves," *Radiation Measurements*, vol. 46, no. 8, pp. 664–668, 2011. 35

[164] J. A. Harvey, N. P. Haverland, and K. J. Kearfott, "Characterization of the glow-peak fading properties of six common thermoluminescent materials," *Appl Radiat Isot*, vol. 68, no. 10, pp. 1988–2000, 2010. 35

[165] S. D. Singh, "A review on the lifetime of trapped electrons relevant to TL glow peaks," *International Journal of Luminescence and its applications*, vol. 3, no. 1, pp. 11–14, 2013. 35

[166] C. Systems and Controls. (2010) modified chemical vapor deposition (MCVD). [Online]. Available: http://www.custom-sys.com/Projects/mcvd.html

[167] D. Wood, K. Walker, J. B. MacChesney, J. R. Simpson, and R. Csencsits, "Germanium chemistry in the MCVD process for optical fiber fabrication," *Lightwave Technology, Journal of*, vol. 5, no. 2, pp. 277–285, 1987. 38

[168] M. Affonseca, P. Andreo, M. Arib, H. Bjerke, B. Casar, L. Czap, S. Duane, H. Ferreira, J. Grindborg, and G. Hartmann, *Implementation of the international code of practice on dosimetry in radiotheraphy (TRS 398): review of testing results.* IAEA-International atomic energy agency, 2005. 43

[169] K. Chung, H. Choe, J. Lee, J. Kim, and S. Chang, "A computer program for the deconvolution of thermoluminescence glow curves," *Radiation protection dosimetry*, vol. 115, no. 1-4, pp. 343–349, 2005. 45

[170] K. D. Dambul, G. A. Mahdiraji, F. Amirkhan, D. M. Chow, G. K. W. Gan, W. R. Wong, M. R. Abu Hassan, S. Ismail, S. A. Ibrahim, N. Tamchek, and F. R. M. Adikan, "Fabrication and development of flat fibers," in *Photonics Global Conference (PGC), 2012*, Conference Proceedings, pp. 1–3. 51

[171] A. Ranjbar, M. Charles, S. Durrani, and K. Randle, "Electron spin resonance and thermoluminescence dosimetry of clear fused quartz: Its possible use for personal, high dose and high temperature dosimetry," *Radiation Protection Dosimetry*, vol. 65, no. 1-4, pp. 351–354, 1996. 62

[172] T. Izak-Biran, S. Malchi, Y. Shamai, and Z. B. Alfassi, "Low pre- and post-irradiation fading of Lif:Mg,Ti (TLD-100, TLD-600, TLD-700) using a preheat technique," *Radiation Protection Dosimetry*, vol. 64, no. 4, pp. 269–274, 1996. 65

[173] R. A. Vasilache, S. Tanase-Nicola, and R. Tiron, "Characteristics of TLD-100 fading and its influence on the calibration of personal dosemeters," *Radiation Protection Dosimetry*, vol. 85, no. 1-4, pp. 183–185, 1999. 65

[174] Y. S. Horowitz and D. Yossian, "Computerised glow curve deconvolution: application to thermoluminescence dosimetry," *Radiation Protection Dosimetry*, vol. 60, no. 1, pp. 3–3, 1995. 84

[175] A. T. Abdul Rahman, N. K. Abu Bakar, M. Chandra Paul, and D. A. Bradley, "Ultraviolet radiation (UVR) dosimetry system and the use of Ge-doped silica optical fibres," *Radiation Physics and Chemistry*, no. 0, 2014. 95

PUBLICATIONS, CONFERENCES AND AWARDS

Publications

- "Optical fiber based dosimeter sensor: beyond TLD-100 limit."
  G. Amouzad Mahdiraji, M. Ghomeishi, E. Dermosesian, S. Hashim, N.M. Ung, F.R. Mahamd Adikan, D.A. Bradley
  Sensors and Actuators A: Physiacal (Q1)
  (Volume: 222, Year: 2015, Pages: 48-57)

- "Enhancing the radiation dose detection sensitivity of optical fibres."
  G. A. Mahdiraji, M. Ghomeishi, E. Dermosesian, F. R. Mahamd Adikan, H. A. A. Rashid, M. J. Maah, D. A. Bradley
  Applied Radiation and Isotopes (Q2)
  (Volume: 100, Year: 2015, Pages: 43-49)

- "Developing small vacuum spark as an x-ray source for calibration of an x-ray focusing crystal spectrometer."
  M. Ghomeishi, M. Karami, and F. R. Mahamd Adikan
  Review of Scientific Instruments (Q2)
  (Volume: 83, Year: 2013, Pages: 103-110)

Conference and Proceedings

- "The Thermoluminescence Response of Undoped Silica PCF for Dosimetry Application." CLEO2013 Pacific Rim / Kyoto, Japan 2013.

- "Study of Traps in Optical Fibre TLD via Glow Curve Analysis." IRRMA2014 / Valencia, Spain 2014

- "Analysis of Optical Fibre Defects Using Thermoluminescence Glow Curve method." ICP2014 / Kuala Lumpur, Malaysia 2014.

Awards

- **Gold medal** for "*Accurate Radiation Capturing Glass*" - Malaysian Technology Expo 2014, Kuala Lumpur.

- **Silver medal** for "*Optical Fibre Based High Sensitive Dosimeter*" - Innovation and Creativity EXPO i-INOVA 2013, Malaysia.

CHAPTER A: HIGH DOSE IRRADIATION RESULTS

In this appendix is tried to present the TL results of various available optical fibres which are exposed to high dose irradiation from of ^{60}Co γ ray or EPS-300 electron beam. Most of the samples were saturated so fast, however, the linear part is shown at inset of the figures when possible.

Following samples contain doped and undoped fibres with different cross-sectional shapes. Undoped fibres were fabricated using F300 preform which is high purity suprasill glass, or using HXWG preform which contains some OH impurities in compare with F300 type.

In the case of electron beam irradiation using EPS-3000, the following parameters were considered during the irradiation (Table A.1):

Table A.1: EPS-3000 Electron beam irradiation parameters.

Accelerator Voltage	Beam Current	Beam Dose	Beam Width	Conveyor Speed
2.0 MeV	1 mA	5 kGy/pass	60 cm	1.88 m/min

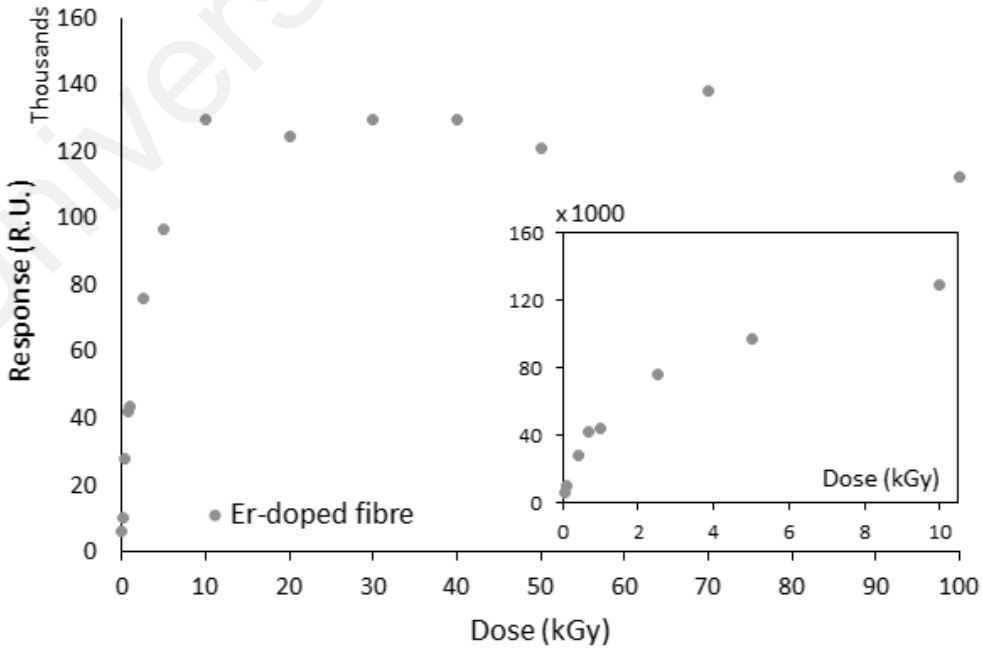

Figure A.1: Er-doped fibre exposed to ^{60}Co. Inset: linear part almost upto 10 kGy.

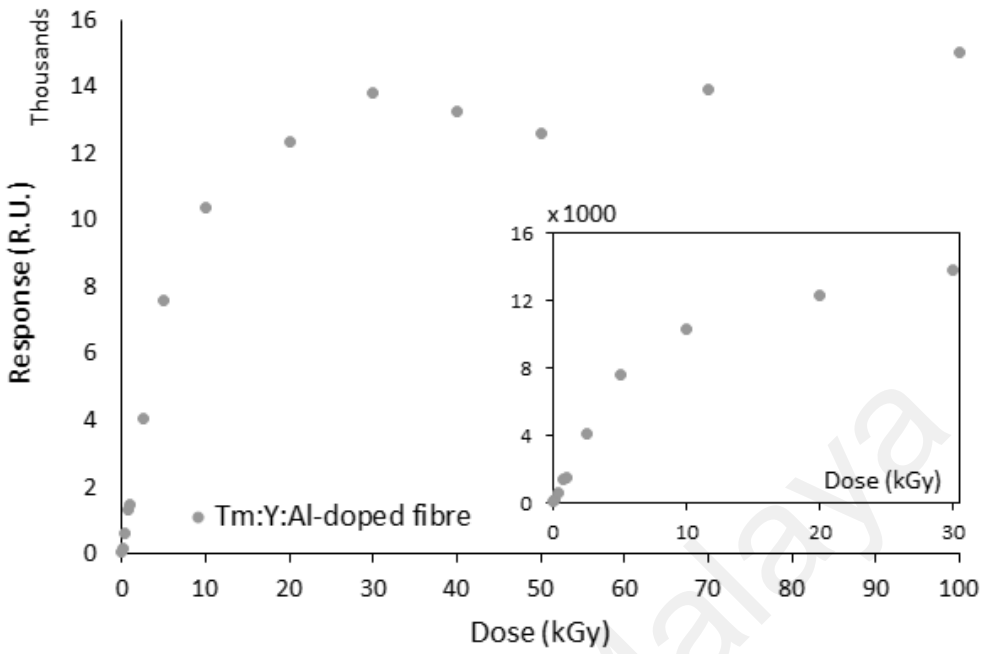

Figure A.2: Tm:Y:Al-doped fibre exposed to ^{60}Co. Inset: linear part almost up to 30 kGy.

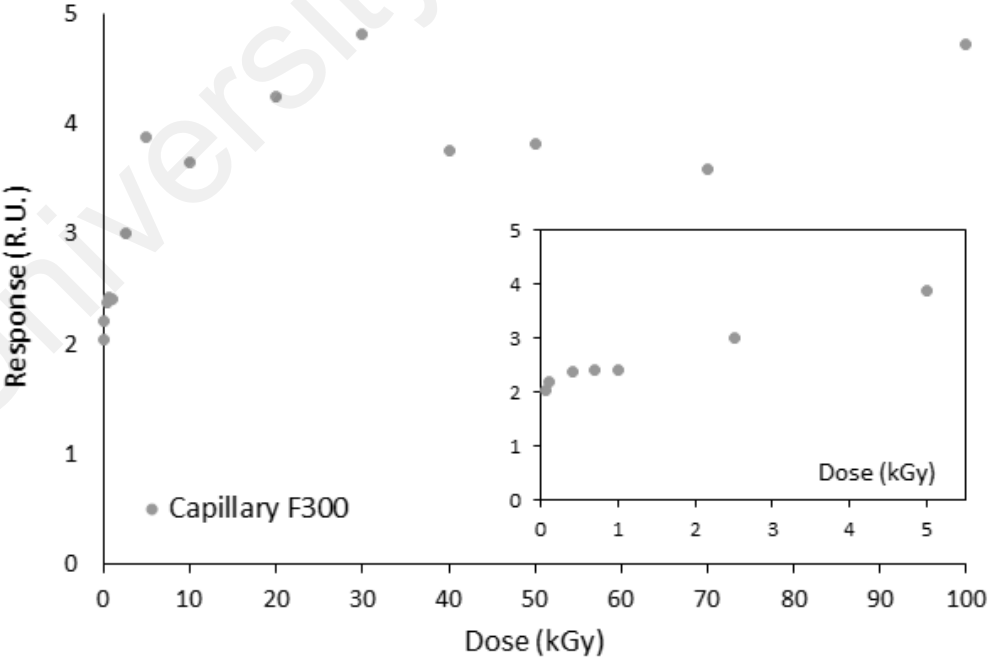

Figure A.3: Capillary-F300 fibre exposed to ^{60}Co. Inset: linear part almost up to 5 kGy.

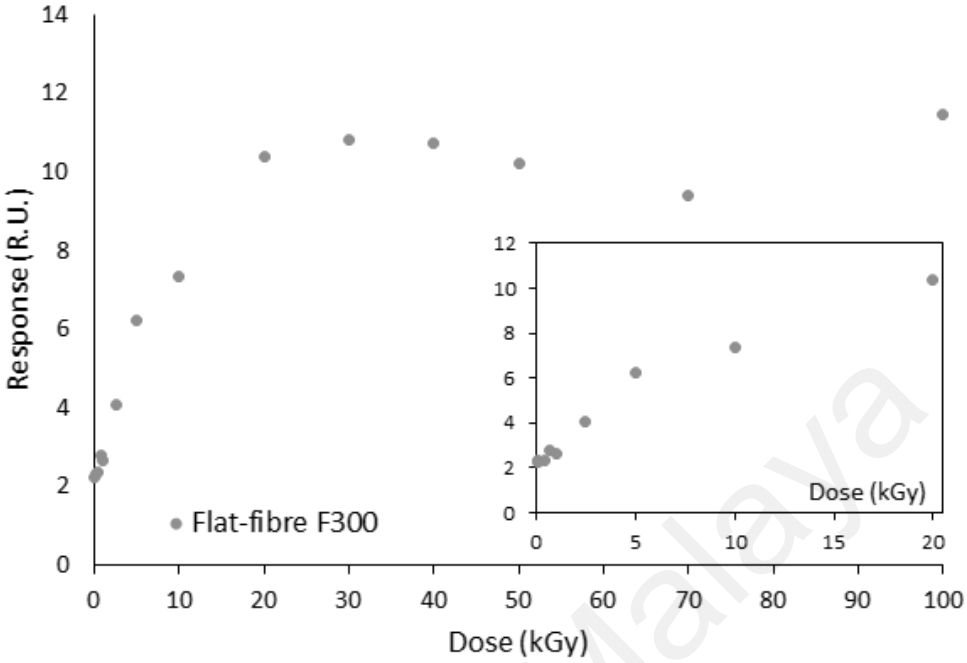

Figure A.4: Flat-F300 fibre exposed to ^{60}Co. Inset: linear part almost up to 20 kGy.

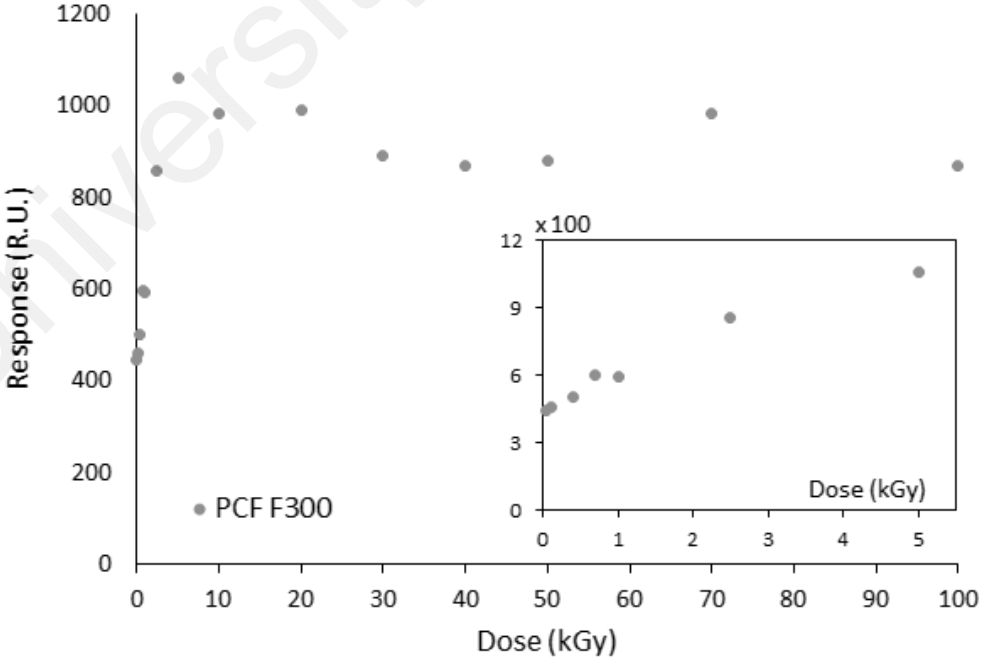

Figure A.5: PCF-F300 fibre exposed to ^{60}Co. Inset: linear part almost up to 5 kGy.

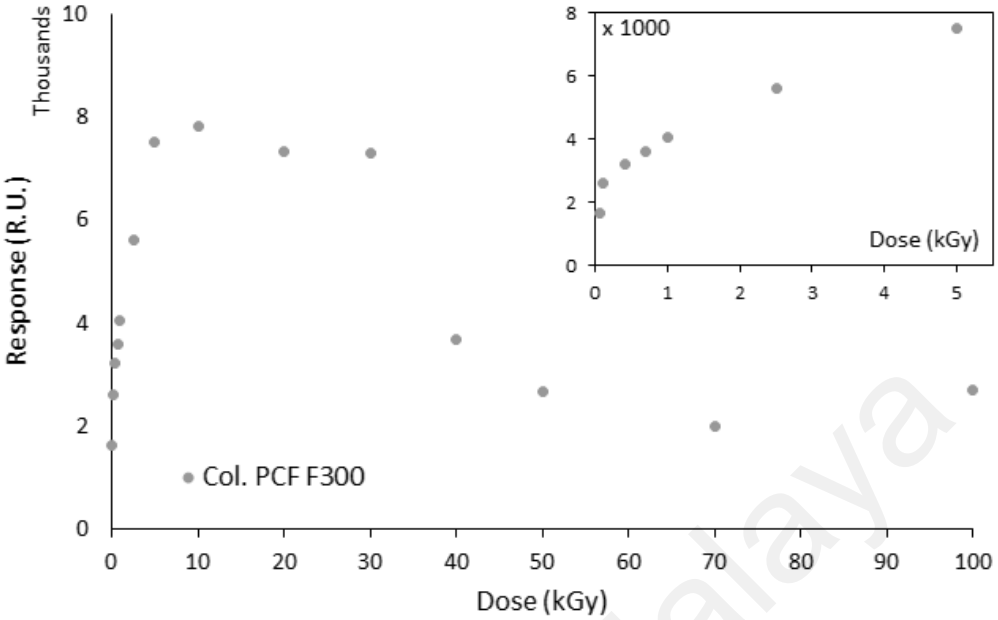

Figure A.6: Collapsed PCF-F300 fibre exposed to ^{60}Co. Inset: linear part almost up to 5 kGy.

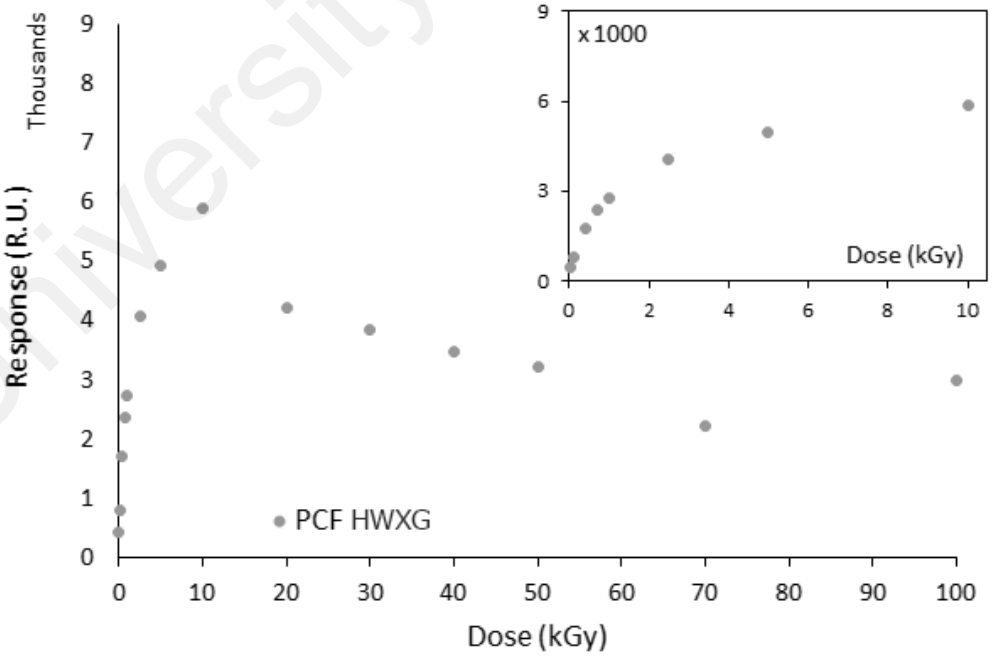

Figure A.7: PCF-HXWG fibre exposed to ^{60}Co. Inset: linear part almost up to 10 kGy.

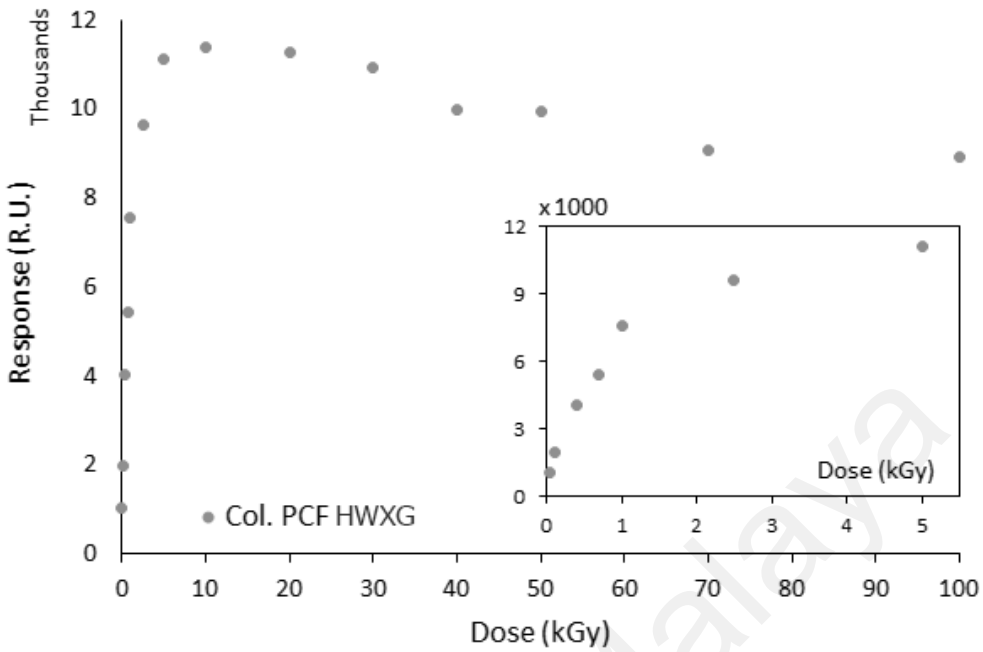

Figure A.8: Collapsed PCF-HXWG fibre exposed to ^{60}Co. Inset: linear part almost up to 5 kGy.

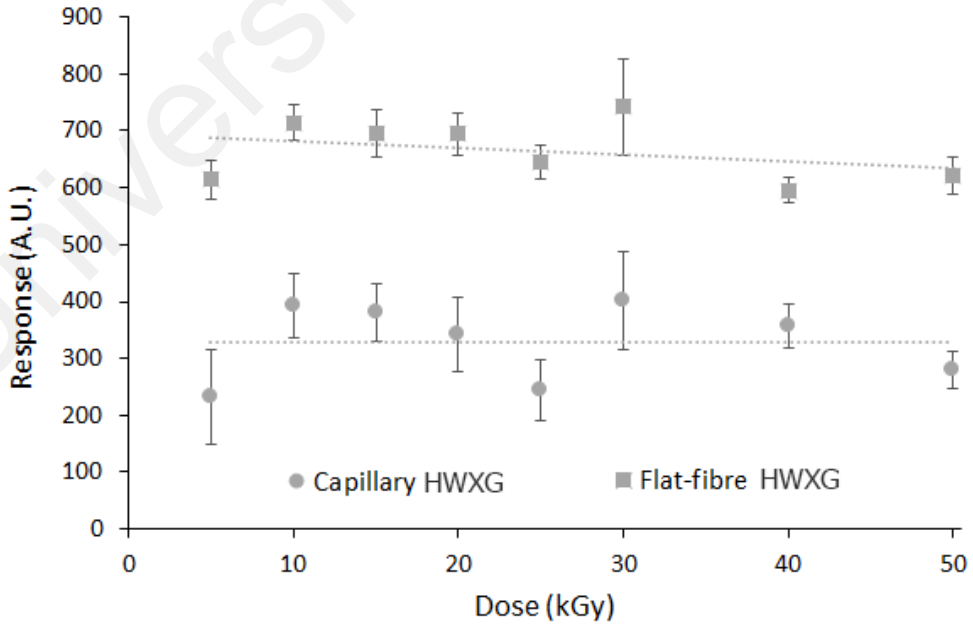

Figure A.9: Capillary and flat-HXWG fibres exposed to electron beam. All samples are fully saturated.

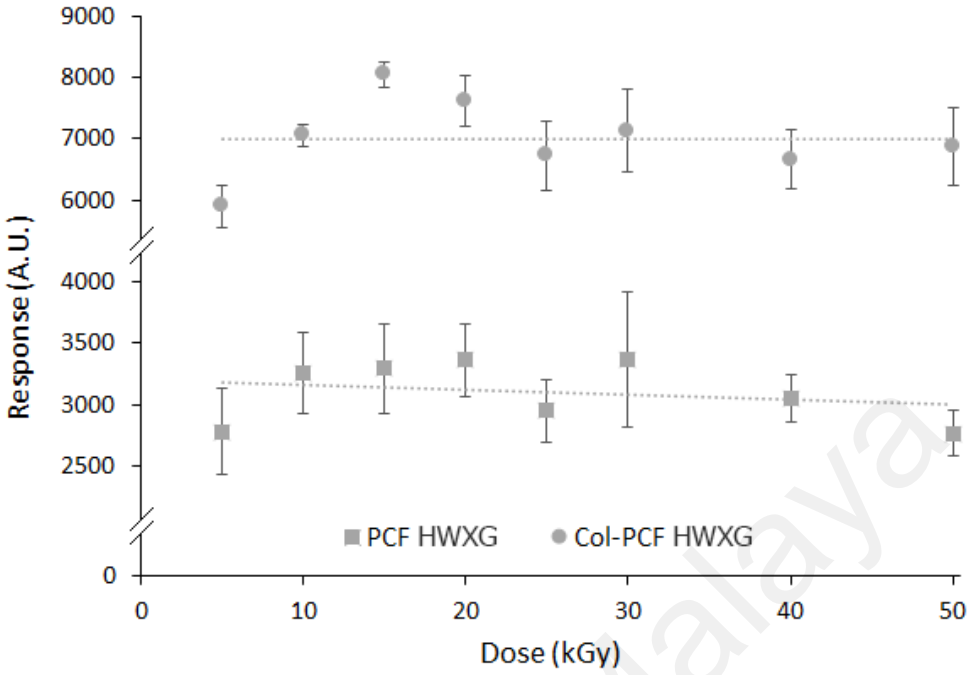

Figure A.10: PCF and Collapsed PCF-HXWG fibres exposed to electron beam. All samples are fully saturated.

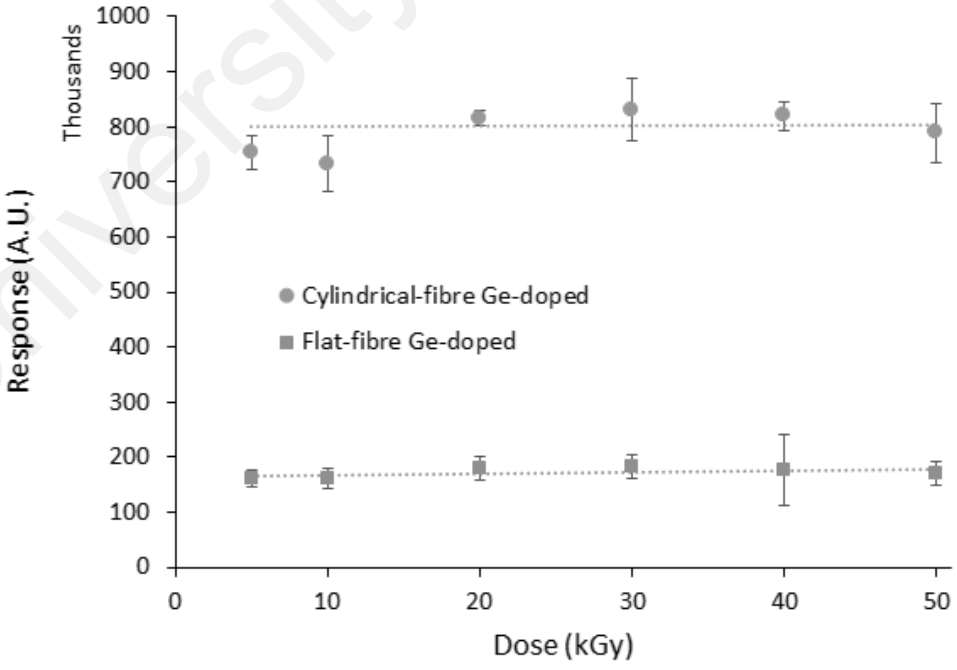

Figure A.11: Ge-doped cylindrical and flat fibres exposed to electron beam. All samples are fully saturated.